Copper at the Interface of Chemistry and Biology: New Insights into hCtr1 Function and the Role of Histidine in Human Cellular Copper Acquisition

by

Kathryn Haas

Department of Chemistry
Duke University

Date:_____
Approved:

_____
Dr. Katherine Franz, Supervisor

_____
Dr. Stephen Craig

_____
Dr. Alvin Crumbliss

_____
Dr. Dennis Thiele

Dissertation submitted in partial fulfillment of
the requirements for the degree of Doctor
of Philosophy in the Department of
Chemistry in the Graduate School
of Duke University

2010

ABSTRACT

Copper at the Interface of Chemistry and Biology: New Insights into hCtr1 Function and the Role of Histidine in Human Cellular Copper Acquisition

by

Kathryn Haas

Department of Chemistry
Duke University

Date:_____
Approved:

_____
Dr. Katherine Franz, Supervisor

_____
Dr. Stephen Craig

_____
Dr. Alvin Crumbliss

_____
Dr. Dennis Thiele

An abstract of a dissertation submitted in partial fulfillment of the requirements for the degree of Doctor of Philosophy in the Department of Chemistry in the Graduate School of Duke University

2010

Abstract

Mechanisms of copper homeostasis are of great interest partly due to their connection to debilitating genetic and neurological disorders. The family of high-affinity copper transporters (Ctr) is responsible for extracellular copper acquisition and internalization in yeast, plants, and mammals, including human. The extracellular domain of the human high-affinity copper transporter (hCtr1) contains essential Cu-binding methionine-rich MXXM and MXM (Mets) motifs that are important for copper acquisition and transport. The hCtr1 extracellular domain also contains potential copper binding histidine (His) clusters, including a high-affinity Cu^{2+} ATCUN site. As of yet, extracellular His clusters have no established significance for hCtr1 function. We have made model peptides based on the extracellular copper acquisition domain of hCtr1 that is rich in His residues and Mets motifs. The peptides' Cu^{+} and Cu^{2+} binding properties have been characterized by UV-Vis and mass spectrometry. Our findings have been extended to a mouse cell model and we show that His residues are important for hCtr1 function likely because of their contribution to strong copper-binding sites in the hCtr1 extracellular domain responsible for copper acquisition.

Copper's pro-oxidant property is also medicinally promising if it can be harnessed to induce oxidative stress as a cancer chemotherapy strategy. Our lab has designed a photocleavable caged copper complex that can selectively release redox-active copper in response to light. The thermodynamic copper binding properties of these potential chemotherapeutics have been characterized.

Dedication

Dedicated to You.

Contents

List of Tables

List of Figures

List of Abbreviations

Abs	absorbance
Ac	acetyl
Ala	alanine
ALS	amyotrophic lateral sclerosis (Lou Gehrig's Disease)
ATCUN	amino terminal copper nickel
Atox1	copper chaperone for ATPase7a/b
ATP	adenosine triphosphate
BAPTA	1,2-bis(o-aminophenoxy)ethane-N,N,N',N'-tetraacetic acid
BC	bathocuproine
BCA	bicinchoninic acid
BCS	bathocuproine disulfonate
BPS	bathophenanthroline disulfonate
calcd	calculated
CCD	charge coupled device
CCS	copper chaperone for SOD
Ctr	copper transport protein
$Ctr1^{-/-}$	MEF Ctr1 knockout cell line
DFO	desferrioxamine
DMEM	Dulbecco's modified eagle medium
DNA	deoxyribonucleic acid
DTPA	diethylenetriamine pentaacetic acid
EDTA	ethylenediamine tetraacetic acid

EGTA	ethylene glycol tetraacetic acid
ESI-MS	electrospray ionization mass spectrometry
FBS	fetal bovine serum
Fmoc	fluorenylmethyloxycarbonyl
GdnHCl	guanidinium hydrochloride
hCtr1	human copper transport protein 1
$hCtr1^{+/+}$	MEF $Ctr1^{-/-}$ reconstituted with hCtr1
hCtr1ntHA	hCtr1 mutant protein with all N-terminal His mutated to Ala
$hCtr1ntHA^{+/+}$	MEF $Ctr1^{-/-}$ reconstituted with hCtr1ntHA
HEPES	4-(2-hydroxyethyl)-1-piperazineethanesulfonic acid
His	histidine
HPLC	high performance liquid chromatography
HSA	human serum albumin
HSAB	hard soft acid base
L	ligand
LFSE	ligand field stabilization energy
Ln	lanthanide
M	metal
MBD	metal binding domain
MEF	mouse embryonic fibroblast
MeOH	methanol
Met	methionine
Mets motif	Met-rich motifs (MXM and MXXM)
MNKP	Menkes disease protein

MRI	magnetic resonance imaging
myc	peptide tag of the sequence EQKLISEEDL
Nle	norleucine
NTA	nitrilotriacetic acid
Opti-MEM®	reduced serum minimal essential media
P	peptide or peptide mass ion
PAL-PEG-PS	polyethylene glycol polystyrene peptide synthesis resin
PET	positron emission tomography
PNGaseF	N-glycosidase
Redox	reduction-oxidation reaction
ROS	reactive oxygen species
SIH	salicylaldehyde isonicotinoyl hydrazone
SOD	Cu/Zn superoxide dismutase
SPECT	single photon emission computed tomography
TGN	transgogli network
TMD2	transmembrane domain 2
TPEN	N,N,N′,N′-tertrakis-(2-pyridylmethyl)-ethylenediamine)
UV-Vis	ultraviolet-visible spectroscopy
WNDP	Wilson's disease protein
wt	wild type
yCtr1	yeast copper transport protein 1
yCtr2	yeast copper transport protein 2
yCtr3	yeast copper transport protein 3
β-ME	betamercaptoethanol, 2-mercaptoethanol

Acknowledgements

I am grateful to many people, both direct and indirect, in preparation of this dissertation. First I thank Katherine Franz for her unwavering support and guidance over the six years of my graduate career. The opportunities you have given me are unique and much appreciated. I feel lucky to have you as an advisor. I also owe a great debt to my committee members. Thank you Dennis Thiele for generously inviting me into your lab in order to take this project from the test tube to live cells. Your excitement for science is contagious and it resonates through your team of students and post docs. I am grateful for the experience of working with the Thiele Lab and am glad to be part of the wonderful science you do. Thanks also to Steven Craig, who reviewed this document in record time and provided invaluable feedback in its early stages. I owe many thanks to Alvin Crumbliss, whose expertise in metal binding has been invaluable throughout my graduate career and in preparation of this dissertation. Thank you all for your contributions to this work.

I am also very fortunate for the many friends and colleagues I have found over the years and who have helped me both directly and indirectly with this work. I would like to especially thank past and present members of the Franz Lab, whose support and friendship helped to make graduate school a great experience. Thanks to Lou Charkoudian who is the best lab mate and running buddy I could ever have. Thanks to Katie Ciesienski, who made this journey with me from beginning to end. Thanks to Lynne Heyman, Jeff Rubino, Marina Dickens, and Drew Folk who contributed to intellectually stimulating conversations about science and fun conversations about life. My grad school experience wouldn't have been the same without you!

I especially want to thank the undergraduate students who worked with me on this project in the Franz lab. Thank you Daniel White for your hard work and especially for you many questions about copper binding to human serum albumin. And thank you Allison Putterman for your countless hours of data collection and questions about hCtr1 that helped this project progress. Your curiosity is an inspiration! The simple questions are sometimes the most important and the most overlooked. I am grateful to both of you for help on this project and know you will do well with whatever you decide to pursue!

I also owe a great debt of gratitude to the past and present members of the Thiele Lab. I owe special thanks to Michelle Turski as both a friend and a great mentor. Thank you for spending your last months at Duke training me in molecular biology. I also thank Dominique Waldvogel who spent many hours drinking coffee with me and having great conversations about copper transport. Thanks to Byung Kim, Kent Wood, Scott McNaughton, Sandra Vergara, Yasuhiro Nose, Dan Neef, and Tracy Nevitt who all played a role in helping interpret data and designing experiments for this project. You all contributed in invaluable ways to this work. I appreciate the training and help I got from all of you. Thank you!

I thank Andrea Lutteran and Amanda Jane Hoertz who helped me early in my career with aspects of this project that did not make it into this document. Your time and efforts are much appreciated and the training I got from you was invaluable later in my career. Thank you!

Special thanks goes to my mom, Deborah Maguire. You have always been a great example for me to follow. I also appreciate you taking on responsibilities at home so that I could finish this work. Thank you for being there for me now and always!

I owe special acknowledgment to James Praise for invaluable help in editing and revising early drafts of this dissertation. I especially thank you for being a strong support and my best friend over many years.

Last but not least, thanks to all that I could not list here, but have participated in and contributed to the great fun of learning over the years.

1. Introduction to Metal Homeostasis in Cellular Biology[i]

1.1 Function of Metals in Biological Systems.

Metals serve an essential role in many aspects of human civilization and have defined Ages of human history. The period of time from about 3300 BC to 1200 BC is often referred to as the Bronze Age. During this period our ancestors first started using metal and learned to mix various elements with copper to make a strong alloy, called bronze. This Age yielded significant advancement in crafting of sharper knives and stronger weapons out of metal instead of rock, wood and bone. Around 1200 BC the human race found an even harder metal and discovered a much stronger alloy called steel. This period is known as the Iron Age. More recently, periods of time known as Gold Rushes have caused huge changes in population distributions and wealth in some countries. Metal has obvious importance in our modern way of life. Today, iron and steel are used for making buildings, machines, automobiles, jewelry, cooking pots, tools, weapons, vehicles, electronics, surgical instruments and symbolic structures like the Eiffel Tower and the Statue of Liberty. Gold, silver, and copper still serve as currency for trade and exchange of goods and services.

Even before human history existed, metals influenced the evolution of life. Metal ions are essential in biology and perform a vast array of important functions. They are used to create both macroscopic and microscopic structures, perform electron transfer reactions, and act as signals between cells. They play key roles in maintaining life and are essential to every organism. In fact, you would have a hard time finding one important process within a living cell that does not depend on a metal ion in the context of either function or structure.

---

[i] Parts of this chapter have been published in Haas, K. L.; Franz, K. J., Application of Metal Coordination Chemistry To Explore and Manipulate Cell Biology. *Chem. Rev.* **2009,** *109* (10), 4921-4960.

What are the properties of metal ions that impart utility to biology? Because inorganic elements comprise the bulk of the periodic table, the diversity of these properties is likewise broad and has been thoroughly covered by several books in the field of bioinorganic chemistry.[1-3] A brief summary of the general chemical properties of metals is given below.

1. Charge. In aqueous solution, metal ions are positively charged, but that charge can be manipulated depending on the coordination environment, so that a metal complexed by ligands can be cationic, anionic, or neutral.

2. Interactions with ligands. Metal ions bind to ligands (both organic and inorganic) via interactions that are often strong and selective. The ligands impart their own functionality and can tune properties of the overall complex that are unique from those of the individual ligand or metal. The thermodynamic and kinetic properties of metal–ligand interactions influence ligand exchange reactions.

3. Structure and bonding. Metal–ligand complexes span a range of coordination geometries that give them unique shapes compared to organic molecules. The bond lengths, bond angles, and number of coordination sites can vary depending on the metal and its oxidation state.

4. Lewis acid character. Metal ions with high electron affinity can significantly polarize groups that are coordinated to them, facilitating hydrolysis reactions.

5. Partially filled d-shell. For the transition metals, the variable number of electrons in the d-shell orbitals (or f-shell for lanthanides) imparts interesting electronic and magnetic properties to transition metal complexes.

6. Redox activity. Coupled with the variability of electrons in the d-shell is the ability for many transition metals to undergo 1-electron oxidation and reduction reactions.

Biology has taken advantage of these chemical properties of metals to perform several functional roles, which are summarized in Table 1. This is by no means an exhaustive list, but rather a primer to highlight important themes. Some metal ions, particularly the alkali and alkaline earth metals, are stable in aqueous solution as cations, making Na^+, K^+ and Ca^{2+} ideal for maintaining charge balance and electrical conductivity.[2] On the other hand, the distinct architectures accessible via metal–ligand bonding interactions impart important structural roles to metal ions that encompass both macroscopic structural stabilization, as in biomineralized tissues,[4] as well as molecular structural stabilization, as in proteins and nucleic acids that are stabilized in a preferred fold by metal ions.[5-8] Metal–ligand bonding is also significant in its reversibility. Nature takes advantage of this reversibility to bind and release metal ions like Ca^{2+} and Zn^{2+} to and from proteins or other storage repositories in order to propagate various biochemical signals.[5, 9] The presence of various metal ions themselves can be their own signal to adjust DNA transcription, as in the case of metalloregulatory proteins.[10, 11] Reversible metal–ligand coordination is also exploited to bind and release molecules to and from a metal center, a prime example being O_2 binding and release from hemoglobin.

The reactivity of metallic centers in biology rests mostly in their Lewis acid or redox-active characters. Metal centers that are strong Lewis acids can activate coordinated ligands for reactivity, for example a water molecule coordinated to a Zn(II) center becomes a potent nucleophile for amide bond hydrolysis of a protein substrate.[12] In terms of redox activity, a wide variety of transition metals that can access variable oxidation states are found incorporated as enzyme cofactors that carry out oxidation/reduction chemistry. Electron transfer units like cytochromes, iron-sulfur clusters, and blue copper proteins shuttle electrons to other proteins that require redox

chemistry for their function, while other redox proteins catalyze multielectron oxidation/reduction reactions directly on a substrate. Examples here involve oxygen metabolism, including the reduction of dioxygen to water by cytochrome c oxidase, and hydrocarbon oxidation catalyzed by cytochrome P-450 enzymes, to name just a few.

When it comes to applying inorganic compounds to biology, chemists are not restricted to the naturally bioavailable set of metals and can take advantage of the properties of biologically exotic elements, including second and third row transition elements and the lanthanide (Ln) elements. This expansion leads to the list of functional roles of inorganic elements applied to biology shown in Table 2. Many of the functions listed in Table 2 mirror those of Table 1, but they are applied in novel ways. For example, the structures of kinetically inert metal complexes are found to interact with proteins and nucleic acids in unique ways, and the acid-base and redox activity of native and non-native metals can be used in new ways. Metal complexes can also impart additional functionality not found naturally. The most striking addition to the list is in visualization, where the photophysical, magnetic, and radioactive properties of metals make possible studies based on luminescence, magnetic resonance, PET, and SPECT imaging modalities.

Table 1: Functional roles of inorganic elements found in biology, with selected representative examples

Function	Inorganic Element	Representative Examples
Charge Balance	Na, K, Ca	K^+ channels responsible for electrical conduction in nervous systems[2]
Structure (macroscopic)	Ca, Si	Biominerals in bone, teeth, and shell[4]
Structure (protein structure)	Zn, Ca	Zn finger proteins, extracellular Ca proteins[5, 8]
Structure (nucleic acid structure)	Mg, Mn	Mg^{2+} stabilization of transfer RNA and the hammerhead ribozyme[6, 7]
Signaling	Ca, NO, Zn	Release of Ca^{2+}, Zn^{2+} and NO instigate diverse biochemical signaling pathways[5, 9, 13]
Signaling to DNA	Hg, Cu, Zn, Pb, As, Sb, Cd, Ni, Fe, Mn, Co, Ag	Metal-responsive transcriptional regulators (metalloregulatory proteins)[10, 11]
Acid-Base Catalysis	Zn, Fe, Ni, Mn, Mg	Hydrolysis reactions carried out by carboxypeptidase, purple acid phosphatase, urease, arginase, etc.[12]
Atom or Group Transfer	V, Fe, Co, Ni, Cu, Mo, W	Dioxygen transport (hemoglobin); alkyl group transfer (cobalamin)[3]
Electron Transfer	Fe, Cu, Mo	Iron-sulfur proteins, cytochromes, blue copper proteins[14]
Redox Catalysis	V, Mn, Fe, Co, Ni, Cu, W	Enzymes involved in oxygen metabolism; nitrogen fixation; radical formation[15]

Table 2. Functional roles of inorganic elements applied to biology, with selected representative examples

Function	Inorganic Element or Molecule	Representative Examples
Structure	Ru, Rh, Pt	Kinetically inert complexes serve as structural scaffolds for complexes that interact in novel ways with biomolecules[16-25]
Signaling	Ca, NO	Compounds that release Ca, NO, or other signaling molecules[25, 26]
Acid-Base Catalysis	Co, Zr, Pt, Ln	Complexes that induce hydrolytic cleavage of biomolecules[25, 27]
Visualization: Luminescence magnetic resonance radioactive x-ray	 Tb, Eu, other Ln Gd, Mn ^{99m}Tc, ^{64}Cu, others Os, Ln	 Subcellular imaging agents[25, 28] Metal-responsive MRI imaging[25, 29] SPECT, PET imaging[30, 31] Heavy atom derivatives for biomolecular X-ray structure determination[25, 32-39]
Alteration of Metal Bioavailability	Fe, Cu, Zn, Ca, other	Chelating agents that alter normal metal homeostasis[25, 26, 40-44]
Bonding	Zn, Ni, others	Metal–ligand bond formation for analyte sensing, metalloprotein inhibition, or protein labeling[25, 45-57]
Ligand Exchange	Gd, Co, others	Change in coordination sphere to increase MRI signal or release bioactive molecule[25, 58, 59]
Electron Transfer	Rh, Ru	Photoinduced electron transfer to produce potent photooxidants[20-22, 25, 60]
Redox	Fe, Cu, others	Oxidative degradation of proteins, DNA; chelation to manipulate redox activity[25, 61-67]

The work presented in this dissertation will focus on the transition metal copper in its role as a naturally occurring biological cofactor and its unnatural role in inorganic coordination compounds that can be used to manipulate cellular copper status. Chapter 2 describes the properties of a naturally occurring protein copper binding site, while Chapter 3 focuses on implications of this binding site on cellular trafficking and regulation of copper. The work in Chapter 4 demonstrates how the properties of inorganic coordination complexes with copper and other metals can be applied in the context of inorganic chemical biology and can be used as probes and tools to understand or control biological processes.

First though, it is important to understand how the coordination environment in a protein is important for biological selection and control of metal ion and oxidation state and how principles that govern metal preference for donor groups and coordination geometry can be utilized by scientists to control cellular metal localization and bioavailability. In the following sections the relevant principles of metal-ligand coordination chemistry and how these principles are used to control metal status in biological experiments will be briefly discussed. In the following sections, a particular focus will be on the biologically relevant transition metals iron, copper and zinc.

1.3 Principles of Metal-Ligand Coordination Chemistry

The principles governing metal–ligand complex stability and specificity depend on the properties of both the metal ion and the chelating agent, as summarized briefly in the following sections. More comprehensive reviews on ligand design for selective complexation of metal ions in aqueous solution are available.[68-73] This discussion sets the stage for understanding the properties of protein and small molecule metal binding sites presented throughout this work.

1.3.1 Donor Atom Preference

The principle of Hard and Soft Acids and Bases (HSAB) was developed in 1965 by R.G. Pearson following criterion paved by Irving, Williams, Arhland, Chatt, and Davies.[74] The classification is based on an atom's polarizability. Non-polarizable acids or bases are small with high charge density and are classified as "hard", and polarizable acids and bases that are usually large with low charge density are classified as "soft". Acids and bases that have intermediate hard/soft character are classified as "borderline". The HSAB principle predicts that hard acids prefer hard bases, soft acids prefer soft bases, and borderline acids prefer borderline bases. Pearson's classifications of metal ions (Lewis acids) and their ligands (Lewis bases) are shown in Table 3, which serves as a useful starting point for predicting the preference of metal ions for ligands with various donor groups. For example, soft donor groups such as thioethers (R_2S) and thiolates (RS^-) prefer soft metal ions, like Cu^+, whereas hard oxygen donors such as carboxylates and phenolates are appropriate for hard metal ions, like Fe^{3+}.[74]

In fitting with the Lewis acid–Lewis base description of metal–ligand coordination, it would seem apparent that increasing the Lewis basicity of the donor would enhance metal–ligand bonding. While this principle can be used to tune metal–ligand affinity, other factors must also be considered. For example, increasing the basicity of a phenolate also increases its pK_a. Since metal ions compete with protons for ligand binding in aqueous solution, such an adjustment might actually decrease the effective metal binding at a desired pH. Because of proton competition, overall stability constants (β) do not reflect the actual affinity of a ligand for a metal under biologically relevant solution conditions. A pH-dependent conditional binding constant (K_{cond}) can be calculated from known β and pK_a values.[75-77] Alternatively, an apparent binding constant (K_{app}, also called K_{eff} for effective binding constant) can be measured directly as

the equilibrium constant under the specified solution conditions of pH and buffer components. An in-depth explanation of the relationship between β, K_{cond}, K_{app} is given in Appendix A. For convenience, binding constants are often inverted and discussed as dissociation constants (K_D).

Table 3. Classification of select metal ions and donor atoms according to Pearson's HSAB Principle

Hard Lewis Acids	Borderline Acids	Soft Acids
H^+, Li^+, Na^+, K^+, Be^{2+}, Mg^{2+}, Ca^{2+}, Sr^{2+}, Sc^{3+}, Ti^{4+}, Zr^{4+}, Cr^{3+}, Al^{3+}, Ga^{3+}, La^{3+}, Gd^{3+}, Co^{3+}, Fe^{3+}	Fe^{2+}, Co^{2+}, Ni^{2+}, Cu^{2+}, Zn^{2+}, Pb^{2+}, Bi^{3+}, Rh^{3+}, Ir^{3+}	Cu^+, Au^+, Ag^+, Tl^+, Hg^+, Pd^{2+}, Cd^{2+}, Pt^{2+}, Hg^{2+}
Hard Lewis Bases	**Borderline Bases**	**Soft Bases**
F^-, OH^-, H_2O, ROH, Cl^-, RO^-, R_2O, $CH_3CO_2^-$, NH_3, RNH_2, NH_2NH_2, CO_3^{2-}, NO_3^-, O_2^-, SO_4^{2-}, PO_4^{3-}, ClO_4^-	NO_2^-, Br^-, N_3^-, N_2, $C_6H_5NH_2$, pyridine, imidazole	RSH, RS^-, R_2S, S_2^-, CN^-, RNC, CO, I^-, R_3As, R_3P, C_6H_5, C_2H_4, H_2S, HS^-, H^-, R^-

1.3.2 Chelate Rings, Steric Strain, and Preorganization

Polydentate ligands that present multiple donor atoms for metal binding provide greater complex stability compared with monodentate analogs due to the chelate effect. This effect can be maximized if the number and size of the chelate rings are optimized for the size of the cation in a way that minimizes steric strain upon metal binding. The chelate rings formed when two donor groups from the same ligand bind a metal center are most favorable for 5- and 6-membered rings. Adjacent 6-membered rings formed from polydentate ligands, however, can induce unfavorable steric strain that is relieved in ligands containing adjacent 5- and 6-membered rings.[69, 70] In general, ligands that minimize steric strain in the complex on coordination of the ligand to the metal ion and/or that preorganize their donor atoms spatially as required for complexation are

preferred for high-affinity binding.[71] Macrocycles that incur minimal strain upon metal complexation can therefore retain their metal ion by tight complexation.

1.3.3 Complex Geometry

A metal ion may prefer certain binding geometries to others based on its number of valence d electrons. This preference is based on Ligand Field Stabilization Energy (LFSE), a full description of which can be found in standard inorganic chemistry text books.[78, 79] Comparing the geometric preferences of iron, copper, and zinc illustrates the point. The common biologically relevant oxidation states of iron are Fe^{2+} and Fe^{3+}, which prefer octahedral and distorted octahedral geometries. Copper, on the other hand, exists primarily as Cu^{+} and Cu^{2+}, with Cu^{2+} favoring square planar, square pyramidal, or axially distorted octahedral geometries due to Jahn-Teller distortions of its d^9 electron configuration. Its reduced Cu^{+} form has a filled d^{10} configuration with no preference for geometry based on LFSE and can therefore be found in a range of coordination geometries including 2-, 3-, and 4-coordinate sites. The geometry of the ligand field can influence the redox state of copper. For example, ligands that impose a tetrahedral arrangement that is unfavorable for Cu^{2+} but reasonable for Cu^{+} will destabilize the Cu^{2+} form, shifting the reduction potential more positive in favor of Cu^{+}. The ligand-induced change in reduction potential can be used to purposefully select a desired oxidation state. Geometric preferences imposed by the ligand are also important for differentiating Cu^{2+} and Zn^{2+}. Because Zn^{2+} is d^{10} and has no geometric preference based on LFSE, tetrahedral zinc complexes are common.

LFSE is also a factor in the trend observed in the Irving-Williams series of relative complex stabilities of first-row divalent metal ions: $Mn^{2+} < Fe^{2+} < Co^{2+} < Ni^{2+} < Cu^{2+} > Zn^{2+}$. In general, complex stability increases as the ionic radius decreases across the series, but Cu^{2+} shows a sharp spike in stability that can be attributed to LFSE

obtained through Jahn-Teller distortion, and Zn^{2+} shows a diminished stability due to a lack of LFSE for its d^{10} configuration. The greater stability of copper(II) complexes compared with zinc(II) complexes revealed by this series indicates an inherent challenge in designing chelating agents that are selective for Zn^{2+} over Cu^{2+}, although sites that impose tetrahedral geometry will prefer Zn^{2+} to Cu^{2+}.

1.4 Chemical Manipulation of Metal Status in Cell Biology

Altering the bioavailability of metal ions by using metal chelating agents is an important strategy for both clinical therapies and for studying cellular processes related to metal ion transport, storage, use and trafficking. When using live cells in probing for biomolecules related to metal homeostasis, a typical approach is to change the availability of one metal, and observe changes in cell processes, especially transcription. Up-regulation or down-regulation of specific genes can indicate the proteins either directly or indirectly related to metal ion handling. The ability to increase or limit the bioavailability of only one target metal is crucial to the integrity of the experiment and interpretation of results. In order to limit the availability of only one metal ion at a time, "selective" metal chelators are often employed, where the selectivity is a measure of its affinity for a particular metal ion over others. Rarely, however, does selectivity imply exclusivity. Many metals are close enough in their HSAB character, their geometric preference and other properties that make it difficult to select for one specific metal in the presence of others. So while an agent may have a thermodynamic preference for a particular metal ion, it does not mean that it binds that metal at the exclusion of all others. Indeed, the complex equilibria that exist in the compartmentalized environment of a cell (even more so in a whole organism) make metal selection a tricky proposition. The following sections highlight some of the most widely used chelating agents for

selectively reducing bioavailable metal ions in cell biology and point out potential pitfalls. The structures are shown in Figure 1.

It is also beneficial to use reagents that selectively increase metal ion concentration. Metal salts are often used as dietary or cell culture media supplement and are a simple way to increase overall concentration of metal ion. In order to increase local concentration of metal ion in a controlled way, inorganic complexes that can release specific metal ions based on reactivity or localization have been developed. This class of reagents has utility in both cell culture and medicine and will be addressed in Chapter 4.

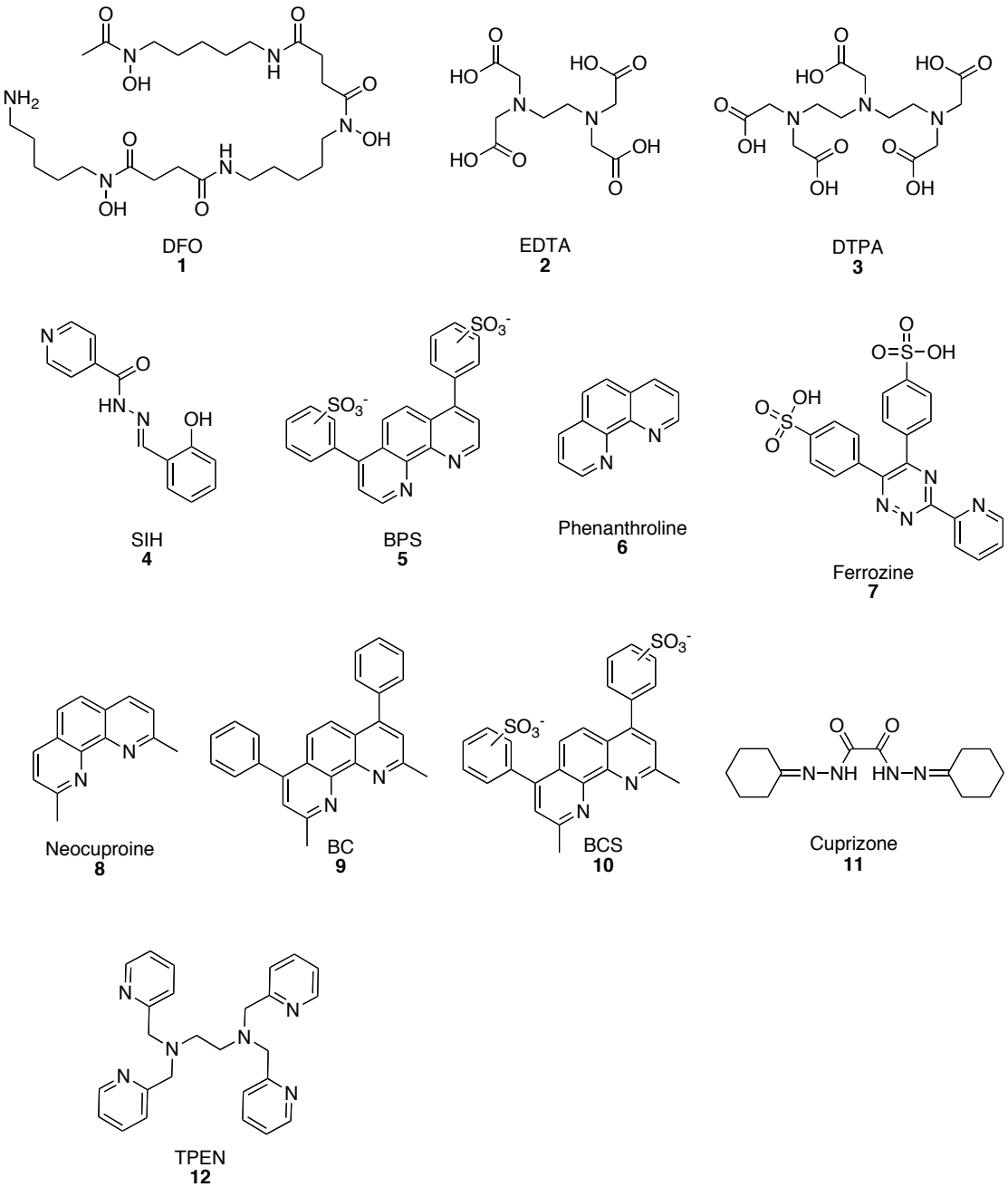

Figure 1. Commonly used chelators in cell biology.

1.4.1 Iron Chelators

The well-known redox activity of iron makes it a useful metal cofactor for biology, but also poses a potential risk because it can participate in redox cycles with oxygen to produce damaging reactive oxygen species (ROS) through the Fenton reaction (Equation 1).[80-82] The catalytic capacity of iron in Fenton reactions requires it to cycle between Fe^{2+} and Fe^{3+}, which means that the reduction potential of the iron center is a key determinant in its ROS-production.[83] Chelating agents that shift the reduction potential to favor either Fe^{3+} or Fe^{2+} without redox cycling can in principle keep iron from producing ROS. Chelating agents for both oxidation states are discussed below.

$$Fe^{2+} + H_2O_2 \rightarrow Fe^{3+} + OH^- + OH^{\bullet} \qquad \textbf{Equation 1}$$

$Iron^{3+}$ is unique to biological transition metal ions in that it has a high charge-to-radius ratio and as a hard acid forms high-affinity complexes with hard oxygen ligands. Ligands can therefore be designed to have a thermodynamic preference for Fe^{3+} over dicationic metal ions like Cu^{2+} and Zn^{2+}. For a comprehensive discussion on designing ligands for iron chelation, see the review by Liu and Hider.[84] The iron siderophore literature is also helpful for understanding selective iron sequestration.[85] It is important to repeat, however, that a high affinity for a particular metal ion does not imply that other metal ions do not also bind with considerable affinity. Most Fe^{3+} chelators also have reasonable affinity for Cu^{2+} and Zn^{2+} that can lead to depletion of these metals, especially with prolonged exposure to the chelating agent.

A common iron(III) chelator used both in the laboratory and the clinic is desferrioxamine (DFO, **1**), a naturally occurring siderophore that binds Fe^{3+} with three hydroxamate groups to give a six-coordinate complex. DFO is one of the first chelators used to treat iron overload disorders and it is still widely used today. DFO is also used in the laboratory for cell studies to control iron bioavailability. It is charged and hydrophilic and does not diffuse easily across the cell membrane. It is believed to enter mammalian cells only by endocytosis, and effects labile iron pools in the cytoplasm and most drastically inside of endosomes. It is slow to chelate intracellular iron at room temperature, but increases efficiency at 37 °C due to increased endocytosis. [86] DFO is a potent and selective chelator for Fe^{3+} that inhibits iron-dependent ROS formation and is itself an antioxidant.[87, 88]

The difficulty of DFO in crossing biological membranes and its subsequent slow rate of intracellular iron chelation has spurred the search for other Fe^{3+} chelating agents. General chelators like EDTA (ethylenediamine tetraacetic acid, **2**) and DTPA (diethylenetriamine pentaacetic acid, **3**) have high affinity for Fe^{3+} but also bind several metal ions and are not considered selective. There is a very large body of literature on the design of iron chelators for medical applications[84, 89, 90] so the focus here is rather to highlight select examples with utility for manipulating iron concentrations in cell culture. In this context, the tridentate chelator salicylaldehyde isonicotinoyl hydrazone (SIH, **4**) has emerged as a useful lipophilic chelator that readily crosses biological membranes.[91-94] It forms a 2:1 ligand:Fe(III) complex that inhibits iron-dependent ROS formation.[95, 96] In addition to protecting cells against iron-induced oxidative stress, another application of SIH has been in the determination of labile iron pools in cells by fluorescent chelators. The general protocol for these measurements has been to use a fluorescently-labeled, cell-permeable chelator that is quenched upon iron binding, then

use SIH to compete iron from the probe to restore fluorescence. The extent of restored fluorescence gives an estimate of the chelator-accessible, or labile, iron pool.[97, 98] SIH is not without its drawbacks, however. While its affinity for Fe^{3+} is high, it also complexes Cu^{2+} and Zn^{2+}.[99] In addition, it has a short half-life in cell culture media and plasma due to hydrolysis of the hydrazone linkage.[100]

Chelators for Fe^{2+} are also used to control iron bioavailability. The oxidation states Fe^{2+} and Fe^{3+} differ in terms of their ligand preferences and the ease for which they can be selectively chelated over other metals based on donor atom identity. Because of its lower charge density and larger size, Fe^{2+} is more similar in HSAB character to other biologically relevant transition metal ions, especially Cu^{2+} and Zn^{2+}. Although it may be difficult to select Fe^{2+} over other borderline metals, Fe^{2+} has a preferred ligand field geometry that is different from Cu^{2+} and Zn^{2+}. Fe^{2+} is a d^6 metal which has a favorable LFSE in a low-spin octahedral complex. Chelators with borderline donor groups that can also adopt an octahedral geometry can potentially select Fe^{2+} over other bio-metals. One chelator that fits these criteria is bathophenanthroline disulfonic acid (BPS, **5**), a sulfonated water-soluble derivative of phenanthroline (**6**) that is frequently used in cell culture as an iron-limiting reagent.[101, 102] BPS forms a tris-chelate iron(II) complex with octahedral geometry and is membrane impermeable due to its charged sulfate groups.[103] Because of its large positive reduction potential, BPS is known to cause non-specific reduction of Fe(III) chelates.[104] Although it has good affinity for Fe^{2+}, it does complex other metals, especially Cu^{2+}, which is not surprising considering variable chelate stoichiometry with BPS and related phenanthroline derivatives.[76] BPS can easily form a bis complex with square planar geometry preferred by Cu^{2+}.

Ferrozine (**7**) is another commonly used chelator for Fe^{2+} in cell culture to create a "defined Fe medium" or "Fe-depleted medium".[105-107] It selects for Fe^{2+} by forming a tris

complex of borderline donor atoms in an octahedral binding geometry with a very large binding constant. Like BPS, ferrozine is known to cause non-specific reduction of Fe(III) chelates.[100] There is evidence that ferrozine forms ternary complexes with Fe and amino acids, especially histidine, which act as potential antioxidants.[108]

In addition to using chelating agents to limit iron bioavailability, irons salts are also used to supplement cell culture media. An understanding of iron coordination chemistry is also helpful to avoid potential problems. Unchelated Fe^{2+} ion is more soluble and more bioavailable than unchelated Fe^{3+}, both because Fe^{2+} is a substrate for divalent metal ion transporters in mammalian cells and because Fe^{3+} rapidly hydrolyzes in water to give insoluble iron hydroxides. Typical cell culture conditions exist in an oxygen-rich environment, so it must be kept in mind that Fe^{2+} salts added to the culture medium or aqueous buffers are likely to oxidize readily to Fe^{3+}, which may not be soluble. In cell culture media, amino acids or other components in the media likely keep iron in solution, but addition of simple iron salts to standard laboratory buffers, especially phosphate buffers, will result in insoluble and bio-unavailable iron.

1.4.2 Copper Chelators

Like iron, the redox chemistry of $Cu^{2+}/^{+}$ makes it essential to biological processes, but also potentially dangerous if it is not handled properly by the cell and becomes available for Fenton-like chemistry to produce ROS. Typically under the oxidizing extracellular environment, copper exists as Cu^{2+}, but in the reducing conditions inside the cell, it likely exists in the reduced Cu^{+} oxidation state. Soft character makes Cu^{+} unique among the biological metal ions, so it has potential to be selected based on ligand donor groups. In addition, Cu^{+} is a d^{10} ion, giving it flexibility in geometric arrangements. This means Cu^{+} can adopt tetrahedral, trigonal, or even linear geometries that are disfavored by other metals. Zn^{2+} is also a d^{10} ion, but is harder

in character than Cu^{+}, so can be minimized as an interfering species based on ligand donor choice. Zn^{2+} is also a smaller metal ion, so chelate ring size can be a determining factor.

2,9 Dimethyl-substituted phenanthroline ligands are well known to select for Cu^{+}. Neocuproine (**8**), bathocuproine (BC, **9**), and bathocuproine disulfonate (BCS, **10**) are the three commonly used 2,9 dimethyl-substituted phenanthroline chelates used in cell culture.[109-115] Unlike phenanthroline, these ligands disfavor octahedral tris-chelate or square-planar bis-chelate coordination modes because of steric interference of the methyl substituents. Instead, when binding to a metal in a bis complex, the metal is forced into a tetrahedral binding geometry with the two chelate ligands nearly perpendicular to each other. This tetrahedral geometry combined with the large bite size of the five-membered chelate ring effectively binds Cu^{+} over other metals. However, these ligands do have significant interaction with Cu^{2+} and are known to bind to Cu^{2+}, forcing it into a tetrahedral geometry and inducing its reduction to Cu^{+}. BC-bound Cu(II) is a stronger oxidizing agent by 0.5 V compared to uncomplexed Cu^{2+}, which highlights the fact that these "Cu(I)-selective" chelators are not innocent chelators of Cu^{+}.[116-118] Although they may be able to promote reduction of Cu^{2+} to Cu^{+}, once the reduced state is reached, it is stabilized and does not participate in redox cycling.[119] In fact BCS has been shown to inhibit Cu-dependent redox cycles.[115]

Bathocuproine (**9**) is not very water-soluble, so a sulfonated version (BCS) was developed to give a more soluble derivative.[103] Because BCS is charged and not membrane permeable, it is commonly used in cell studies as an extracellular Cu-limiting agent. Because Cu^{2+} is the dominant extracellular form of copper, it should be considered that BCS is a potential promoter of Cu^{2+} reduction. Neocuproine (8) is more

hydrophobic, and is used for intracellular and extracellular copper chelation since it can diffuse over the cell membrane.

Cuprizone (oxalic acid bis(cyclohexylidene)hydrazide, **11**) is another chelator used to selectively bind Cu^{2+} in cell studies,[109, 112] however, the actual nature of its copper complex has long been under debate. There is strong evidence that cuprizone stabilizes a Cu^{3+} oxidation state in a square planar d^8 complex.[120-122] The cytotoxic and neurotoxic effects of cuprizone may be related to Cu^{2+}-Cu^{3+} redox cycling induced by this chelator under biological conditions.[120, 123]

1.4.3 Zinc Chelators

The only relevant oxidation state for zinc is Zn^{2+}. It has borderline HSAB character, and it is d^{10} with no real preference for ligand field geometry. Zn^{2+} is very close to Cu^{2+} in size and charge density, and can be difficult to select for over Cu^{2+}. TPEN (N,N,N',N'- tetrakis-(2-pyridylmethyl)-ethylenediamine, **12**) is the most common zinc chelator used in the literature,[114, 124-130] however there is an apparent misconception that TPEN is Zn^{2+}-specific. In fact, the affinity of TPEN for Fe^{2+} (log K_a 14.6) is relatively significant, while its affinity for Cu^{2+} (log K_a 20.6) is higher than that for Zn^{2+} (log K_a 18.0).[131, 132] There are several studies that show TPEN affects cellular concentrations of zinc and copper, and that replenishing either metal into TPEN-treated cells will rescue the cells from TPEN-induced apoptosis.[129] Another study shows that levels of iron are affected in addition to copper and zinc when TPEN is added to cell culture.[133] Part of the reason that TPEN can have such significant affinity for Zn^{2+}, Cu^{2+} and Fe^{2+} is its potential variability in chelate binding geometry. TPEN has six possible donor groups, and for Zn^{2+} and Fe^{2+} all six are used to chelate the ion in an octahedral geometry. Cu^{2+}, which is destabilized by octahedral geometry, is chelated by only 5 of the 6 possible donor groups and forms a distorted square pyramid with high stability. It is necessary to

consider the Cu, Fe, and Zn binding properties of TPEN before interpreting the results of an experiment where TPEN is used as a "selective" chelator.

1.5 Human Cellular Copper Transport and Homeostasis

Copper is an important metal cofactor required for several cellular metabolic processes, including oxidative phosphorylation (ATP synthesis), antioxidant activity, connective tissue formation, pigmentation, iron metabolism, and neurotransmitter synthesis. In humans, enzymes and proteins which require copper include copper-zinc superoxide dismutase, cytochrome C oxidase, lysyl oxidase, ceruloplasmin, dopamine β-hydroxylase, tyrosinase, peptidylglycine monooxygenase, clotting factors V and VIII, angiogenin, hephaestin, and perhaps others (Figure 2).[134] Copper is useful in these enzymes because it can take part in biological electron transfer reactions due to its two biologically-accessible oxidation states, Cu^{+} and Cu^{2+}. Controlled redox cycling between these two oxidation states imparts function to the enzymes that require copper as a cofactor, however uncontrolled redox cycling due to systemic overload of copper or local dysfunction in the proteins that handle copper is known to cause debilitating human diseases. Aberrant copper is also toxic because it binds promiscuously to proteins and can occupy binding sites meant for other metals. Displacement of native metal causes dysfunction in proteins that would not normally include copper as a cofactor.[135, 136] These aspects define a paradoxical state of copper where it is both essential to biological processes, and also potentially toxic.

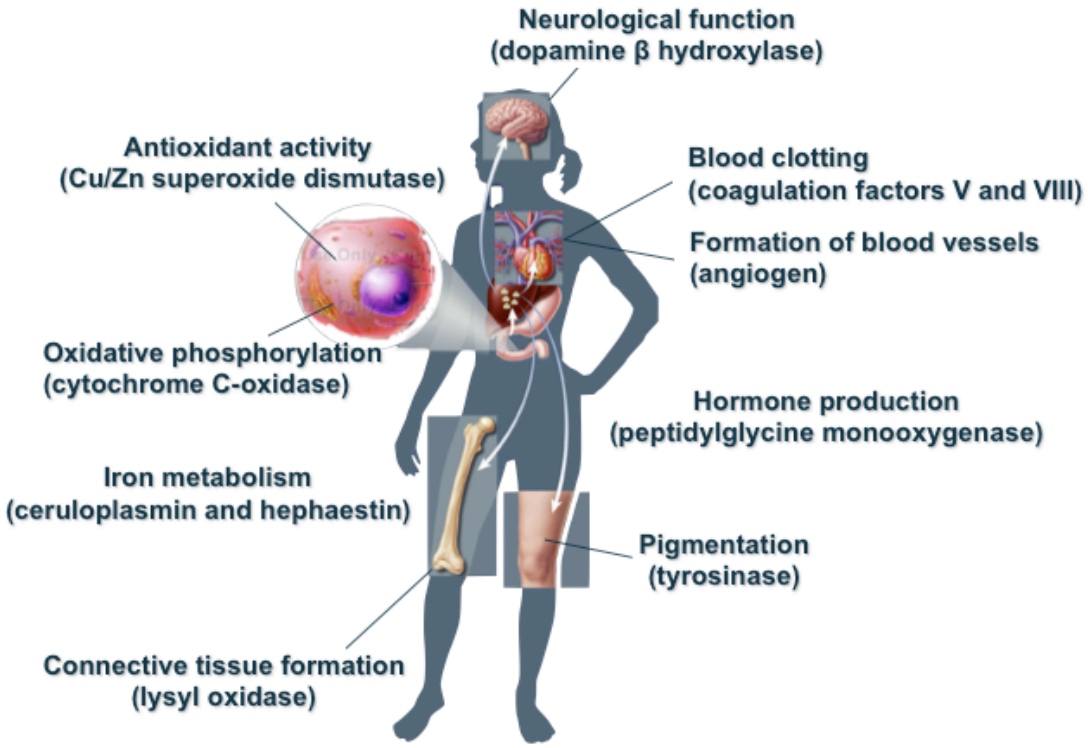

Figure 2. Copper in human health. Copper is an essential cofactor in several enzymes that are important to cellular and systemic metabolism. Parts of this image were taken from www.cda.org.uk.

Menkes and Wilson's diseases are two examples of degenerative conditions that stem from point mutations in the copper trafficking proteins responsible for excretion of copper from the cell via the trans golgi network. Menkes disease is caused by mutation of the copper transporting ATPase 7A (MNKP) protein and results in reduced transport of dietary copper across the basolateral membrane of enterocytes to hepatic portal circulation and additional blockage in copper transport across the blood-brain barrier. The result of this dysfunctional transporter results in systemic copper deficiency, especially in the central nervous system. Patients affected with Menkes disease demonstrate neurological impairment, convulsions, skeletal abnormalities, tortuosity of

cerebral blood vessels, skin laxity, hypopigmentation, and usually do not survive to see their second birthday.[137, 138]

Mutation in a related protein, the copper transporting ATPase 7B (WNDP), causes Wilson's disease. In this case, progressive intracellular accumulation of copper in some tissues, especially liver, leads to acute or chronic hepatitis, cirrosis, and hepatic failure. Accumulation of toxic copper in the brain can also lead to neurological and psychiatric abnormalities including Parkinsonian like symptoms, tremors, dystonia, abnormal behavior, personality changes and depression.[137-139]

Amyotrophic lateral sclerosis (ALS), or Lou Gehrig's disease, is another devastating disease linked to mutation in a copper handling protein. Approximately 15-20% of patients with autosomal dominant familial ALS demonstrate point mutations in copper-zinc superoxide dismutase (SOD), the cytosolic enzyme responsible for conversion of toxic superoxide to oxygen and hydrogen peroxide (antioxidant activity). These point mutations are thought to cause SOD to acquire toxic properties via dysregulation of the copper cofactor, ultimately leading to increased oxidative stress. ALS is characterized by progressive muscle atrophy due to degeneration of large motor neurons and spasticity and hyperreflexia due to lesions of the upper motor neurons. Patients with ALS usually die from complications due to intercurrent illnesses.[137, 138, 140]

The essential yet toxic nature of copper requires that it is tightly regulated in biology both intra- and extracellularly. Over the past few decades, intense investigation on the proteins that govern copper homeostasis has lead to a critical progress in our understanding of the mechanisms involved in copper uptake, transport, and efflux from the eukaryotic cell.[134, 141-144] The proteins involved in copper homeostasis are incredibly conserved in their structure, function and mechanisms across all species investigated, including plants, microbes, and mammals. It is clear from these studies that Nature has

evolved to handle copper in a very carefully controlled manner.[145-148] Figure 3 shows a current model of copper homeostasis in eukaryotes based on a recent review on copper homeostasis.[141]

Copper is acquired from the extracellular environment via plasma membrane copper transport proteins. Studies in yeast first led to identification of the copper transport proteins yCtr1 and yCtr3, founding members of a family of copper transport proteins (Ctr), which are widely conserved in yeast, fungi, plants, and mammals.[149-151] Genetic studies in yeast, human, mouse, and drosophila confirm that Ctr is in fact required for copper acquisition and internalization. Yeast have two copper transporters responsible for extracellular copper acquisition, yCtr1 and yCtr3, and one vacuolar copper transporter, yCtr2, responsible for mobilization of intracellular copper stores.[152, 153] Although the human genome contains two putative copper transporters, only hCtr1 has been demonstrated to be involved in cellular copper acquisition.

Ctr1 proteins localize to the plasma membrane, and contain three transmembrane domains, an extracellular N-terminal domain and an intracellular C-terminal. A three-dimensional (3-D) crystal structure of hCtr1 has recently confirmed that the copper transporter forms a homotrimer to create a cone shaped pore in the plasma membrane.[154, 155] The 3-D image shows that the pore opening is bordered by the second transmembrane domain (TMD2) of each monomer. It has been known for some time that Ctr1 TMD2 contains an essential MXXXM domain. Mutagenesis of either methionine in TMD2 renders the protein inactive for copper transport.[156, 157] From the 3-D crystal structure, it is apparent that the MXXXM domain of TMD2 contributes to binding a total of two copper ions inside the Ctr1 pore.

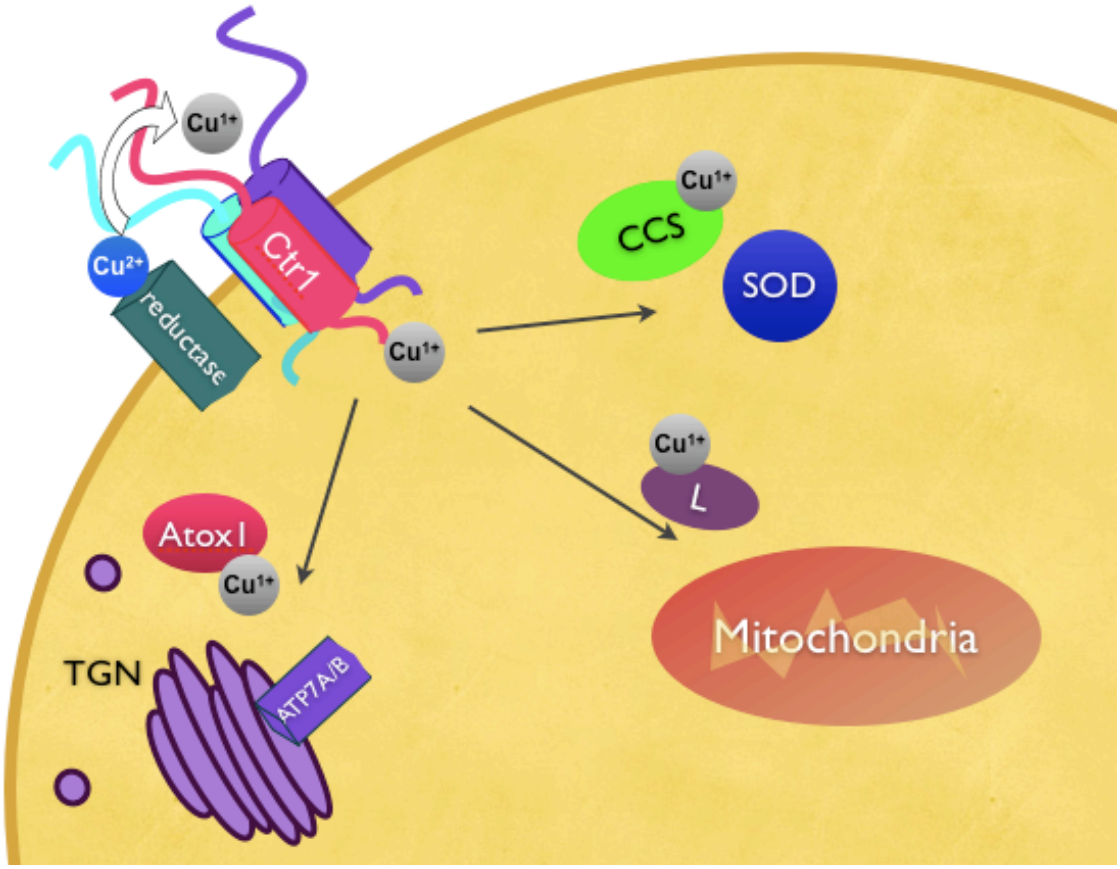

Figure 3. Mammalian cellular copper homeostasis.[141] Mammalian cells acquire copper from the extracellular environment via the plasma membrane copper transporter, Ctr1. Copper^{2+} in the extracellular environment must be reduced because Ctr1 selectively transports Cu^{+}. The mechanism of reduction and copper acquisition by mammalian Ctr1 is currently unknown. It is proposed that, like in yeast, a mammalian cell surface copper reductase is responsible for the one electron reduction of copper. However such a mammalian reductase has not yet been identified. Copper^{+} that enters the cell through Ctr1 is eventually passed to the intracellular copper chaperones CCS, Atox1, and the unidentified cytoplasmic mitochondrial chaperone. CCS is the chaperone for the cytoplasmic enzyme, Cu/Zn superoxide dismutase (SOD), which is responsible for antioxidant activity. Mutations in SOD are linked to some familial forms of the disease, ALS. AtoxI delivers Cu^{+} to the copper transporting ATPases, ATP7a and ATP7B (Menkes and Wilson's disease proteins), for transport into vesicles for excretion. This image is based on a recent review of eukaryotic copper metabolism.[141]

Unfortunately, the 3-D images reveal little about the structure of the N and C-terminal domains, indicating that the extracellular and intracellular domains may have variable structure.

It is well established that Ctr proteins in all species selectively transport Cu^{+} and therefore Ctr-dependent copper uptake requires a cell surface reductase. In yeast, Cu^{2+} is reduced at the plasma membrane by the iron and copper reductases Fre1 and Fre2.[158, 159] Although there have been implications to some proteins that may serve this role in mammals,[160] conclusive evidence for the identity of a mammalian cell surface copper reductase is lacking. Some mechanism for reducing extracellular Cu^{2+} must exist in mammals, although the identity of the enzyme or other reductant is currently unknown.

Once it is carried across the membrane, Cu^{+} must be shuttled to the correct protein targets within the cell to be incorporated as a cofactor. Nature has developed a tightly regulated network of intracellular proteins that function exclusively to assure that Cu^{+} gets to its appropriate targets safely and without compromise.[146, 147] The need for these copper chaperone proteins likely stems from the low concentration of total copper and the extremely low concentration of "free" or aquated (< 1 atom/cell) copper in the cell.[146, 147] Copper chaperone proteins have been found to interact directly with their target proteins in order to incorporate copper safely into its enzyme binding sites. It has been found that controlled copper transfer between copper chaperones and their targets is accomplished by direct interaction.[161, 162] Although the mechanism by which copper is transferred from Ctr1 to the copper chaperones is unknown, it is probably not an exception to this rule. Copper acquired through Ctr1 is shuttled to three major targets; cytochrome-C-oxidase in the mitochondria, copper-zinc superoxide dismutase (SOD) in the cytoplasm, and the trans gogli network (TGN) for excretion.

Copper is transported to the trans gogli network's Cu^{+}-transporting ATPases, ATP7a and ATP7b via the copper chaperone AtoxI . AtoxI binds Cu^{+} by specific interactions through a CXXC metal binding domain (MBD). This same CXXC metal binding sequence is conserved in the six MBD found at the cytoplasmic domain of ATP7a and ATP7b. These ATPases are energy dependent copper pumps that transport copper into vesicles for excretion.

The cytoplasmic copper chaperone to the mitochondria is a yet uncharacterized ligand, but several proteins have been identified that are responsible for copper shuttling and transfer to cytochrome C oxidase inside the mitochondrial space. These chaperones inside the mitochondria include Cox17, Cox11, and structurally similar proteins Sco1 and Sco2.[141]

Copper that is destined for the antioxidant protein, SOD, is shuttled by the chaperone known as CCS, which consists of three important domains that are individually responsible for the roles of copper binding, SOD recognition, and cargo transfer.[163] At the N-terminal of CCS, Domain 1 is responsible for copper binding and contains a CXXC motif and resembles the AtoxI metallochaperone MBD. Domain 2 of CCS is responsible for recognition of the SOD target. It is almost identical to SOD but lacks one residue that renders SOD catalytically active. At the C-terminal of CCS, Domain 3 is a short amino acid sequence that is essential for copper transfer to SOD. The mechanism for transfer from CCS to SOD has been elucidated and involves a direct interaction between the chaperone and its target.[161, 162]

2. Spectroscopic Studies of Copper Binding to N-Terminal hCtr1 Model Peptides

2.1 Background and Significance

Mechanisms of intracellular copper regulation are beginning to be well understood, however, understanding of the chemical mechanisms of cellular copper acquisition from the extracellular environment is lacking.[141, 142, 145, 164, 165] Human Ctr1 is a 190 amino acid protein with three transmembrane domains, an intracellular C-terminal domain containing conserved histidine and cysteine residues that have been shown to bind Cu^{+}, and an extracellular N-terminal domain implicated in copper acquisition that contains unique methionine sequences MXXM and MXM, called "Mets motifs" that are also shown to bind Cu^{+} (Figure 4).[156, 157, 166, 167] The protein forms a homotrimer in the plasma membrane to create a cone-shaped pore that is capable of transporting monovalent copper through the cell membrane.[154, 155, 168, 169] Metal ion transport is passive and it is well established that the Ctr1 specifically transports Cu^{+}, partly based on evidence that yCtr1 transport is dependent on Cu/Fe metalloreductases Fre1 and Fre2 in yeast.[158, 159] Two conserved methionine residues in the second transmembrane domain are essential for Ctr1-dependent copper transport and another Mets motif in the N-terminal domain near the extracellular pore is important for high-affinity copper acquisition.[156]

Little is known about the mechanism by which the human copper transporter, hCtr1, acquires copper from the extracellular environment and passes the metal ion to cytoplasmic copper chaperone proteins,[134] and much of what is known about mammalian Ctr1 has derived from yeast model studies. Both human and yeast Ctr1 proteins have an extracellular domain rich in MXM and MXXM Mets motifs that are

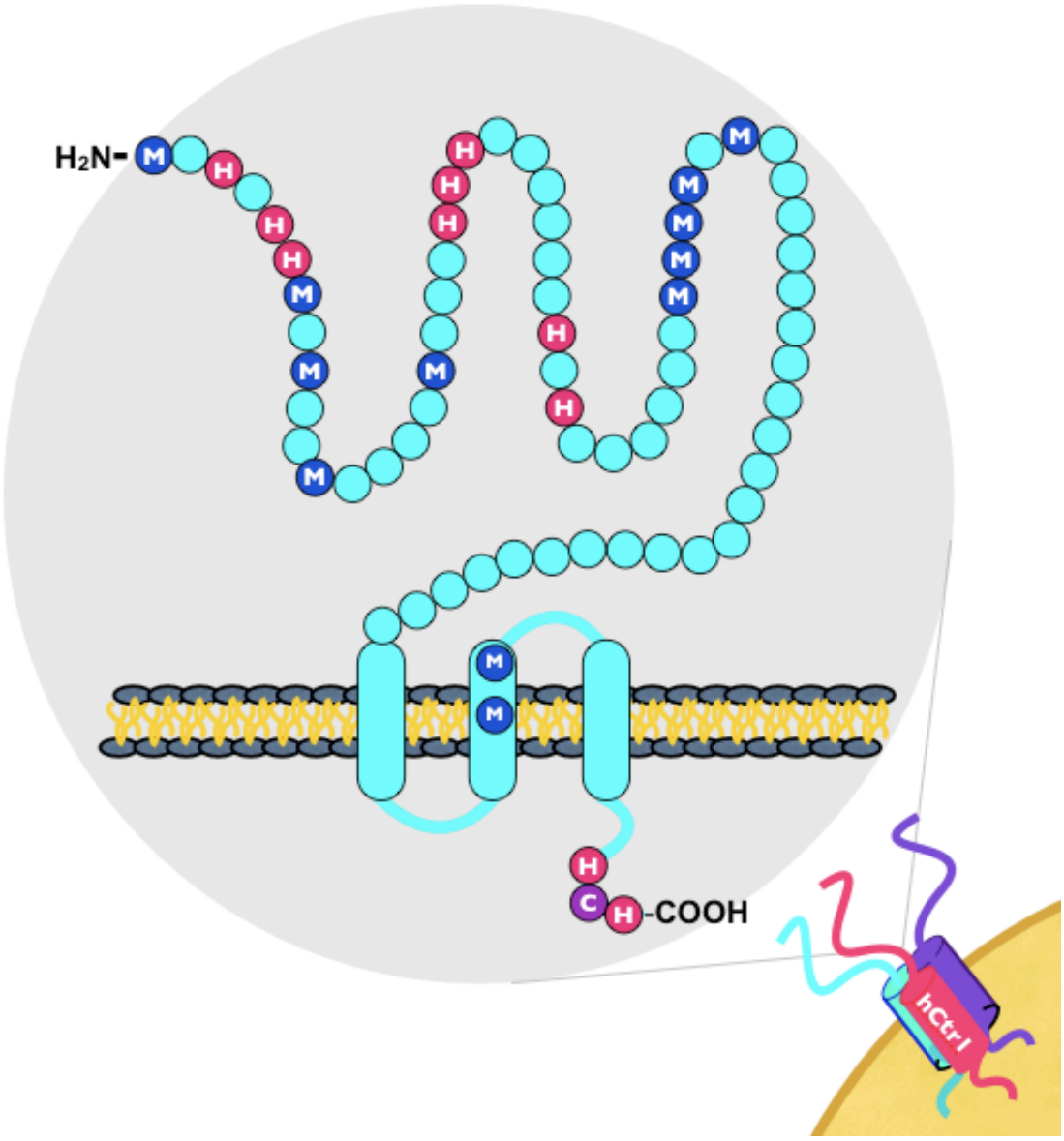

Figure 4. Cartoon of hCtr1. Human Ctr1 forms a homotrimer in the plasma membrane with an N-terminal extracellular domain equipped with His (H) and Met (M) potential metal-binding residues. All extracellular His and Met residues are labeled. Mutagenesis studies in yeast and mammalian cells have shown functional significance only for two methionines in the N-terminal that are closest in sequence to the first transmembrane domain. According to the same studies, all other N-terminal residues seem to be insignificant in hCtr1-dependent copper acquisition and transport. The functionally significant TMD2 methionines and C-terminal cysteine and histidine residues are also labeled.

capable of binding Cu^{+} with μM affinity and are presumed to be responsible for recruiting Cu^{+} to the Ctr pore.[170] In the yeast cell model, Cu^{2+} is first reduced by Fre1/2 at which point Ctr Mets motifs may pick up the Cu^{+} and transport it through the cell membrane. Unlike the N-terminal domain in yeast, hCtr1 has extracellular His-rich clusters that are conserved throughout several mammalian species. Although early studies in yeast cell models and HEK293 cells found no role for the histidines (His) in hCtr1, there are reasons to suspect that extracellular His-rich regions in this protein may be important for copper acquisition in human and other mammals.

Histidine is a well-known copper-binding amino acid and has an established role in biology as a copper-binding ligand.[171] Aside from general His residues, hCtr1 contains a H_2N-XXH amino terminal copper/nickel (ATCUN) high affinity Cu^{2+} binding (log K=12.0, picomolar K_D) sequence. This ATCUN site is similar to the ones found in several biologically important Cu^{2+}-binding proteins, including human serum albumin (HSA),[172] hepcidin,[173] histatin-5 and -3,[174, 175] human sperm protamine P2a,[175] neuromedin-C,[176] and endostatin.[177] The ATCUN domain has high affinity for Cu^{2+} that is a result of ultimate formation of a thermodynamically stable, four coordinate Cu(II) chelate with nearly square planar geometry. The histidine in the third position from the free amine acts as an anchor to recruit copper (Figure 5). The binding event is associated with consequent lowering of the adjacent amide proton in the direction of the N-terminal from above pK_a 12 to below 5. This subsequently lowers the next adjacent amide proton to below or close to 5 due to thermodynamic stability gained by the free N-terminal amine wrapping around to form a square planar chelate.

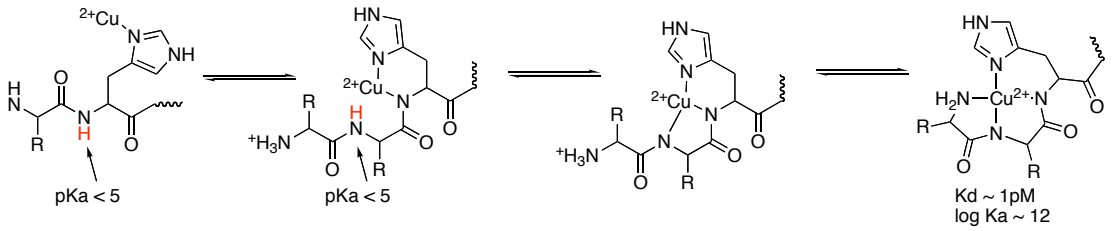

Figure 5. ATCUN binding site forms a neutral, stable square planar Cu(II) complex.

One amino acid removed from the N-terminal ATCUN site is a bis-His (HH) sequence. This HH site is interesting because of its potential to form a stable Cu(I) complex. Recent work by Karlin & Shearer on model peptides with similar HH sequences in vitro show that bishistidine can stabilize Cu(I) in a linear two coordinate environment so that the Cu(I) complex is stable to oxidation even when O_2 is bubbled through solution.[178-182] Addition of a third imidazole group to the bishistidine Cu(I) complex results in a tridentate coordination environment that displays reversible redox behavior (Figure 6).[179, 181, 182] The HH motif in hCtr1 is surrounded by other His residues that could serve as a third donor and impart interesting redox properties on this protein. In addition, the HH motif is bordered by a Mets motif of the form MXMXXM. Mets motifs of this type have been shown to bind Cu^{+} in yeast Ctr1 model peptides with μM affinity and mutagenesis has confirmed the importance of methionine in Ctr-dependent copper transport.[156, 170] Farther down the sequence toward the extracellular pore of hCtr1, there are two other His clusters and one other Mets motif. Despite early results from biochemical characterization of this protein that show significant functional roles only for extracellular Mets motifs, the existence of the albumin-like ATCUN site and other His residues suggests that hCtr1 should also be capable of interacting with copper via His.

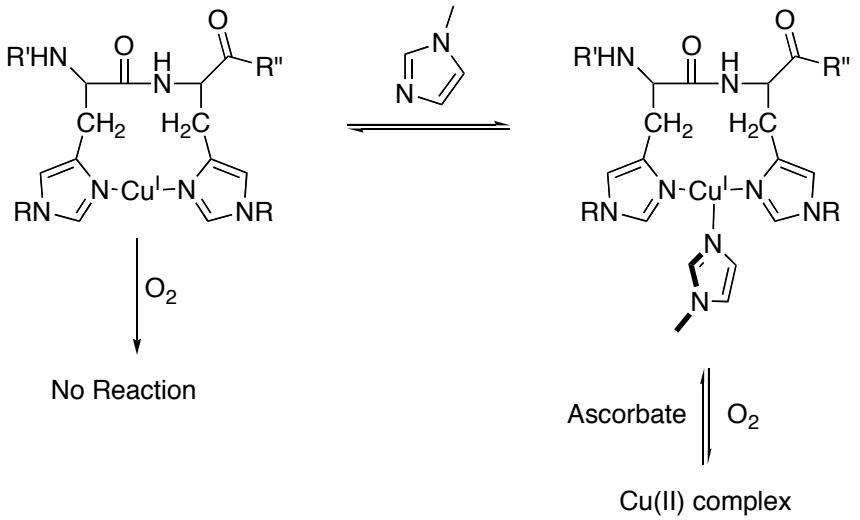

Figure 6. Bis-histidine copper complexes display interesting redox properties.[178-182] Regioselectively protected bishistidine (HH) peptides were used to first demonstrate the interesting properties of HH copper complexes. HH can bind to Cu(I) in a two coordinate linear environment. This two coordinate Cu(I) complex was shown to be stable to oxidation, even when O_2 is bubbled through solution. Upon addition of a third imidazole N-donor, the complex becomes a three-coordinate Cu(I), which is readily oxidized. This has been extended to short peptides containing an HH domain. The resultant Cu(II) complex can be easily reduced by the reducing agent, ascorbic acid. This type of 3-coordinate Cu(I) complex shows reversible redox behavior. R=peptide or Fmoc. R'=peptide or OMe. R"= peptide, $OCPh_3$ or OH. This image was designed based on independent but related work by Karlin and Shearer.[178-182]

It is interesting that Ctr1 in several mammalian species contain His in their extracellular domain, whereas yeast do not have these domains. A possible explanation for this phenomenon can be rationalized based on the extracellular environments of mammalian and yeast cells. In humans and other mammals, most cells are in an environment where extracellular pH is ~7.4. At this pH Cu^{2+} is not soluble in its aquated form and is likely to be present only in stable complexes with proteins (i.e. HSA) or amino acids (i.e. His). In contrast, yeast acidify their extracellular environment to a pH close to 4. At this low pH, Cu^{2+} can be soluble in its aquated form, but its binding to His would be very weak due to competition with H^+. In general His binding to metal is pH

dependent, and at pH close to 4, it is unlikely to interact significantly with copper. His would be ineffective as an extracellular copper binding residue in yeast Ctr, but would be quite useful to mammalian cells for extracellular copper acquisition.

Mammalian Ctr's containing these His domains may in fact acquire copper by a different mechanism than yeast Ctr's that contain only Mets Cu^{+}-binding motifs. In this study, we focused mainly on the first 14 amino acids of hCtr1 because of the wealth of interesting potential copper binding sites in this region. This region contains one of the well-characterized Mets motifs that have been shown to bind Cu^{+} in yeast Ctr1 models,[170] an interesting HH site, and a likely Cu^{2+}-binding ATCUN site. We set out to characterize the Cu^{+} and Cu^{2+} binding properties of model peptides based on the first 14 amino acids of hCtr1. In addition, we used a peptide containing the second hCtr1 N-terminal Mets motif, MMMMXM. This sequence contains the conserved N-terminal MXM domain that is functionally significant for Ctr1-dependent Cu acquisition according to mutagenesis studies in both yeast and human.[156, 157] This additional peptide domain will serve as a good reference to compare copper binding with other hCtr1 N-terminal domains.

2.2 Results

2.2.1 Characterization of Cu^{+} Binding of N-terminal hCtr1 Mets Motifs

Short model peptides based on sequences found in hCtr1 were synthesized by standard Fmoc solid-phase peptide synthesis protocol using a Protein Technologies PS3 automated peptide synthesizer on PAL-PEG-PS resin. Three peptides were used in the characterization of Cu^{+} binding to hCtr1 Mets motifs, and the sequence of each peptide is listed in Table 4. Peptides hCtr7-14 and 38-45 each contain one of the two different Mets motifs found in N-terminal hCtr1. A non-native lysine has been added to the C-terminal end of sequences hCtr7-14 and hCtr38-45 to improve solubility in water. These

two peptides are also acetyl capped (Ac) on their N-termini, while the hCtr1-14 peptide is left uncapped, as in the native protein. Peptide hCtr1-14 contains the same Mets motif found in hCtr7-14, but includes an histidine-rich cluster and an additional Met residue.

Table 4: hCtr1 native sequence model peptides containing Mets motifs.

Peptide	Sequence
hCtr1-14	H_2N M D H S H H M G M S Y M D S
hCtr7-14	Ac M G M S Y M D S K
hCtr38-45	Ac S M M M M P M T K

Effective dissociation constants were calculated by two separate indirect methods using Electrospray Ionization Mass Spectrometry (ESI-MS) quantitative analysis of peptide and using UV-Vis kinetic studies of the copper catalyzed oxidation of ascorbic acid.

2.2.1.1 Characterization of Cu^+ and Cu^{2+} Binding by ESI-MS

Peptide binding to the monovalent and divalent oxidation states of copper was determined by ESI-MS. Peptide binding to $Cu^{2+}$was assessed by adding one equivalent of $CuSO_4$ to 20 μM solutions of each peptide in Table 4. These solutions were directly injected into the ESI-MS. To create a reducing environment so that Cu^+ binding could be observed, $CuSO_4$ in conjunction with the reducing agent ascorbic acid were used. A large excess of reducing agent (5 mM) was used to assure full reduction of Cu^{2+}. This excess ascorbate ensures reduction of copper but also lowers the pH to approximately 4. Due to this low pH and the pH-dependent binding of Cu to histidine, the experimental conditions here allowed assessment of Cu^+ binding to methionine only, as histidine binding would be negligible at low pH in the presence of excess ascorbic acid.

Solutions of peptide were analyzed in the absence and presence of excess ascorbate and varied concentration of $CuSO_4$ from 0-10 equivalents. Figure 7 shows the mass spectra of 20 μM peptide (Figure 7a, d), 20μM peptide plus 20μM $CuSO_4$ (Figure 7b,

e), 20μM peptide plus 20μM $CuSO_4$ in 5mM ascorbate solution (Figure 7c, f), for hCtr1-14 (Figure 7a-c), and hCtr7-14 (Figure 7d-f). The spectra for hCtr38-45 are not shown, but are similar to the spectra of hCtr7-14.

The spectrum of 20 μM hCtr1-14 shows two peaks at m/z = 1663.9 and m/z = 832.4, which correspond to $[HP]^+$ and $[H_2P]^{+2}/2$, where P stands for the peptide mass ion and H is an associated proton (Figure 7a). These values agree well with calculated values of m/z = 1664.6 for a singly-charged peptide plus one proton, and m/z = 832.8 for half the mass of the doubly-charged peptide with two protons. In the presence of 20 μM $CuSO_4$, two additional peaks appear at m/z = 1726.7 and m/z = 863.7 (Figure 7b). These two new peaks correspond to Cu^{2+}-bound peptide $[PCu(II)]^+$ and $[PCu(II)]^{+2}/2$ and agree well with calculated values of m/z = 1726.1 and m/z = 863.6, respectively. Peaks for peptide and Cu(I)-bound peptide bound are seen with the addition of 20 μM $CuSO_4$ in the presence of 5 mM ascorbate (Figure 7c). In this case, the peaks corresponding to copper-bound peptide appear at m/z = 1727.7 and m/z = 864.7, corresponding to $[PCu(I)]^+$ and $[HPCu(I)]^{+2}/2$, and agreeing well with calculated values of peptide plus copper, m/z = 1727.1, and half the mass of peptide bound copper plus one proton, m/z = 864.08. Other peaks from noise are also apparent in this spectrum because the intensity of all hCtr1-14 peaks dramatically decreases in the presence of ascorbate.

In the case of the Mets-only peptides, hCtr7-14 and hCtr38-45, formation of a Cu(II) complex was not observed. The spectrum of hCtr7-14 shows a mass ion at m/z = 1089.9, which agrees well with the calculated m/z = 1090.4 for $[HP]^+$. The doubly charged mass ion is not seen. As expected, no peak for Cu(II)-bound peptide is seen

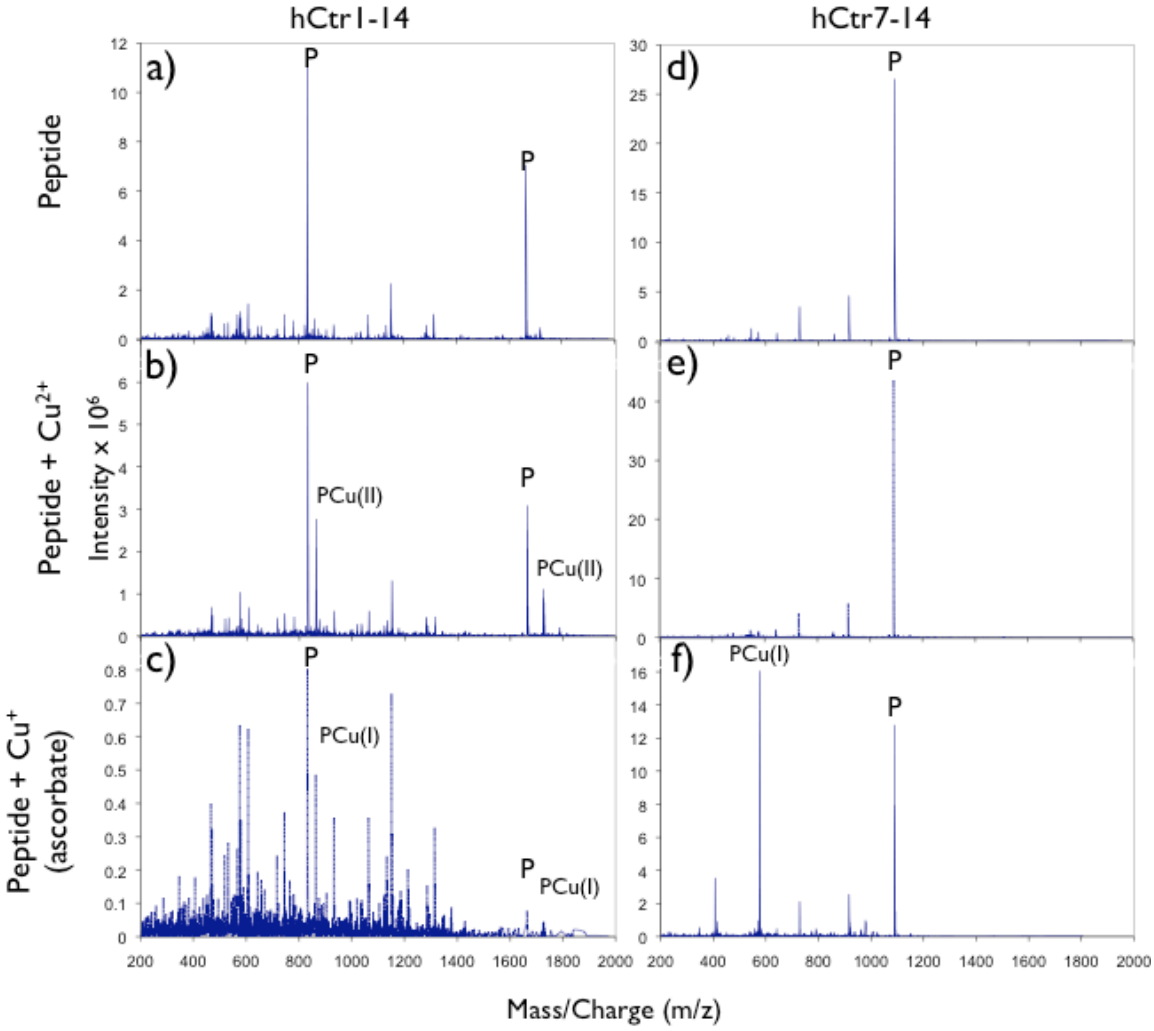

Figure 7. Mets-peptides bind Cu^{+} but require His residues to bind Cu^{2+} by MS. a) ESI-MS of 20 μM solution of hCtr1-14 peptide. hCtr1-14 contains a His cluster and a Mets motif. The P^{+} (peptide mass ion) and $P^{+2}/2$ peak appear at 1663.9 and 832.4 *m/z*, respectively. b) Solution of 20 μM hCtr1-14 and 20 μM $CuCl_2$. Peaks for peptide remain and two peaks for $[HPCu(II)]^{+}$ and $[PCu(II)]^{2+}$ appear at 1726.7 and 863.7 m/z, respectively. c) 20 μM hCtr1-14 plus 20 μM $CuCl_2$ and 5 mM ascorbate. In the presence of 5 mM ascorbate, Cu^{2+} should be reduced to Cu^{+}. Peaks corresponding to peptide are visible and new peaks for $[PCu(I)]^{+}$ and $[HPCu(I)]^{2+}$ appear at 1727.7 and 864.7 m/z, but barely distinguishable above background noise. This dramatic drop in signal intensity is likely due to protonation of His at low pH. d) 20 μM hCtr7-14 peptide, containing only a Mets motif. A peak for the peptide M^{+} appears at 1089.9 m/z. e) 20 μM hCtr7-14 plus 20 μM $CuCl_2$. This Mets-only peptide does not show Cu^{2+} binding in the MS, indicating that Mets motif alone does not bind to divalent Cu. e) 20 μM hCtr7-14 plus 20 μM $CuCl_2$ and 5 mM ascorbate. A new peak for $[HPCu(I)]^{2+}/2$ appears at 576.3 m/z.

with the addition of 1 equivalent of $CuSO_4$. Upon the addition of $CuSO_4$ under reducing conditions a new peak appears at m/z = 576.3, corresponding to copper complex $[HPCu(I)]^{+2}/2$, and agrees well with the calculated value of m/z = 576.5. Although no peak around m/z = 1152.98 is seen for the singly charged $[PCu]^{+}$, the doubly charged mass ion is sufficient to indicate hCtr7-14Cu(I) complex formation.

The spectrum of hCtr38-45 gives a mass ion of m/z = 1127.9, close to the calculated m/z = 1128.5 for $[HP]^{+}$. Similarly to hCtr7-14, no doubly charged mass ion is seen in the peptide spectrum, and the addition of 20 μM $CuSO_4$ does not give a mass ion corresponding to m/z for the hCtr38-45Cu(II) complex. As expected, the addition of $CuSO_4$ in the presence of reducing agent, ascorbate, gives a peak at m/z = 595.3, close to the calculated value of m/z = 596.0. This doubly charged mass ion indicates Cu(I) complex formation. As in the case of hCtr7-14, no peak for $[PCu]^{+}$ is seen at m/z = 1191.0. A summary of the results from ESI-MS experiments is shown in Figure 8.

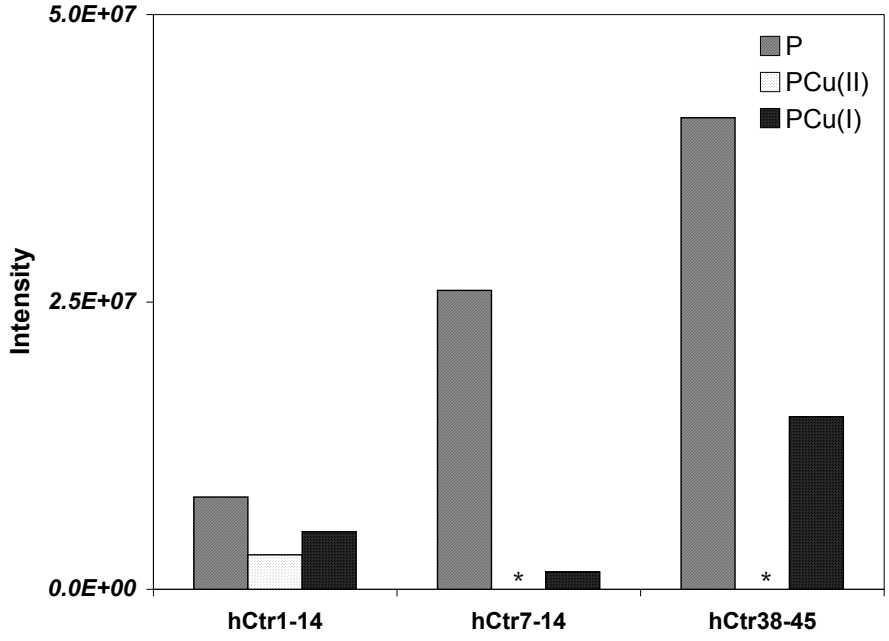

Figure 8. Copper binding to hCtr1 model peptides by ESI-MS. * Little or no affinity for Cu^{2+} predicted by absence of P-Cu(II) mass ion in ESI-MS analysis of solutions of 1:1 P:Cu.

These experiments show that hCtr7-14 and hCtr38-45 Mets motif peptides readily bind Cu^{+}, but have low, if any, affinity for Cu^{2+}. hCtr1-14 binds Cu^{+} via a Mets motif, and is unique in that it is also capable of binding Cu^{2+} due to the His residues that are not available in the other two model peptides.

hCtr114 shows low intensity compared to the other two peptides. This is likely an effect of His in hCtr114 being easily ionized and reducing the intensity of P^{+} signal (compared to P with multiple charges).

2.2.1.2 Calculation of Cu^{+} Binding Constants by Quantitative ESI-MS.

To determine the relationship between peptide concentration and peptide mass ion (P^{+}) intensity by ESI-MS, peptide solutions of varying concentration from 0-25 μM in the presence or absence of excess ascorbate were analyzed by MS and used to form a calibration curve showing peak intensity as a function of peptide concentration in solution. Peptides hCtr7-14 and 38-45 were analyzed for Cu^{+} binding in the presence of ascorbate. Both peptides show a linear dependence of P^{+} intensity on solution concentration (Figure 9a). Because the peak intensity of 20μM hCtr1-14 was very low in the presence of ascorbate in previous ESI-MS experiments it was not analyzed by this method.

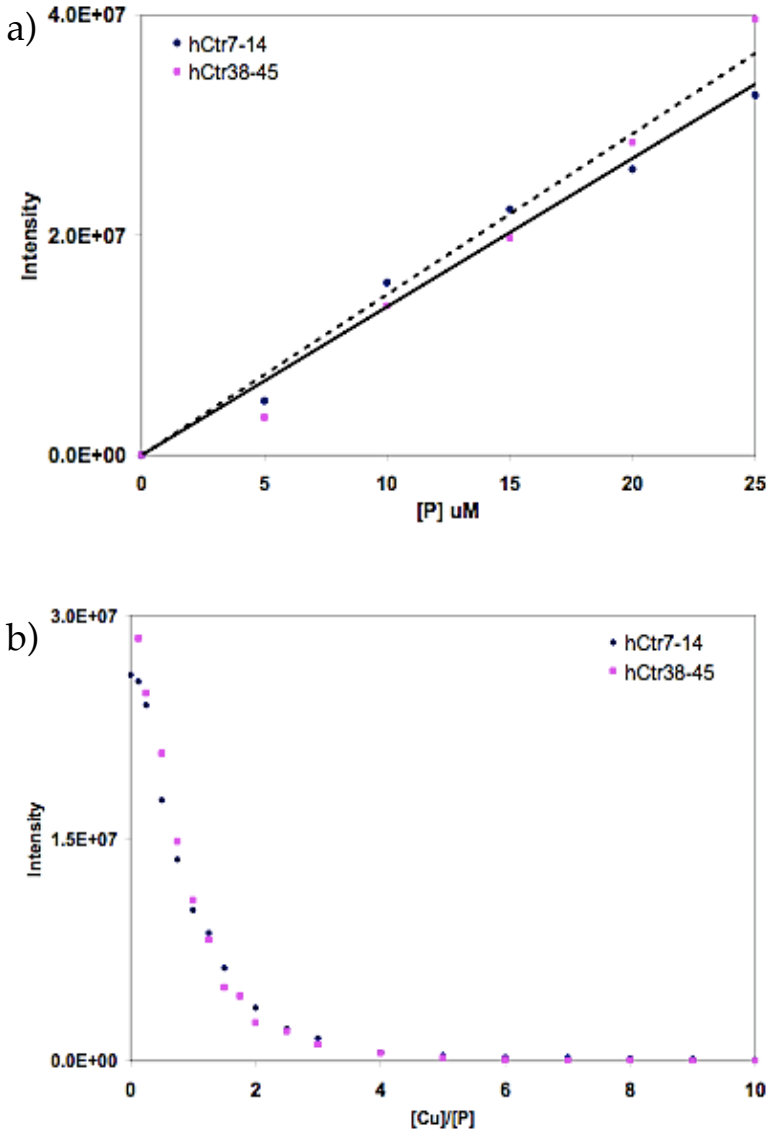

Figure 9. Quantitative ESI-MS to determine peptide-Cu^+ binding constants via Mets motifs. a) Linear dependence of peptide P^+ peak intensity on concentration of peptide in solution. b) Intensity of free peptide P^+ decreases with increasing copper.

The change in peptide P^+ intensity was measured as $CuSO_4$ was titrated into solution from 0-200 μM. As the concentration of copper increased, P^+ intensity decreased and the P-Cu doubly charged mass ion ($[PCu(II)]^{2+}/2$) increased. At high copper concentrations (>8 eq. Cu) multiple copper binding was seen. However, the multiple copper binding seen here is probably not biologically relevant due to the high concentrations of copper required. Assuming a 1:1 binding stoichiometry, the formation of P-Cu(I) complex can be represented by Equation 2, and the expression for K_D is shown by Equation 3, where P is free peptide, Cu is free copper, and PCu is peptide-copper complex.

$$PCu \rightarrow P + Cu \qquad \textbf{Equation 2}$$

$$K_D = \frac{[P][Cu]}{[PCu]} \qquad \textbf{Equation 3}$$

The amount of free peptide was calculated using the respective calibration curves between 0.5 and 2 equivalents of copper. With the calculated value of $[P]_{free}$, effective K_D's were calculated (Equation 3) for each peptide. Values for calculated K_D's are shown in Table 5. These calculated values match well with the concentration of biologically available copper in the human body and the reported K_M of Ctr1 for a variety of organisms.[156, 166]

Table 5: Effective K_D values calculated for 1:1 peptide-Cu(I) complex of hCtr1 model peptides from quantitative ESI-MS and ascorbate oxidation assay methods.

Peptide	K_D for Cu(I) by ESI-MS	K_D for Cu(I) by ascorbate oxidation assay
hCtr1-14	-	16 ± 4 μM
hCtr7-14	5.7±0.8 μM	9 ± 3 μM
hCtr38-45	3.3±0.9 μM	3 ± 4 μM

2.2.1.3 Analysis of Peptide-Cu^{+} Binding by Oxidation Rate of Ascorbate.

At pH below 7 and in the absence of catalytic metal ion, ascorbate does not autoxidize and displays a pH dependent UV absorption in the range 245-265 nm. In the presence of redox-active metal ion, however, ascorbate (H_2Asc) is readily oxidized. In the case of Cu^{2+}-catalyzed oxidation, the rate-limiting step includes one electron-transfer from ascorbate anion ($HAsc^-$) to dioxygen via metal complex, forming ascorbate radical anion ($Asc^{\bullet -}$). The reaction is first order with respect to both $HAsc^-$ and free metal ion.

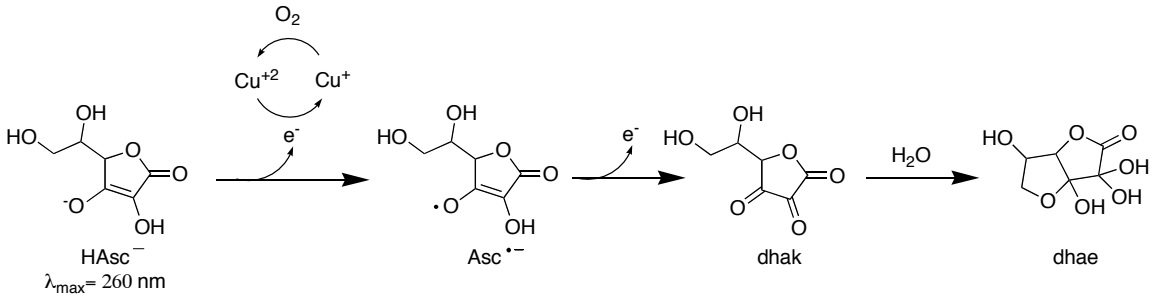

Figure 10. Metal dependent oxidation of ascorbate.

The $Asc^{\bullet -}$ radical is further oxidized in a fast one-electron step to a keto intermediate (dhak) which then cyclizes to form dehydroascorbic acid (dhae). Reaction progress can be monitored by loss of absorption around 245-265 nm. Metal chelators are known to suppress the rate of metal-catalyzed oxidation with rate being inversely related to chelate stability. Therefore, metal binding stability of a given chelator can be assessed by observing the rate of metal-catalyzed oxidation of ascorbic acid as a function of chelator concentration.

Equation 4 represents the rate of the Cu^{2+}-catalyzed oxidation of ascorbate, and Equation 5 represents the observed rate constant (k_{obs}). Combining these two expressions gives the first-order rate expression in Equation 6.

$$\frac{d[\mathrm{HAsc}^-]}{d\mathrm{T}} = k[\mathrm{HAsc}^-][\mathrm{Cu}^{2+}] \qquad \textbf{Equation 4}$$

$$k_{obs} = k[\mathrm{Cu}^{2+}] \qquad \textbf{Equation 5}$$

$$\frac{-d[\mathrm{HAsc}^-]}{d\mathrm{T}} = k_{obs}[\mathrm{HAsc}^-] \qquad \textbf{Equation 6}$$

Solutions of 120 μM ascorbate were prepared with various concentrations of $CuSO_4$ from 0-16 μM and the reaction was observed by monitoring the disappearance of the ascorbate absorbance band at 260 nm. According to Equation 5, k_{obs} can be found from the slope of the line of $-d[HAsc^-]$ vs. time. This observed Cu-catalyzed ascorbate oxidation rate is linearly dependent on [Cu] under our working copper concentrations from 0-16 μM, and thus provides a standard curve, shown in Figure 11, to determine $[Cu]_{free}$ from k_{obs} (Equation 5).

The k_{obs} was calculated for peptide concentrations from 0-30μM and used to determine the $[Cu]_{free}$. Knowing the values of total peptide and copper added to the solution allows us to calculate the final variable needed determine K_D (Equation 3) using equations 7 and 8.

$$[\mathrm{P}]_{total} = [\mathrm{P}]_{free} + [\mathrm{PCu}] \qquad \textbf{Equation 7}$$

$$[\mathrm{Cu}]_{total} = [\mathrm{Cu}]_{free} + [\mathrm{PCu}] \qquad \textbf{Equation 8}$$

The calculated dissociation constants are found in Table 5. Although the δ values are rather large compared to the K_D value, the calculated dissociation constants for hCtr7-14 and 38-45 are in the same order of magnitude as those calculated using ESI-MS

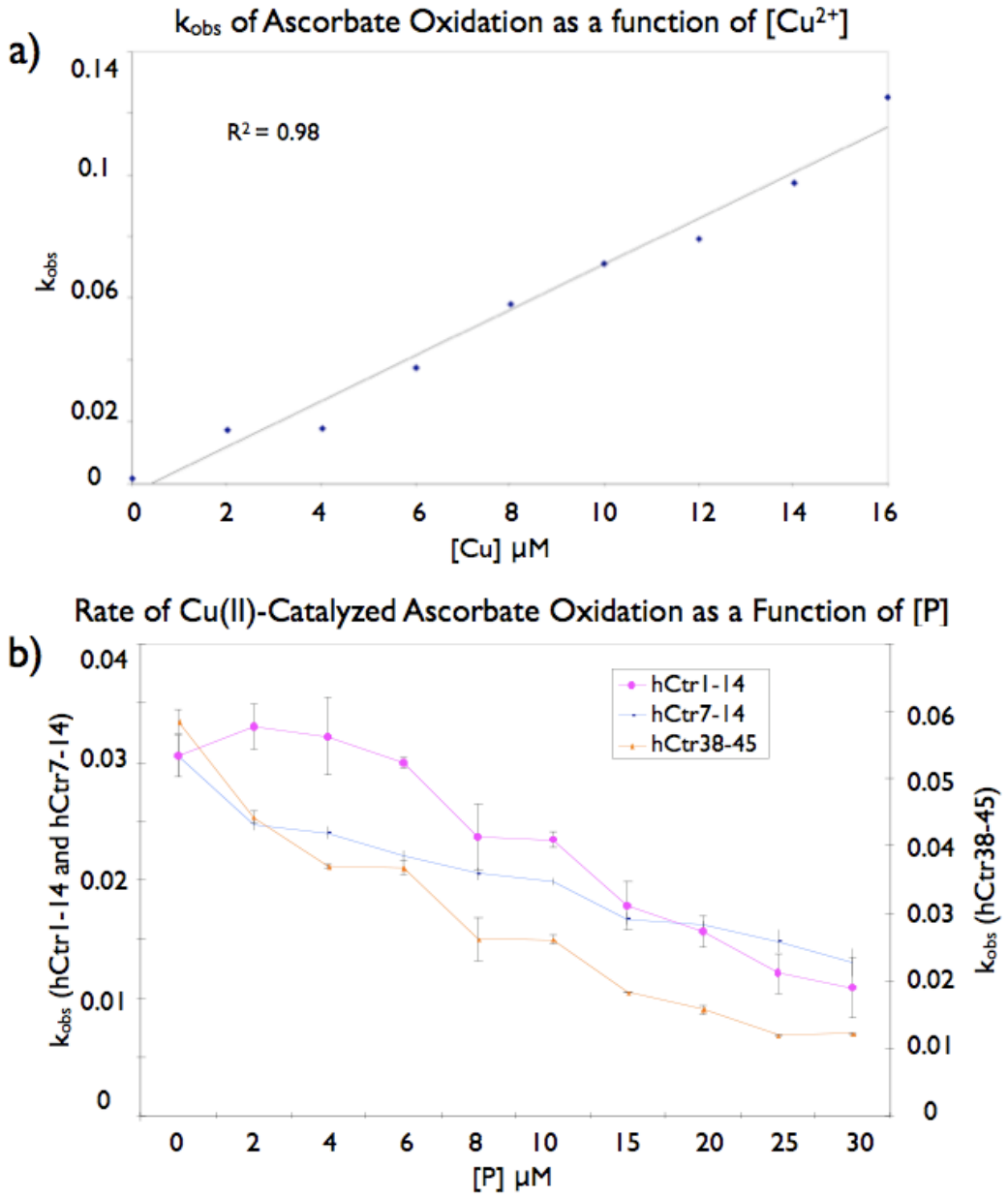

Figure 11. P-Cu binding slows the rate of Cu-catalyzed ascorbate oxidation in 120µM H_2Asc solution. a) Standard curve showing the rate of ascorbate oxidation as a function of $[Cu(II)]_{free}$ from $[CuSO_4]$ from 0 to 16 µM. b) Rate of Cu-catalyzed oxidation at 8 µM $CuSO_4$ as a function of Cu-chelating peptide concentration. As [P] increases from 0-30 µM, the k_{obs} decreases. The rate of reaction was then monitored as a function of peptide concentration using the same peptides shown in Table 1. Peptide was added to solutions of 120µM ascorbate (pH~4.5) and 8 µM $CuSO_4$.

experiments presented in the previous section. This experiment could be potentially complicated for the following reasons: First in the equations used to calculate K_D, we assume 1:1 P-Cu binding. However, hCtr1-14 may be able to bind multiple copper atoms at a time since it has sites for both Cu^+ and Cu^{2+} binding. Also, the presence of histidine ligands may have an undetermined effect on the Cu-catalyzed ascorbate oxidation rate depending on how the peptide controls the first coordination sphere of bound copper and whether the His can participate in copper binding in the presence of low concentration of ascorbic acid (120 μM).

All peptides suppress the rate of copper catalyzed ascorbate oxidation at concentrations above 8 μM. However, hCtr1-14 seems to slightly increase the rate at low peptide concentrations (Figure 11b). An explanation for this phenomenon is offered in the case of monodentate ligands that favor Cu^+ over Cu^{2+}, as follows. In anaerobic conditions and in the absence of a metal chelate, the oxidation of $HAsc^-$ to $Asc^{\bullet -}$ is unfavorable, but when Cu^{2+} is available, this unfavorable oxidation is overcome by favorable reduction of $Cu^{2+}$and Cu^+-ligand complex formation. The anaerobic oxidation is not a catalytic cycle, however, because Cu^+ complex is more stable that Cu^{2+}, and therefore Cu^+ is not readily re-oxidized to Cu^{2+}. This initially catalyzes the $Cu^{2+} \rightarrow Cu^+$ reaction, but slows the rate of $HAsc^-$ oxidation as Cu^+ product accumulates. In this case we have a peptide ligand that may prefer Cu^+ binding. The peptide may be able to control the first coordination sphere of copper such that after PCu(I) complex is formed, it is not reoxidized. In the case of a metal chelate that favors Cu^+ over Cu^{2+}, the aerobic oxidation is suppressed; however initial anaerobic oxidation is catalyzed. This may explain the initial acceleration of $HAsc^-$ oxidation rate seen for hCtr1-14.

Previous MS studies have shown that Mets motif peptides bind Cu^+ exclusively.[170] This makes sense because soft thioether ligands should prefer the soft Cu^+

oxidation state. However, His-rich peptides are known to bind the harder Cu^{2+} oxidation state due to the harder imidazole N-ligands. For this reason, we would not expect hCtr7-14 and hCtr38-45 with only Met binding sites, to bind copper from $CuSO_4$ unless the system is put under reducing conditions to provide Cu^{+}. On the contrary, hCtr1-14 would be expected to bind copper under conditions that favor both Cu^{2+} and Cu^{+} because it has both His and Met ligands to bind the two respective oxidation states.

As expected, both "Mets-only" peptides, hCtr7-14 and hCtr38-45, show a copper complex by ESI-MS only in the presence of reducing agent indicating that these peptides have low affinity for Cu^{2+} but readily bind Cu^{+}. In the case of hCtr1-14, where both a Mets motif and several His residues are present on the peptide, a Cu^{2+} complex was seen by ESI-MS. Copper binding through His residues was confirmed by the appearance of a M→L charge transfer band at 525 nm (see next section, Figure 14). Under reducing conditions, a Cu^{+} complex was detected with ESI-MS and could be distinguished from a Cu^{2+} product by the difference in mass ion.

The intensity of peaks for hCtr1-14 is reduced significantly when ascorbic acid is present. This could be explained by the presence of the His residues which are readily protonated at the low pH of 5 mM ascorbic acid (measured pH≈3). The low intensity of these peaks makes them just distinguishable above the background noise of the instrument.

K_D values calculated from ESI-MS experiments are between 1-6 μM. These values are on the same order of magnitude as found previously for a model yeast Ctr peptide (2.5 μM)[170] and with the K_M values (1-5 μM) reported for Ctr1 in a variety of organisms[156].

The ascorbic acid oxidation assay shows expected results for hCtr7-14 based on a previous study on "Mets only" model peptides of yeast Ctr.[170] In this previous work, a

peptide with Mets motif, MXXMXXM, showed a curve similar to that seen here for hCtr7-14 and 38-45, with Mets motifs MXXMXM and MMMMXM, respectively. Mutant peptides with norleucine replacing various methionine residues showed a curve more similar to that seen here for hCtr1-14, with a small acceleration of rate at low peptide concentrations.[170] The K_D values calculated by the ascorbate oxidation assay for hCtr7-14 and 38-45 are in the same order of magnitude as those found by ESI-MS. In the case of hCtr1-14, the method for calculating K_D may be complicated due to the interfering His ligands and the possibility of forming a peptide complex with more than one copper species.

These experiments show us that both methionine and histidine ligands of hCtr1 N-terminal model peptides are capable of binding copper. Methionine ligands in these model peptides are selective for the monovalent copper species. It is likely that histidine prefers divalent copper, however that is not proven with the experiments presented here. Experiments in the following sections address histidine binding to Cu^+ and Cu^{2+}.

2.2.2 N-terminal hCtr1 Model Peptides Require Histidine for High Affinity Cu^+ and Cu^{2+} Binding

Model peptides of the first 14 amino acids of hCtr1 (hCtr1-14) including several mutant peptides were synthesized. As mentioned above, hCtr1-14 contains three His residues and four Met residues. To determine the amino acids important for copper binding, Met and His residues in hCtr1-14 were systematically substituted for norleucine (Nle) or alanine (Ala), respectively. In the case of His to Ala or Met to Nle substitution, two lysines were added to the peptide C-terminus to increase water solubility. Peptide apparent or relative affinities for Cu^+ and Cu^{2+} were determined by copper competition experiments (Sections 2.2.2.1 and 2.2.2.2). The model peptide sequences and calculated binding constants are shown in Table 6.

In the following sections "high" affinity sites refer to those binding copper(I) with nanomolar (log K_a~10) affinity or copper(II) with picomolar (log K_a=12) affinity or better. "Low" affinity sites refer to anything with affinity two orders of magnitude or more reduced from high affinity sites.

Table 6. hCtr1 model peptide sequences and calculated Cu^+ and Cu^{2+} binding constants. Cu^+ binding constants are calculated from copper competition with BCA (See section 2.2.2.1). Cu^{2+} binding constants are calculated from copper competition with NTA (See section 2.2.2.2).

Peptide	Sequence	Cu(I) log K_a	Cu(II) log K_a
hCtr1-14	M D H S H H M G M S Y M D S	10.2 ± 0.2	12.8 ± 0.3
HA	M D A S A A M G M S Y M D S K K	*	6.7 ± 0.7
H3A	M D A S H H M G M S Y M D S K K	9.1 ± 0.2	**
H5A	M D H S A H M G M S Y M D S K K	10.01 ± 0.09	13.1 ± 0.3
H6A	M D H S H A M G M S Y M D S K K	9.71 ± 0.02	13.0 ± 0.1
H56A	M D H S A A M G M S Y M D S K K	8.86 ± 0.03	12.67 ± 0.06
MNleH56A	Nle D H S A A Nle G Nle S Y Nle D S K K	*	13.09 ± 0.07
MNle	Nle D H S H H Nle G Nle S Y Nle D S K K	9.55 ± 0.04	12.4 ± 0.2
Ac-hCtr114	Ac M D H S H H M G M S Y M D S		10.92 ± 0.04

* Peptide does not compete with BCA for Cu^+

** Data does not fit model, peptide forms ternary species with Cu^{2+} and HEPES or NTA

2.2.2.1 hCtr1-14 High Affinity Cu^+ Binding Requires Histidine.

This lab has previously reported apparent affinity constants of yeast Ctr1 model peptides with Cu^+ and the apparent affinity constants for hCtr1 Mets motif model peptides are reported in Table 6. The Ctr1 model peptide-Cu(I) association constants were obtained for Mets motif peptides using a gas-phase ESI-MS method and ascorbic acid as a copper reductant.[170] These methods are not applicable to study metal binding to histidine because in the presence excess of ascorbic acid, H^+ ions compete with metal

binding. Instead, we use a solution competition study employing the colorimetric Cu^+ indicator, bicinchoninic (BCA), as a competitive ligand for Cu^+.

Solutions of $BCA_2Cu(I)$ were titrated with up to 50 equivalents of peptide. In these experiments, a large excess of peptide ensures that a 1:1 P:Cu(I) species is present, even in the case where the peptide may have multiple potential Cu^+ binding sites. Assuming a 1:1 P:Cu(I) complex and using a published affinity constant for $BCA_2Cu(I)$ ($\log \beta_1 = 7.3$, $\log \beta_2 = 14.7$)[183] apparent affinity constants for the PCu(I) complexes were determined and are shown in Table 6.

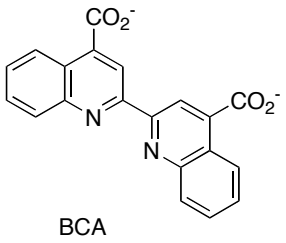

BCA

Figure 12. BCA is a Cu^+ selective chelator.

An example of titration spectra from hCtr1-14 competition with BCA is shown in Figure 13a, where competition can be observed by the decrease of absorbance at 358 and 562 nm. The strongest binding is observed from the hCtr1-14 native sequence, with an apparent $\log K_{PCu(I)}$ of 10.2, corresponding to a 0.1 nanomolar K_D.

According to the current model for hCtr1 function in vivo, the histidines in hCtr1-14 should not be important for Cu^+ acquisition. However, substitution of all three His for Ala (HA peptide) renders the model peptide unable to compete for Cu^+ from the $(BCA)_2Cu(I)$ complex, even with 50 equivalents excess peptide. This experiment demonstrates for the first time that histidines are important for strong Cu^+ binding in an hCtr1 model peptide.

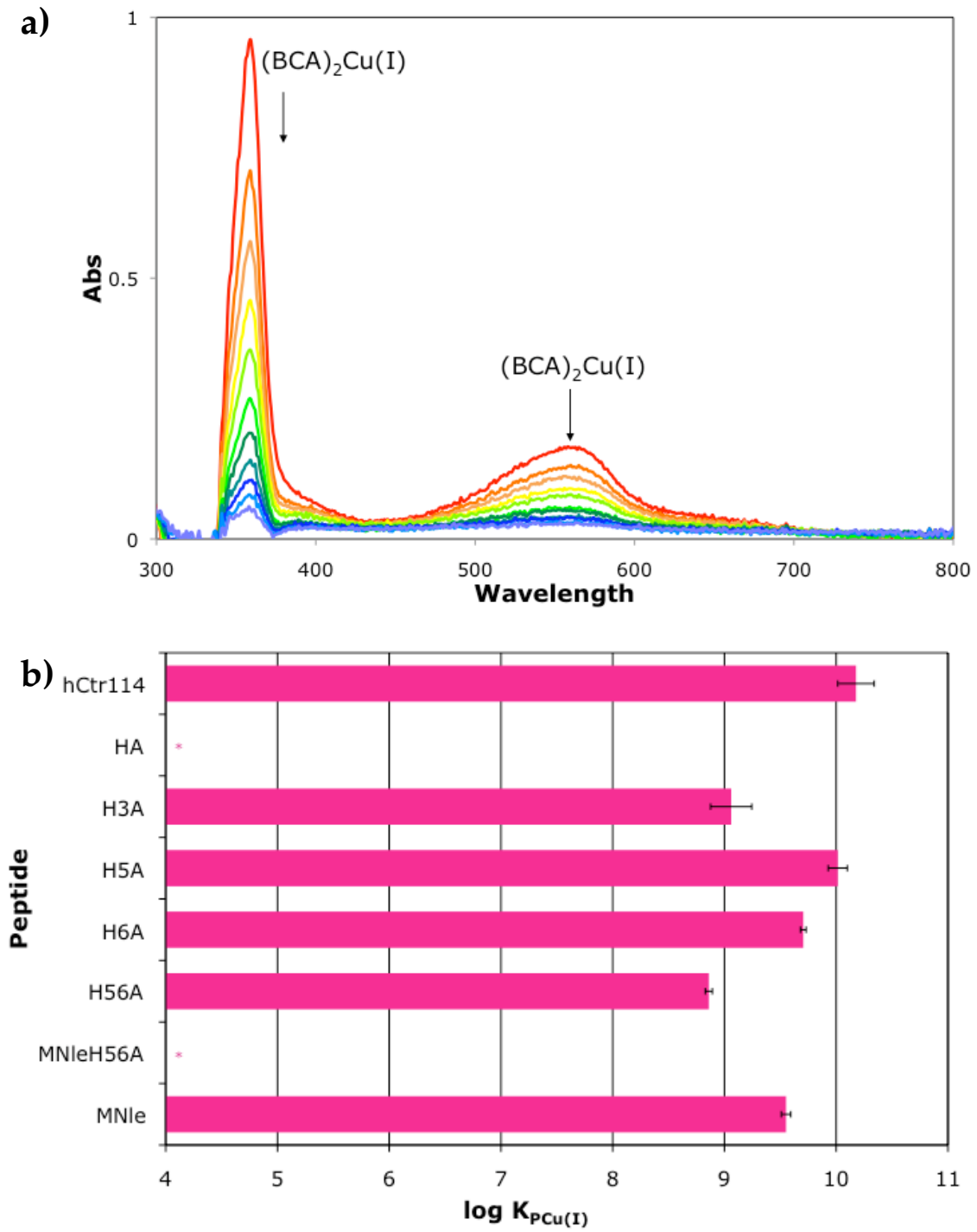

Figure 13. hCtr1 model peptide competition with BCA for Cu^{+}. a) Spectra from a titration of 50 equivalents of hCtr1-14 peptide into 75 μM BCA and 25 μM $[Cu(I)(CH_3CN)_4]PF_6$ with 50 mM HEPES at pH 7.4 and ~1% CH_3CN. b) Apparent Cu(I) binding constants for hCtr1 model peptides determined by titration of 25μM $BCA_2Cu(I)$ with 50 eq of peptide in aqueous solution with HEPES and CH_3CN. *Excess peptide (50 equivalents) does not compete with BCA for Cu^{+}.

Further debunking the current dogma on hCtr1 binding to Cu^{+} via only MXM and MXXM Mets motifs,[141, 156, 157, 170] exchange of all methionines to norleucine has little if any effect on the association constant for the peptide and Cu^{+}. This supports evidence that His residues, rather than Mets motifs alone, are important for high affinity copper binding to hCtr1 model peptides at the physiological pH of 7.4.

Individual His substitution has a less drastic effect on the ability of peptides to compete for Cu^{+} from BCA as compared to the all His to Ala substituted peptide. Mutation of the histidines in the fifth or sixth position have little if any effect, but mutation of these two His together reduced the binding constant by about one order of magnitude. Individual mutation of the histidine in the third position also reduced the binding constant significantly by one order of magnitude. These results may indicate that all three His have some part in the Cu^{+} binding site, but perhaps the fifth and sixth histidine are exchangeable and/or have a cumulative contribution to Cu^{+} complex formation.

Based on the complete loss of Cu^{+} competition in the MNleH56A peptide containing only the third position His, it is clear that Cu^{+} does not bind strongly in the same way that Cu^{2+} does to the ATCUN site alone. This is not surprising because the soft Cu^{+} would not prefer the harder donor character of amide and amine nitrogens according to Pearson's HSAB Principle (Chapter 1).[74] The third position His seems to contribute to Cu(I) binding in a His-only or mixed His/Met donor environment. One possibility for coordination involving the fifth and sixth His is the type of linear two-coordinate bis-His site recently characterized by Karlin and Shearer and shown to possess unique redox chemistry in the presence of other donors.[178-182] The fifth and sixth His alone, however, are clearly not the only important residues contributing to a high-affinity Cu(I) binding site (Figure 13b, Table 6).

2.2.2.2 N-Terminal Model Peptides of hCtr1 Bind Cu^{2+} with High Affinity via an ATCUN-Like Site.

Solutions of peptide and Cu^{2+} in HEPES buffer at pH 7.4 are shown (Figure 14). The native sequence 1-14 of hCtr1 (hCtr1-14) plus $Cu(ClO_4)_2$ shows an absorbance maximum near 525 nm, typical of an albumin-like distorted square planar N,N^-,N^-,N coordination environment with Cu^2.[172-174, 177] The spectrum is nearly identical to that of Cu(II)HSA.[172] Substitution of either all Met to Nle (MNle peptide) or His at the fifth (H5A peptide) or sixth position (H6A peptide) causes no significant change in the PCu(II) spectrum (Figure 14), indicating that none of the Mets or His 5 and 6 are coordinated to Cu^{2+} in the native peptide high affinity binding site. In contrast, mutation of His in the third position from the N-terminal in the H3A peptide results in a absorbance shift, indicating that the coordination environment is different in this mutant peptide. In addition, when the N-terminal amine is capped, the λ_{max} shifts to a longer wavelength indicating a change in coordination environment compared to the native sequence. These data are consistent with albumin type coordination in the native peptide (hCtr1-14) by an ATCUN site in which the Cu^{2+} ion is coordinated by the imidazole nitrogen, two deprotonated amide nitrogens, and the terminal amine.

Apparent affinity constants at pH 7.4 in HEPES buffer were determined using NTA as a competitive ligand. In short, solutions of 1:1 P:Cu(II) were titrated with a total of at least 2 equivalents of NTA and reactions were monitored by UV-Vis (Figure 15a). Titrations were also done in the reverse direction. Binding constants for each model peptide are shown in Table 6.

Copper(II) binds to hCtr1-14 with a conditional log $K_{PCu(II)}$ of 12.9. This strong binding to Cu^{2+} is comparable to that of human serum albumin (HSA, log $K_{HSACu(II)}$= 10.68), the major labile Cu^{2+} carrier in blood. This is physiologically relevant and suggests that hCtr1 may be able to compete with blood proteins for Cu^{2+}.

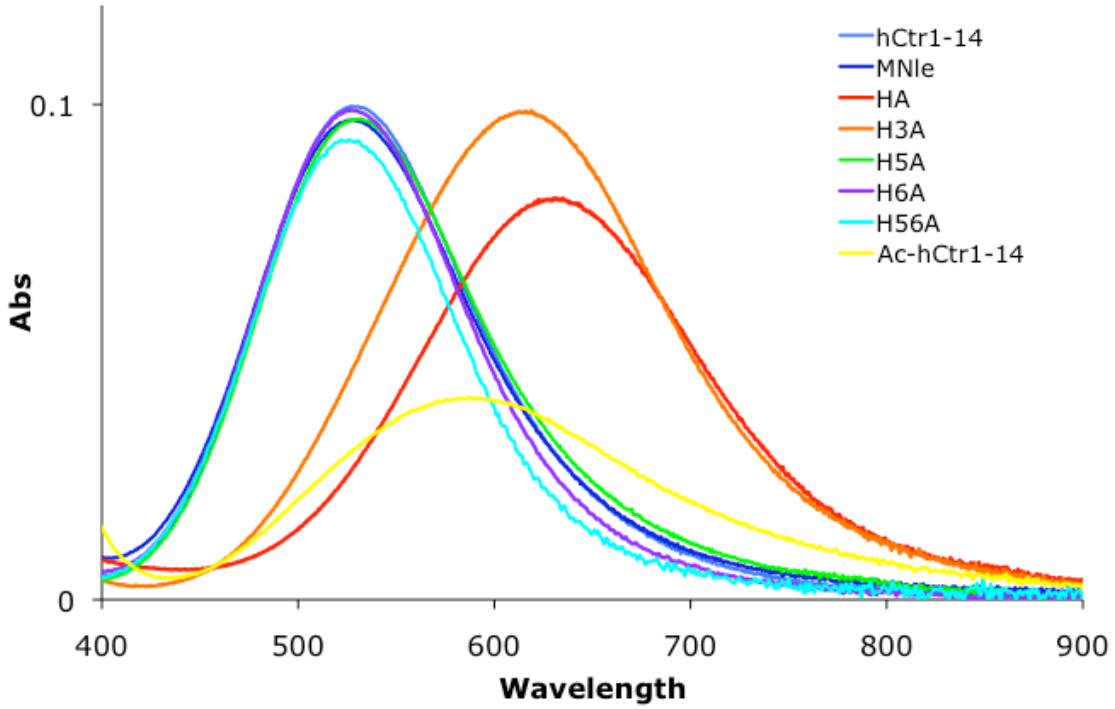

Figure 14. Absorbance spectra of hCtr1 model peptides with 1 equivalent of Cu^{2+} at pH 7.4 in HEPES buffer. Peptides with His in the third position from a free N-terminal display absorbance at 525 nm characteristic of a typical N-terminal ATCUN Cu(II) binding site. Substitution of all His to Ala, individual substitution of the His at position 3 (H3A) or acetyl capping of the N-terminal (Ac-hCtr114) results in a different type of binding site and a shift in λ_{max} compared to the native sequence peptide (hCtr1-14).

Consistent with results discussed above, mutation of all Met and/ or the His in the fifth and sixth positions does not significantly affect Cu^{2+} affinity. Only by mutation of His in the third position from the N-terminus or by acetyl-capping of the N-terminal amine can we detect a significant change in binding affinity, as shown in Table 7 and Figure 15b.

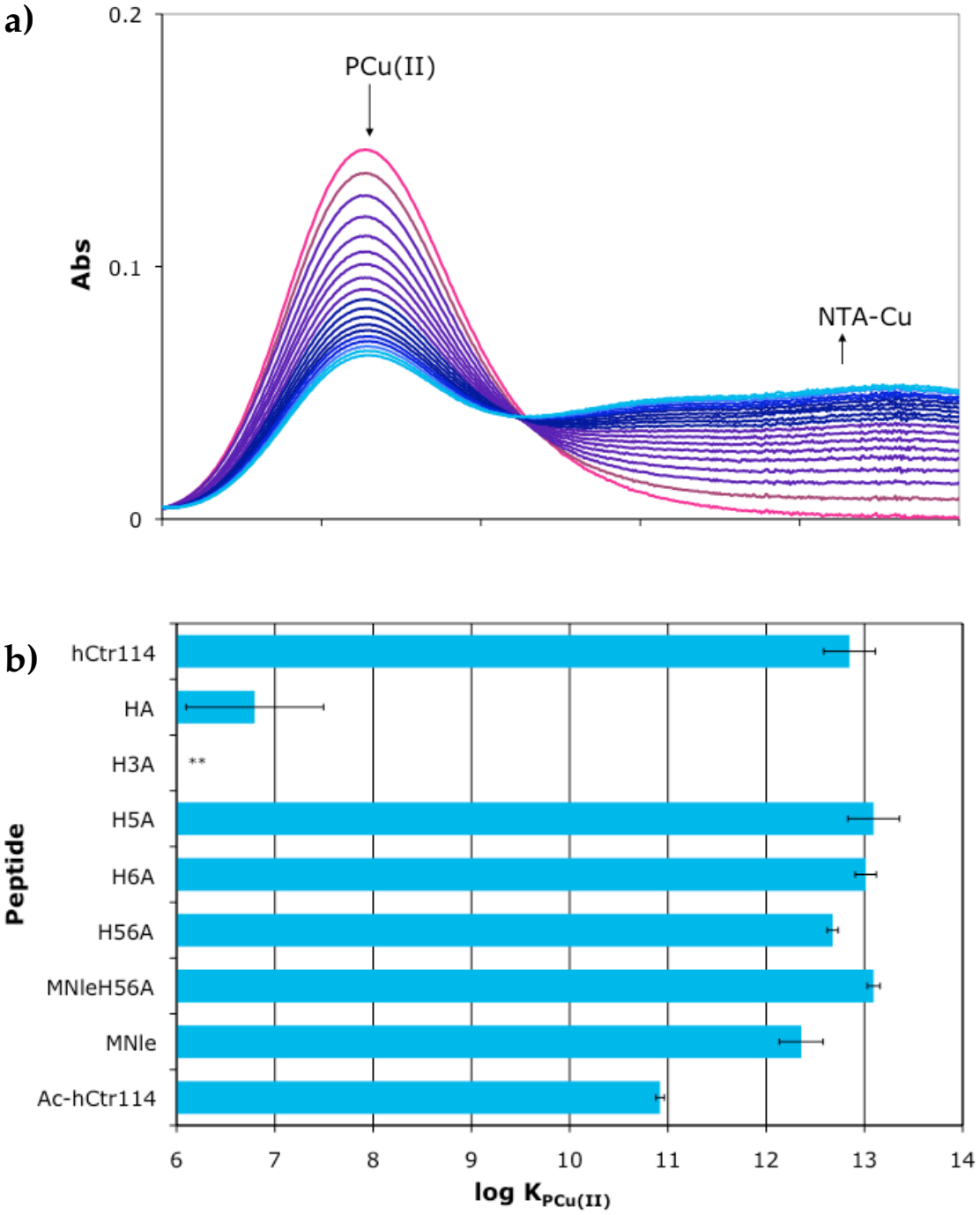

Figure 15. hCtr114 model peptide competition with NTA for Cu^{2+}. a) Spectra from titration of NTA into a 500 μM solution of 1:1 P:Cu(II) in 50 mM HEPES buffer at pH 7.4. b) Conditional binding constants of Cu(II) and hCtr1 model peptides determined by competition with the Cu(II) chelator, NTA. **H3A peptide forms an undefined ternary complex most likely with Cu(II) and HEPES or NTA and titration spectra did not fit the model shown in Table 7.

These results are as expected from an ATCUN-like H_2N-XXH site and demonstrate for the first time that N-terminal hCtr1 model peptides have high picomolar affinity for Cu^{2+}. The strong Cu^{2+} binding affinity found here for hCtr1 model peptides indicates that competition between hCtr1 and extracellular Cu^{2+} carriers, like HSA, is possible and may allow for Cu^{2+} to occupy the hCtr1 N-terminal before reduction to the monovalent state.

2.2.2.3 HH Sequence Facilitates the Ascorbate-Dependent Reduction of Cu(II)-Peptide Complexes.

It is clear from experiments discussed above that model peptides of hCtr1 can bind both oxidation states of copper with significant affinity. It is especially obvious that the histidine residues are crucial for the model peptides' ability to compete with BCA for Cu^{+} and NTA for Cu^{2+}. Mets motifs alone are not sufficient for the high affinity binding necessary to compete for either oxidation state of copper. It is also apparent that the residues crucial for acquisition of Cu^{+} are distinct from the ATCUN site with high affinity (picomolar K_D) for Cu^{2+}. Histidine in the third position from the N-terminal seems to be of shared importance to Cu^{+} and Cu^{2+} affinity, although the overall binding site in each case is different. From Figure 16, it is clear that His is important, but that the site for high affinity (0.1 nanomolar K_D) Cu^{+} binding is distinct from the ATCUN high affinity Cu^{2+} site (Figure 16).

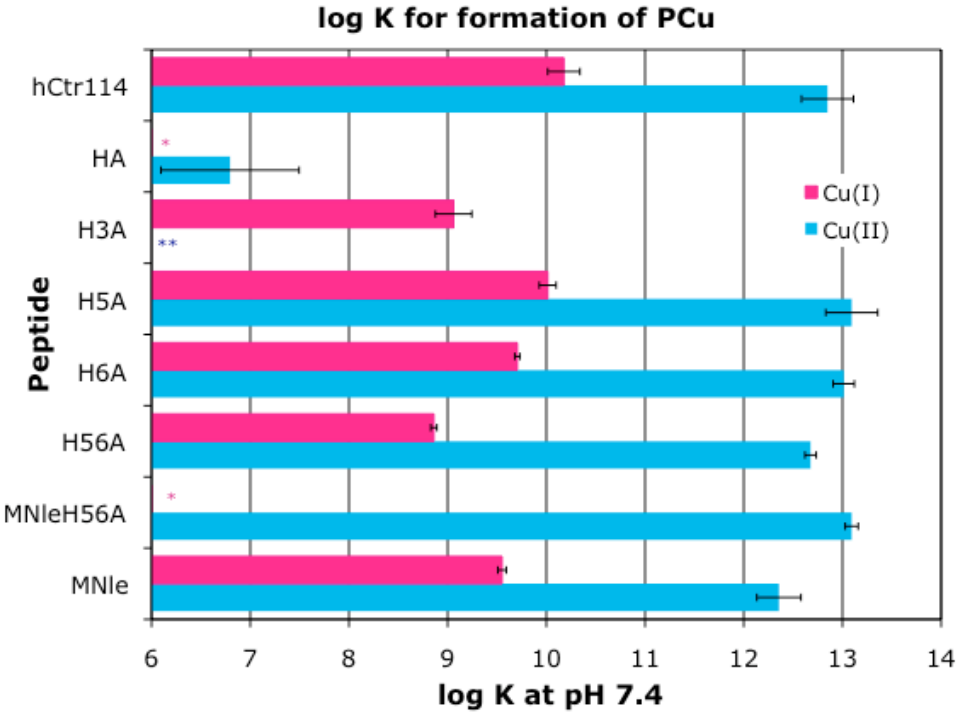

Figure 16. Relative hCtr114 model peptide copper binding constants. Apparent Cu(I) (pink bars) and conditional Cu(II) (blue bars) binding constants for hCtr1 model peptides.

Because these peptides are capable of strong binding to both oxidation states of copper it would be interesting to acquire the reduction potentials of the Cu(II) complexes using cyclic voltametry. The work of both Karlin[181, 182] and Shearer,[178-180] suggests that the presence of HH domains in hCtr1 might impart interesting redox properties to the model peptides. Unfortunately attempts to measure reduction potentials via standard cyclic voltametry protocols failed to produce a measurable signal. This is likely due to low diffusion coefficients or insulation of the Cu ion by the peptide.

Instead, differences in the ability of ascorbate to reduce Cu(II) complexes of the various peptides were measured in the presence of HEPES buffer at pH 7.4. The

experiments were limited to aerobic conditions, and availability of oxygen might allow cycling of copper oxidation states (i.e. after being reduced by ascorbate, the Cu^{+} could be re-oxidized by O_2 from the air). However, if the peptides are able to stabilize Cu^{+} then the re-oxidation to Cu^{2+} will be slowed and PCu(I) complex should accumulate. In fact, this seems to be the case with some of the peptides and clear differences can be noted depending on the presence of the fifth and sixth position His (Figure 17).

In previous work done by Perrone et al., the ascorbate-dependent reduction of Cu^{2+} complex with HSA and a model peptide with the sequence, DAHK, based on the ATCUN motif of HSA were tested via a similar procedure under anaerobic conditions.[184] This previous work found that the Cu^{2+} complex of a peptide with the sequence DAHK was stable in the presence of ascorbic acid whereas HSA complex with Cu^{2+} was reduced to a Cu^{+} species. The copper reduction could be monitored by a decrease of the HSACu(II) signal at 525 nm. We repeated this experiment with HSACu(II) under aerobic conditions and found comparable results under our set of conditions. We therefore tested our hCtr1 model peptides under the same conditions.

The Cu^{2+} complex of hCtr1-14 demonstrates a reduction in the signal at 525 nm over 1 hour after adding 2 equivalents of ascorbate to solution, indicating an ascorbate-dependent reduction to a Cu^{+} complex. Similarly to hCtr114 and HSA, the MNle peptide Cu^{2+} complex could be reduced and assumingly stabilize the Cu^{+} species under these conditions. However, upon substitution of either His in the fifth or sixth position, the PCu(II) absorbance at 525 nm did not change over 1 hour with ascorbate. This indicates that both His 5 and 6 are important for stabilizing the Cu^{+} species and perhaps facilitating the reduction of Cu^{2+} to Cu^{+} complex by increasing the reduction potential.

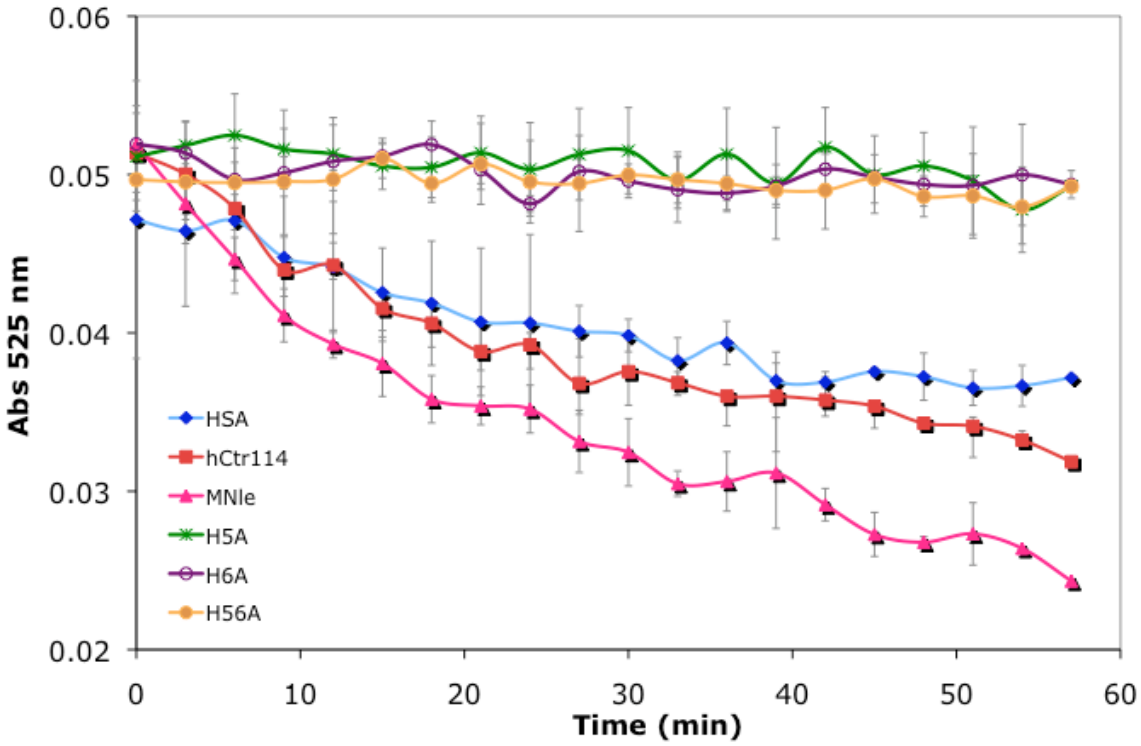

Figure 17. Ascorbate-dependent reduction of Cu(II) in complex with hCtr114 model peptides containing the ATCUN site. Solutions of 500 μM peptide-Cu(II) complex and 1 mM ascorbate in 50 mM HEPES at pH 7.4 monitored for 1 hour with UV-Vis at 525 nm.

The results of this experiment show that the HH site in these hCtr1 model peptides affects the redox properties of the peptide-Cu(II) complexes. This apparent facilitation of Cu^{2+} reduction or simple stabilization of Cu^{+} in the case of peptides containing the HH site has significant implications for the in vivo function of this protein. The similar reactivity of HSA is also interesting. We suggest that perhaps the ascorbate present in the blood (~30 μM) could work as a reductant for Cu^{2+} at the cell membrane in the presence of either HSA or hCtr1. This facilitation of Cu^{2+} reduction in the presence of both hCtr1 and HSA could be an important clue to understanding the mechanism for reduction of Cu^{2+} at the cell membrane and for understanding the mechanism of copper acquisition and transport via hCtr1. In either case, it is very clear

that His may have a functional role in hCtr1 copper acquisition by imparting special redox properties on the peptide copper complex.

2.2.4 Summary of Results from Spectroscopic Studies of Copper Interactions With N-terminal hCtr1 Model Peptides

Presented here is the first evidence that N-terminal hCtr1 model peptides have significant affinity for copper via histidine residues. The presence of an ATCUN site at the N-terminus allows hCtr1 model peptides to bind Cu^{2+} with strong, low picomolar affinity (log $K_{PCu(II)}$~13). This high affinity for Cu^{2+} should allow the hCtr1 protein to compete with biologically relevant extracellular copper carriers, like HSA. This may be important for understanding the mechanism for hCtr1 copper acquisition. Specifically, the high binding affinity of hCtr1 model peptides for Cu^{2+} implies that the protein may be occupied by Cu^{2+} in vivo and perhaps this binding event is important to protein function.

The presence of His also significantly increases hCtr1 model peptide affinity for Cu^{+}. This further suggests a functional significance of hCtr1 N-terminal histidine residues in acquisition of copper. We could speculate that histidine may also be important for competition for copper from extracellular Cu^{+} carriers, like HSA in the presence of ascorbate.

The current model for mammalian copper acquisition for hCtr1 shows that only Mets motifs are important, however the data presented here suggest otherwise. In fact, the model peptides of hCtr1 used in the experiments presented here show that the peptide interacts very weakly with copper via methionines alone. In fact, His is necessary for strong interactions with both oxidation states of copper.

These studies also suggest that the mechanism of in vivo copper reduction in fact may not depend on a membrane reductase, as it does in yeast. We speculate that the

strong Cu^{+} binding found in the model peptides may increase reduction potential of hCtr1-bound Cu^{2+} so that physiological reducing agents, like ascorbic acid, could be sufficient for the necessary reduction to Cu^{+}. Another possibility suggested by this work is that HSA-bound Cu^{2+} can be reduced by ascorbate and then acquired by hCtr1.

The findings here call for further investigation of histidine's role in hCtr1 copper acquisition and transport. These results may also suggest modification of the current model for mammalian copper acquisition. An updated model based on these studies will allow for extracellular His clusters to compete for copper from extracellular copper chelators and may also allow a role for hCtr1 or HSA and ascorbate in the reduction step necessary for copper transport through the plasma.

2.3 Materials and Methods

Peptide Synthesis and Purification

Model peptides based on the first 14 N-terminal amino acids of hCtr1 were synthesized on a Protein Technologies PS3 automated peptide synthesizer on Fmoc-PAL-PEG-PS resin (Applied Biosystems) in 0.1 and 0.05 mmol scales. Couplings of standard Fmoc (9-fluorenylmethoxy-carbonyl)-protected amino acids (Chem-Impex, Novabiochem) were achieved with HBTU (O-benzotriazole-N,N,N′,N′-tetramethyl-uronium hexafluorophosphate; Novabiochem) in the presence of N-methylmorpholine (NMM) in N,N′-dimethylformamide (DMF) for 20 min cycles. Fmoc deprotection was achieved with 20% piperidine in DMF. The N-terminus of peptides were either acetylated with acetic anhydride and NMM or were allowed to remain as a free amine. Side chain deprotection and peptide cleavage from the resin were achieved by treating the resin-bound peptides with a 5-7 mL cocktail of 95% trifluoroacetic acid (TFA), 2.5% ethane dithiol (EDT), and 2.5% triisopropylsilane (TIS) for 2-4 h under N_2. An additional 75-150 μL of EDT and 65-130 μL of bromotrimethylsilane (TMSBr) were added during

the final 30 min to minimize methionine oxidation. After evaporation of TFA to a volume of 1-2 mL under N_2, the peptides were washed three times with diethyl ether, air-dried, and purified by semi preparative reverse-phase HPLC on a YMC C18 column with a linear 40-min gradient from 7 to 97% methanol or acetonitrile in water with 0.1% TFA. The purity was validated to be >95% by analytical HPLC, and the mass of each peptide was confirmed by ESI-MS. hCtr114 calcd for 1663.6: Found ($M + H^+$) 1664.7. hCtr17-14 calcd. for 1089.43; found ($M + H^+$) 1090.0; hCtr138-45 calcd. for 1127.47; Found ($M + H^+$) 1128.2. HA calcd for 1721.7: Found ($M + H^+$) 1722.8. H3A, H5A, H6A calcd for 1853.8: Found ($M + H^+$) 1854.7. H56A calcd for 1787.7: Found ($M + H^+$) 1788.9. MNle calcd for 1848.0: Found ($M + H^+$) 1849.1. Ac-hCtr1-14 calcd for 1705.6: Found ($M + H^+$) 1706.7.

Preparation of Stock Solutions

Stock solutions of peptides were prepared by dissolving lyophilized peptide in 1-1.5 mL of Nanopure water. Concentration was determined using the Edelhoch method.[185, 186] In short, 5-15 μL aliquots of peptide were diluted into 1mL total volume of 6 M guanidinium hydrochloride (GdnHCl) to get an absorbance at 280 nm between 0.1 and 1 absorbance unit. Absorbance of aromatic amino acids, in this case only tyrosine, was measured at 276, 278, 280 and 282 nm. Known extinction coefficients of tyrosine at these wavelengths were used to determine total concentration of peptide. Stock peptide solutions were periodically checked by HPLC and ESI-MS to verify that they remained stable to oxidation or degradation in aqueous solution. $Copper^{2+}$ solutions were prepared in Nanopure water from $Cu(ClO_4)_2 \cdot 6H_2O$ (Strem Chemicals), and were standardized by EDTA (Aldrich) titration in ammonia solution with a mueroxide indicator (Fischer).[187] $Copper^{+}$ solutions were prepared from $[Cu(CH_3CN)_4]PF_6$ (Aldrich) in anhydrous acetonitrile (Aldrich) and were standardized by titrating aliquots of stock

solution into excess of the chromophoric ligand anion bicinchonate (BCA) in doubly deionized water that was boiled and degassed with argon. Concentration was determined from absorption at 562 nm due to the $Cu(I)(BCA)_2$ complex ($\varepsilon = 7900\ M^{-1}$) .[188] Solutions of Cu^+ were stored under argon and re-standardized each day to ensure that Cu^+ had not oxidized.

Mass Spectrometry

Electrospray ionization mass spectrometry (ESI-MS) was performed with an electrospray quadrupole ion trap mass spectrometer (1100 Series LC/MSD Trap, Agilent, Palo Alto, CA) with a conversion dynode detector (Daly). Samples were infused with a Harvard Apparatus (Holliston, MA) syringe pump at 33 μL/min. Ionization was achieved in the positive ion mode by application of +5 kV at the entrance to the capillary; the pressure of the nebulizer gas was 20 psi. The drying gas was heated to 325 °C at a flow of 7 L/min. Full-scan mass spectra were recorded in the mass/charge (m/z) range of 200-2000.

UV-Visible Spectroscopy

Absorption spectra were recorded in 1-cm quartz cuvettes on either a Cary50 Uv-Vis spectrophotometer or an SI Photonics (Tucson, AZ) model 420 fiber optic CCD array UV-Vis spectrophotometer.

Determination of PCu Binding Constants From Solution Phase Studies

Association constants in these experiments are the apparent association constants of copper ion with peptide at pH 7.4 assuming 1:1 binding of peptide (P) and copper.

The K_a values of the peptide-copper complexes (PCu, K_{PCu}) are large enough that titration of Cu into a peptide solution results in over 95% conversion to PCu complex (Equation 9). To calculate K_{PCu} (Equation 10) from spectroscopic techniques, an ideal

equilibrium is one that does not go to completion so that concentrations of all species are present in solution in significant amounts at any one titration point.

By introducing a competitive ligand (L) such that the peptide and ligand are competing for Cu, we create a situation in which all species are present in significant amounts in solution over the course of the titration. It is useful if the binding constants of the two competing species are close and as a general rule for the two competing species, it is ideal to have a no more than six orders of magnitude difference in the two K_{ML} values.

To determine the Cu binding constants of hCtr1 model peptides, competition between each peptide and a competitive ligand was employed. By using a competitive ligand with a known binding affinity for Cu we create an exchange equilibrium between the chelator and our model peptides. An equilibrium constant for the exchange of copper (K_{ex}, Equations 13 and 14) can be determined based on the known concentrations of total copper, peptide and competitive ligand added to solution and from the concentrations of PCu complex and LCu complex determined from absorbance spectra (Equations 9-14).

For example, calculation of binding constants can be done as follows: Starting with the PCu complex in solution and titrating the competitive L into solution will give the exchange equilibrium shown in Equation 13 for which the exchange constant (K_{ex} , Equation 14) can be calculated. If the competing ligand has a known association constant for Cu (K_{LCu}) then the apparent affinity of Cu for peptide K'_{PCu} can be deduced from the calculated K_{ex} using Equation 14. This general treatment can be used for any metal and any set of two competitive ligands that have binding constants that are within a reasonably close range.

$$P + Cu \rightarrow PCu$$ **Equation 9**

$$K_{PCu} = \frac{[PCu]}{[Cu][P]}$$ **Equation 10**

$$Cu + nL \rightarrow L_nCu$$ **Equation 11**

$$K_{LCu} = \frac{[L_nCu]}{[Cu][L]^n}$$ **Equation 12**

$$PCu + nL \rightarrow P + L_nCu$$ **Equation 13**

$$K_{ex} = \frac{[P][L_nCu]}{[PCu][L]^n} = \frac{K'_{PCu}}{K_{LCu}}$$ **Equation 14**

The association constants for the peptide Cu complexes were determined using Specfit[189, 190] software and where appropriate, computer-generated values for K_{CuP} were verified by manual calculation, as explained below.

Calculation of Cu^{2+} Binding Constants Using NTA as a Competitive Ligand

In the case of Cu^{2+} binding to hCtr1 model peptides, the assumption of 1:1 P:Cu complex formation is validated by a linear relationship between absorbance maxima between 400 and 700 nm due to peptide-copper complex (PCu(II)) and ratio of P:Cu(II) up to 1:1 in 50 mM HEPES buffer at pH 7.4. More than one equivalent of Cu^{2+} to P in solution results in precipitation of a light blue solid (copper hydroxide) indicating that each peptide can accommodate only one Cu^{2+} ion in solution.

Titrations here to determine peptide copper affinity were performed with NTA (K_{NTACu} = 10.68, pH 7.4) as a competitive chelator for Cu^{2+}. Solutions of 0.5–1 mM PCu(II) were titrated with at least two equivalents of NTA using a 100 mM NTA stock solution. For peptides that had a low $K_{PCu(II)}$ ($\log K_{PCu(II)} < 10$) titrations were preformed in the reverse direction with peptide being titrated into NTACu(II) solution under the same conditions.

The PCu(II) association equilibrium (Equation 15) and the NTACu(II) association equilibrium (Equation 17) are part of the overall exchange equilibrium (Equation 19). The equilibrium constant expression for the PCu(II) association (Equation 16) and the NTACu(II) association (Equation 18) can be used to define the overall exchange equilibrium constant expression (Equation 20). This expression can be rearranged to solve for the apparent $K_{PCu(II)}$ (Equation 21) because $K_{NTACu(II)}$ is known ($10^{10.68}$) at pH 7.4 and K_{ex} can be determined from titration spectra.

When using NTA as a competitive chelator in HEPES buffer, the experiment is slightly complicated by the fact that HEPES buffer can form a ternary complex with NTACu(II), defined by the equilibrium shown in Equation 22. This ternary complex formation should result in an apparent $K_{PCu(II)}$ ($K^{app}_{PCu(I)}$) value that appears weaker than the actual conditional association constant value at pH 7.4. Fortunately this system has been characterized and a published value for the binding of HEPES to NTACu(II) ($K_T = 10^{1.8}$, Equation 23)[172] can be used to correct the apparent $K^{app}_{PCu(I)}$ derived from Equations 15–21 that does not account for this ternary complex interference. The corrected apparent value, which accounts for ternary complex formation, $K^{appT}_{PCu(I)}$, should be more representative of the conditional binding constant, $K_{PCu(I)}$.

This K_T value and the appropriate equilibrium equations accounting for ternary species formation can also be used to derive a more appropriate equilibrium model (Equation 24). This in turn can be used to find a more accurate apparent $K_{PCu(II)}$ using Equations 26 and 27. In these titrations, the apparent affinity constants for copper(II) binding to peptide were calculated using Specfit according to the model shown in Table 7 (based on the equilibrium in Equation 22) and were corrected by Equation 27 to account for NTACu-HEPES ternary complex formation. Calculated conditional values of $\log K_{PCu(II)}$ are shown in Table 6.

$$P + Cu^{2+} \rightarrow PCu(II)$$ **Equation 15**

$$K_{PCu(II)} = \frac{[PCu(II)]}{[Cu^{2+}][P]}$$ **Equation 16**

$$NTA + Cu^{2+} \rightarrow NTACu(II)$$ **Equation 17**

$$K_{NTACu(II)} = \frac{[NTACu(II)]}{[Cu^{2+}][NTA]}$$ **Equation 18**

$$PCu(II) + NTA \rightarrow NTACu(II) + P$$ **Equation 19**

$$K_{ex} = \frac{[P][NTACu(II)]}{[PCu(II)][NTA]} = \frac{K_{NTACu(II)}}{K^{app}_{PCu(II)}}$$ **Equation 20**

$$K^{app}_{PCu(II)} = \frac{K_{NTACu(II)}}{K_{ex}}$$ **Equation 21**

$$NTACu(II) + HEPES \rightarrow NTACu(II) - HEPES$$ **Equation 22**

$$K_T = \frac{[NTACu - HEPES]}{[NTACu][HEPES]} = 10^{1.8}$$ **Equation 23**

$$PCu(II) + NTA + HEPES \rightarrow P + NTACu(II)HEPES$$ **Equation 24**

$$K^{T}_{ex} = \frac{[NTACuHEPES][P]}{[PCu][NTA][HEPES]} = \frac{(K_T)(K_{NTA})}{K_{PCu}}$$ **Equation 25**

$$K^{appT}_{PCu(II)} = \frac{K_T K_{NTACu(II)}}{K^{T}_{ex}} = K^{app}_{PCu(II)} K_T$$ **Equation 26**

$$\log K^{appT}_{PCu(II)} = \log K^{app}_{PCu(II)} + \log K_T$$ **Equation 27**

Table 7. Model used for the competition of hCtr1 model peptides and NTA for Cu^{2+} in HEPES buffer at pH 7.4. $\log\beta_1$ solved by this model is an apparent values that does not account for the presence of HEPES in solution. β_1 values derived from this model were corrected by 1.8 log units according to Equation 27.

Species	Log β_{lmh}	Cu *m*	NTA *l*	P *l*	H *h*	
CuP		1	0	1	0	refined
Cu(NTA)	12.7	1	1	0	0	Constant
$Cu(NTA)_2$	17.4	1	2	0	0	Constant
NTAH	9.46	0	1	0	1	Constant
$NTAH_2$	11.95	0	1	0	2	Constant
$NTAH_3$	13.76	0	1	0	3	Constant
$NTAH_4$	14.76	0	1	0	4	Constant
CuOH	-8.2	1	0	0	-1	Constant

Calculation of Cu^{1+} binding constants using BCA as a competitive ligand

To determine peptide Cu^+ association constants, the colorimetric Cu^+-selective chelator BCA was employed as a competitive ligand. Although Cu(I) complexes are usually spectroscopically silent, the $Cu(I)(BCA)_2$ complex is colored and has strong absorbance at 358 nm (ε = 42900 M^{-1}) and 562 nm (ε = 7900 M^{-1}).[191, 192] Association constants ($K_{PCu(I)}$) were determined for association of Cu^+ ion and peptide at pH 7.4 in HEPES buffer with up to 1% acetonitrile and assuming 1:1 binding of peptide to Cu^+. Although it may be possible for peptides to bind multiple Cu^+ ions, this assumption is validated by the large excess of peptide present during the course of these experiments. Peptide stock solutions were titrated into 1 mL solutions of $BCA_2Cu(I)$ (50 μM $Cu(CH_3CN)_4PF_6$ and 150 μM BCA) and competition was observed as a disappearance of the $BCA_2Cu(I)$ absorption bands. Calculations were done using Specfit[189, 190] software and an equilibrium model shown in Table 8 and based on the equations 28-34 for the equilibrium in Equation 32. We do not take into account the affect of acetonitrile in

solution. Acetonitrile has low affinity for copper (log K_1=2.63, log K_2=1.39, log K_3=0.28)[193] and formation of pure acetonitile-Cu(I) species in solution is unlikely in the presence of excess BCA (log K_1=log K_2~7.4)[183] and excess peptide (log K_1~10) with high affinity for Cu^+. Incorporation of acetornitrile-copper formation constants into the model in table 8 did not change the refined β_1 values. The extent to which acetonitrile can participate in ternary complex formation with the peptide-Cu(I) complex is unknown and is not addressed in these experiments. For this reason, we note that the constants described for Cu(I) and hCtr1 model peptides are apparent constants and are limited in that they may not reflect the value of purely conditional pH-dependant constants.

$$Cu^+ + BCA \xrightarrow{\beta_1 = K_1} Cu(BCA)$$ **Equation 28**

$$\beta_1 = K_1 = \frac{[CuBCA]}{[Cu][BCA]} = 10^{7.4}$$ **Equation 29**

$$CuBCA + BCA \xrightarrow{K_2} Cu(BCA)_2$$ **Equation 30**

$$K_2 = \frac{[Cu(BCA)_2]}{[CuBCA][BCA]} = 10^{7.4}$$ **Equation 31**

$$Cu^+ + 2BCA \xrightarrow{\beta_2 = K_1 K_2} Cu(BCA)_2$$ **Equation 32**

$$\beta_2 = K_1 K_2 = \frac{[Cu(BCA)_2]}{[Cu][BCA]^2} = 10^{14.7}$$ **Equation 33**

$$Cu(BCA)_2 + P \xrightarrow{K_{ex}} PCu + 2BCA$$ **Equation 34**

$$K_{ex} = \frac{[PCu][BCA]^2}{[Cu(BCA)_2]}$$ **Equation 35**

Table 8. Model used for the competition of hCtr1 model peptides and BCA for Cu^{+} in HEPES buffer at pH 7.4 and up to 1% acetonitrile. $\log\beta_1$ solved by this model is an apparent values that does not account for the presence of HEPES or acetonitrile in solution.

Species	Log β	Cu *m*	NTA *l*	P *l*	H *h*	
CuP		1	0	1	0	refined
Cu(BCA)	7.3	1	1	0	0	Constant
$Cu(BCA)_2$	14.7	1	2	0	0	Constant

Ascorbate Dependent Reduction of Cu(II) complexes of hCtr1 model peptides.

The reducing agent, ascorbic acid, was added to Cu(II) complexes of hCtr1 model peptides to determine the effect of the HH site on the copper redox. Peptides containing an ATCUN site with similar Cu^{2+} binding constants, but changes in the fifth or sixth histidine or methionines were compared for the ability of their Cu(II) complex to be reduced by ascorbate and/or the ability of the peptide to stabilize Cu(I) upon reduction. In a 1 cm quarts cuvette, 600 μM peptide and 500 μM $Cu(ClO_4)_2$ were combined in 50 mM HEPES buffer at pH 7.4. Two equivalents of ascorbate (1 mM) were added to solution and changes in the absorbance of the Cu(II) peptide complex at 525 nm was monitored over 1 hour with a Cary 50 UV-Vis. Ascorbate stock solution (10 mM) was made fresh each day and kept in the dark.

3. Extracellular His domains are Required for Cellular Copper Acquisition in a Mouse Cell Model.

3.1 Background and Significance

Yeast and mammalian studies of Ctr1 have shown that conserved methionines in transmembrane domain 2 (TMD2) are essential for copper transport function. In addition, a conserved Mets motif in the N-terminal region is important for high affinity copper acquisition under copper-limiting conditions. Despite the well-established role of histidine in protein copper binding sites, as well as the conserved nature of Ctr1 N-terminal His across several metazoan species (Figure 18), a role for the N-terminal His clusters in hCtr1 has not been found.[156] Yeast, insect, and human cells expressing mutant hCtr1 lacking extracellular His clusters have demonstrated no significant difference in Cu uptake compared to cells expressing native or wild type Ctr1.[156, 166] These results coupled with the fact that yCtr1 lack His domains has lead to the conclusion that the N-terminal His residues in mammalian Ctr1 have no functional significance for Cu transport.

Despite this evidence, it is intriguing that mammalian species contain conserved histidines in the domain responsible for copper recruitment. Even more interesting is that Ctr1 in Human, Chimp, Mouse, Pig, and Cow all contain a histidine as part of an ATCUN high affinity Cu^{2+} binding site at their N-terminus (Figure 18). Why would evolution select for mammalian Ctr1 containing an ATCUN site and/or other histidine rich clusters in their extracellular domain if they have no significance to protein function?

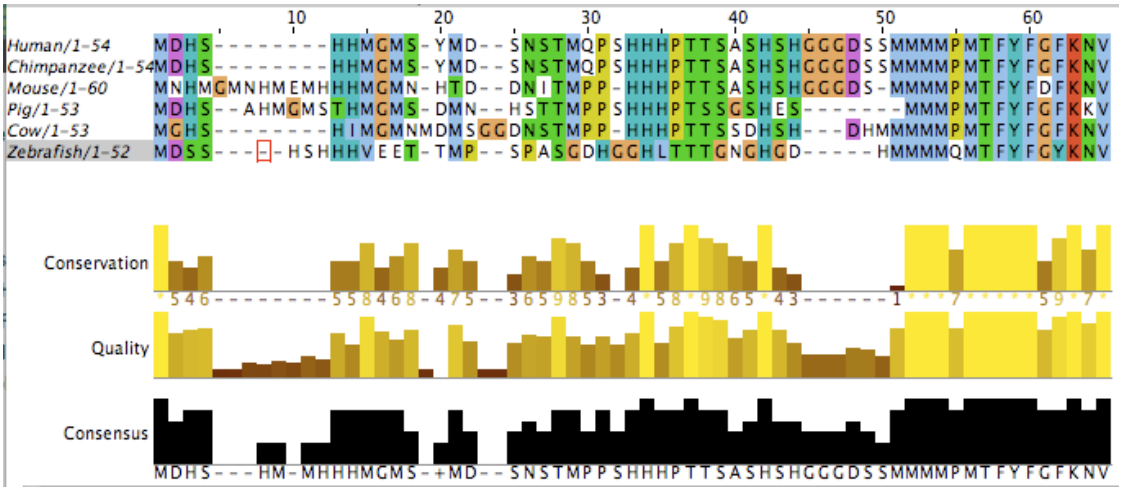

Figure 18. Sequence alignment of Ctr1 from several metazoan species shows conserved Met and His in the extracellular domain. Mammalian species have a conserved ATCUN site and other His-rich clusters in their N-terminal domain. The mammalian Ctr1 from dog and the Norway rat also have His-rich clusters, but they are exceptions in that they do not have an ATCUN site (not shown). Zebra fish and other metazoan species have His-rich clusters (chicken, roundworm not shown) and some even display ATCUN in addition to other His (mosquito, fruit fly not shown). This sequence alignment was generated with the web-based sequence alignment tool, ClustalW.

We have characterized copper binding properties of hCtr1 N-terminal His domains and Mets motifs and have demonstrated that His residues significantly increase copper binding affinity at physiological pH (Chapter 2). With this in mind, we set out to investigate the effect of mutation of the N-terminal hCtr1 His residues on live cells. Although hCtr1 has already been characterized in yeast, mammalian, and insect cell lines, [156, 166] full characterization has not yet been done in a mammalian Ctr1 knockout cell line. Here we are fortunate to have access to a mammalian Ctr1 knockout cell line, generated from Ctr1 null mice by the Thiele Lab at Duke University.[194] A Ctr1 knockout cell line serves as a more sensitive cellular model than was available during the Ctr1 biochemical characterizations originally done by Thiele and Kaplan in 2002.[156, 166] With this cell line it is possible to express a Ctr1 mutant protein exclusively, unlike in the past when mammalian Ctr1 studies were limited to over-expression of mutant Ctr1

in a native system that also expressed endogenous protein. The advantages of using a Ctr1 knockout cell line is demonstrated and discussed further in the following sections.

3.2 Results

3.2.1 Mutation of His to Ala in N-Terminal hCtr1 Causes Copper Deficiency.

Mouse embryonic fibroblast (MEF) cells, including wild type (wt), Ctr1 knockout ($Ctr1^{-/-}$) and , hCtr1 reconstituted ($hCtr1^{+/+}$) homogenous stable cell lines were generated previously.[194] A vector containing cDNA for an hCtr1 mutant with all N-terminal His mutated to Ala (hCtr1ntHA) was generated and expressed in $Ctr1^{-/-}$ cells. Homogeneous stable cell lines were tested by immunoblot protein analysis for expression of Ctr1 and CCS, a copper status indicator. CCS is the copper chaperone for Cu,Zn-superoxide dismutase (SOD) and shows an inverse relationship to copper status. Under normal or high copper conditions CCS is low, and under intracellular copper deficiency CCS is high (Figure 19a).

Mutation of extracellular histidine to alanine should not render the Ctr1 pore unable to transport copper, as is seen with mutation of the Mets motif found in TMD2.[156] Rather, we expect a phenotype consistent with decreased copper transport due to inefficient recruitment of copper to the pore opening. If this hypothesis is correct, we can expect that mutation of N-terminal extracellular His to Ala in the $hCtr1ntHA^{+/+}$ cell lines will partially rescue the copper deficiency seen in $Ctr1^{-/-}$ cells, but not to the same extent as rescue seen in the $hCtr1^{+/+}$.

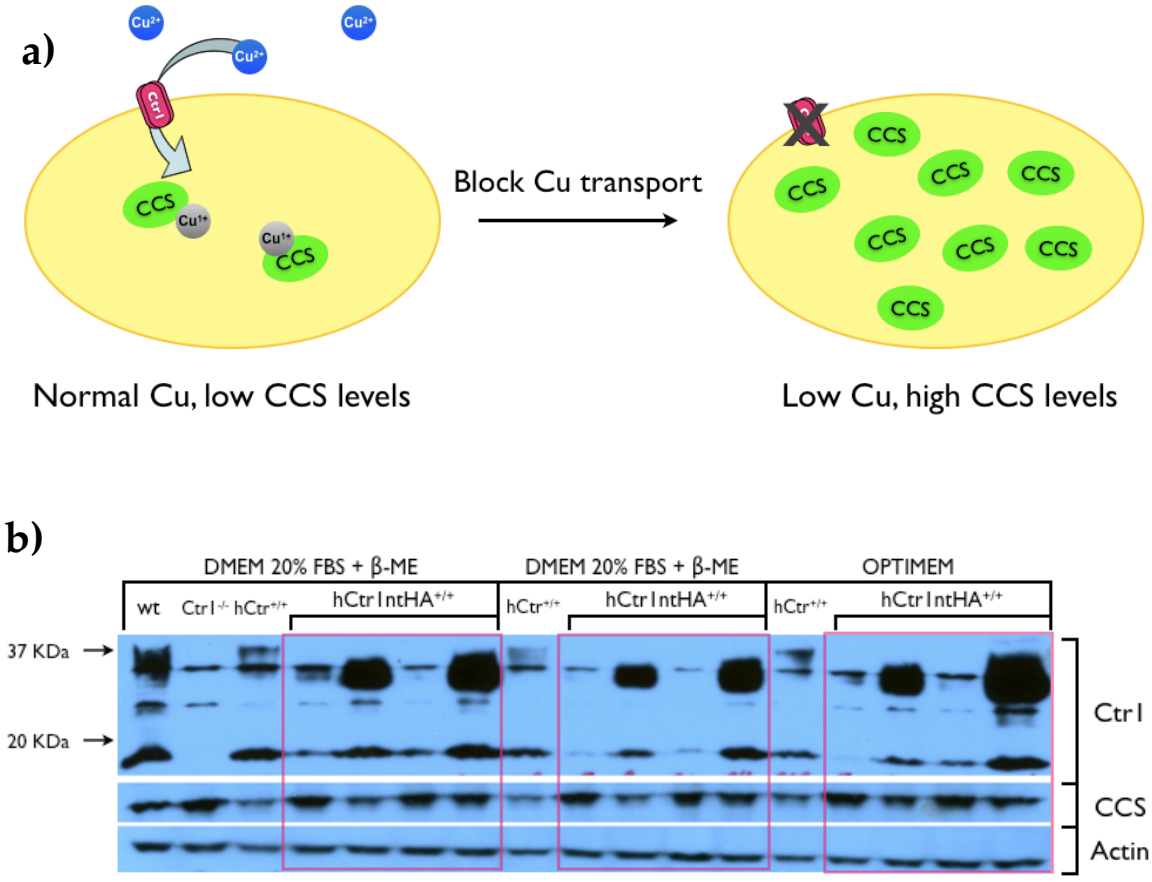

Figure 19. High CCS levels in hCtr1ntHA expressing cells indicate a copper deficient phenotype. a) CCS levels are indicative of intracellular copper status. When copper status is normal, CCS expression levels are low compared to when cells experience copper deficiency. Under intracellular copper starvation, CCS is stabilized and accumulates. b) Immunoblot showing expression levels of proteins recognized by antibodies against Ctr1, CCS and actin in wild type (wt) MEF cells, Ctr1 knockout MEF cells ($Ctr1^{-/-}$), hCtr1 reconstituted stable MEF cells ($hCtr1^{+/+}$) and the N-terminal hCtr1 H to A mutant stable cells (hCtr1ntHA). Cells expressing hCtr1ntHA have high CCS levels compared to the $hCtr1^{+/+}$ control, indicating that His mutation causes an intracellular copper deficiency.

Cell lines were grown in 1) DMEM containing 20% fetal bovine serum (FBS) with or 2) without the reducing agent, 2-mercaptoethanol (beta-mercaptoethanol, β-ME) and 3) Opti-MEM without FBS or β-ME. The different medias were used to ensure that copper availability (in FBS) and presence of the reducing agent (β-ME) did not affect the experiment. In the blot shown in Figure 19b, wild type MEF cells and cells stably expressing hCtr1$^{+/+}$ and hCtr1ntHA$^{+/+}$ all display a protein that is recognized by the specific Ctr1 primary antibody. This Ctr1 antibody recognized several bands. The lowest band around 19 KDa is attributed to the deglycosylated (and perhaps truncated)[195, 196] Ctr1 monomer. The higher group of bands around 35 KDa can be attributed to various N-linked and O-linked glycosylation states as well as potential Ctr1 dimer formation. Cells expressing mutant hCtr1ntHA show various levels of mutant Ctr1 expression, but all show higher CCS levels compared to the hCtr1$^{+/+}$ control. This phenomenon did not depend on the media used, but was perhaps more obvious when cells were incubated in copper-deficient Opti-MEM for 24 hours. These data indicate that the cells expressing the hCtr1ntHA mutant have lower copper levels than cells expressing hCtr1. This phenotype was consistent over several experiments. Please note that the MEF wt control in Figure 19b shows higher CCS levels than expected and this result was not consistent across experiments. Normally, CCS level in wt cells is similar to that in hCtr1$^{+/+}$ cell line (Figure 20).

To further confirm that the cells expressing hCtr1ntHA were demonstrating a phenotype consistent with copper deficiency, an experiment using standard media (DMEM with 20%FBS and β-ME) was repeated for quantitative analysis. As seen in Figure 20, four different homogenous stable cell lines expressing the hCtr1ntHA mutant protein showed intermediate CCS levels compared to Ctr1$^{-/-}$ cells and wt MEF or hCtr1$^{+/+}$ cells. These data are consistent with an intermediate copper deficiency in cells

a)

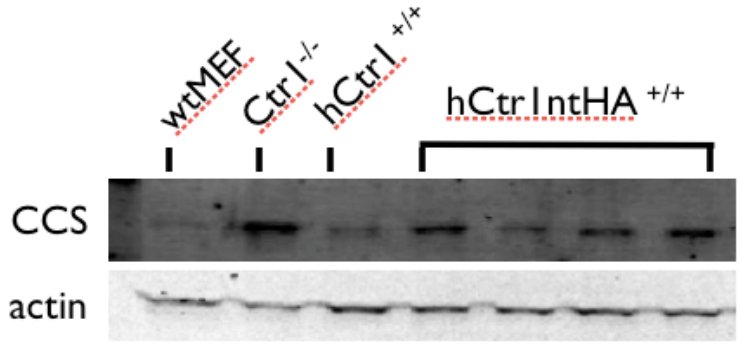

b)

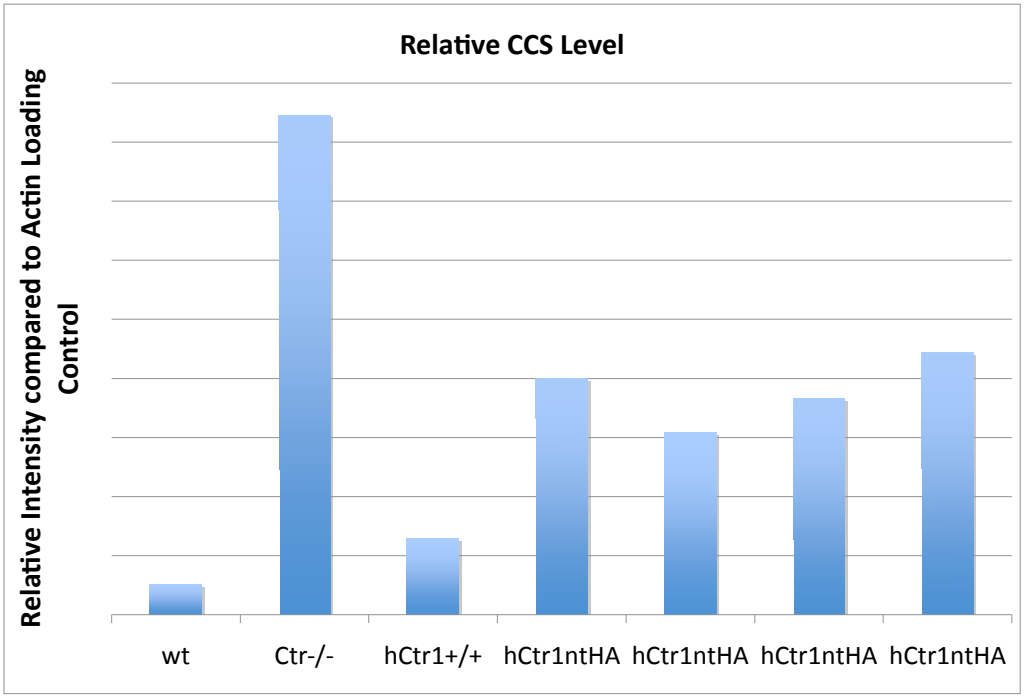

Figure 20. Quantitative analysis of CCS protein levels relative to loading control. a) Immunoblot probed for CCS and actin by Li-COR protein quantification protocol. b) Quantified CCS protein levels relative to actin loading control protein levels.

expressing the His to Ala mutant Ctr1. This quantitative result supports our hypothesis that hCtr1ntHA mutant protein is functional, but less efficient, at recruiting or transporting copper than is its native protein counterpart.

Presented here is the first evidence for functional significance of any of the N-terminal His domains in hCtr1 or any Ctr protein. Due to the importance of His for a high affinity copper binding site for hCtr1 model peptides in vitro (Chapter 2), it is likely that His to Ala mutation lowers the binding affinity of hCtr1 and renders it less efficient at competing for copper with extracellular chelators. This diminished affinity for copper would lower the local concentration of copper at the opening of the hCtr1 pore leading to less copper transport through the membrane. Although this theory predicting lower transport efficiency based on weakened N-terminal copper binding can explain the phenomenon that we see in Figures 19 and 20, it is not the only possible explanation for the copper deficient phenotype observed. Copper transport could also be affected if the mutation of His to Ala caused other physiological changes in the protein and affected its glycosylation state, ability to form multimers, localization status, or copper-stimulated endocytosis. These potential issues are addressed in the following sections.

3.2.2 MEF hCtr1ntHA Demonstrates Plasma Membrane Localization

Immunofluorescent microscopy was employed in order to determine the localization status of the hCtr1ntHA mutant in MEF cells. Cells were fixed and permeabilized in 1:1 MeOH:Acetone and probed with Ctr1 primary antibody. Secondary antibody covalently linked to a Green Fluorescent protein was used to visualize Ctr1 and assess its location in the cells.

Cells expressing hCtr1ntHA mutant show Ctr1 localization similar to wild type and hCtr1$^{+/+}$ cells. The even distribution of signal in hCtr1ntHA mutants is typical of the plasma membrane localization seen for Ctr1.

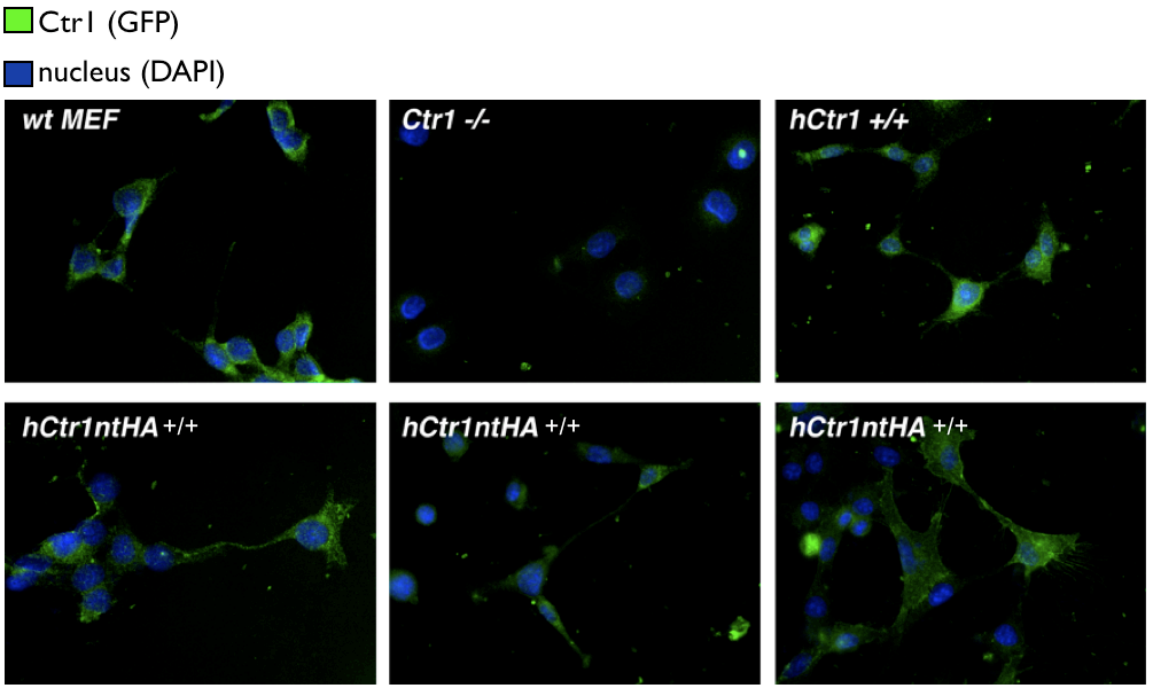

Figure 21. Immunofluorescent imaging of Ctr1 expression in various cell lines. Fixed cells were probed with specific primary antibody for Ctr1 and secondary antibody fused to GFP (green). Slides were mounted with DAPI stain to visualize the nucleus (blue).

3.2.3 hCtr1ntHA Mutant Displays Normal N-Glycosylation Status and Multimerization

Evaluation of N-terminal N-glycosylation status was done using the N-glycosidase, PNGaseF. Cell lysates were incubated at 37°C for 72 hours with or without PNGaseF enzyme and Ctr1 protein mobility on an SDS-PAGE gel was assessed by protein immunoblot analysis. Two exposures of the same immunoblot for Ctr1 are shown in Figure 22. hCtr1ntHA mutants show normal N-glycosylation status, as can be seen by the shift in band size from about 36 KDa to about 27 KDa.

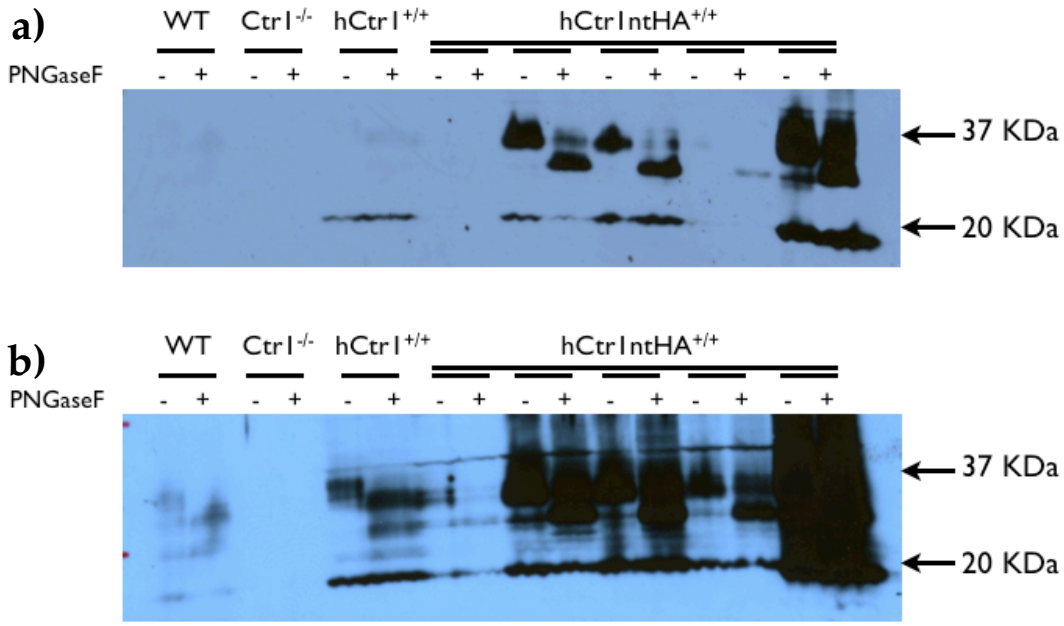

Figure 22. Ctr1 mobility changes in the presence of an N-glycosidase. Immunoblot probed with anti-Ctr1 antibody and exposed to film for a) 2 min and b) 10 min after adding HRP-fused secondary antibody and Luminol with stable peroxides. Shift of the bands around 36 KDa after treatment with the N-glycosidase, PNGaseF, indicate that the proteins are N-glycosylated. A shift can be seen in b) for wild type mCtr1 (WT), hCtr1 (hCtr1$^{+/+}$) and the His to Ala mutant hCtr1 (hCtr1ntHA). In a) the shift is more clear for mutant hCtr1ntHA.

It is debatable whether the lower band around 19 KDa seen in this blot is due to Ctr1 deglycosylated monomer or due to unglycosylated monomer that has been truncated at its N-terminal due to the lack of O-linked glycosylation-dependent

protection from proteolytic degredation.[195, 196] It is clear that the removal of N-linked sugar by PNGaseF does not shift the wt or hCtr1ntHA mutant band to this position around 19 KDa, so we may presume that the O-glycosylation status of these mutants is also normal. Loading controls were not assessed in this experiment since it is sufficient to see a qualitative shift in the Ctr1 band due to deglycosylation. Loading differences can explain the variation in amount of protein seen on these membranes.

Multimerization status of the proteins was assessed by loading identical protein samples with and without the reducing agent, 2-mercaptoethanol (Figure 23). The reducing agent should reduce disulfide bonds that might form between Ctr1 multimers and demonstrate whether the protein band around 36 KDa is partly due to dimerization. There is no obvious change in the 36 KDa band with 2-mercaptoethanol compared to without the reducing agent for either native Ctr1 proteins or mutant. From this we can conclude that the bands around 36 KDa are due mainly to glycosylation of the Ctr1 monomers or that the reducing conditions were not sufficient to affect dimer formation. There is a change, however, in the intensity of a band just above 50 KDa that corresponds to the mass of glycosylated hCtr1 dimer. The intensity of this band changes depending on the presence of reducing agent, indicating the presence of intermolecular disulfide bonds (Figure 23). This band is not seen in the wt or $Ctr1^{+/+}$ cells, probably due to the much higher Ctr1 expression levels seen for the mutants here. The change in intensity of the 50 KDa band indicates that the hCtr1ntHA mutants are capable of forming multimers and that the added 2-mercaptoethanol is sufficient for disulfide bond reduction.

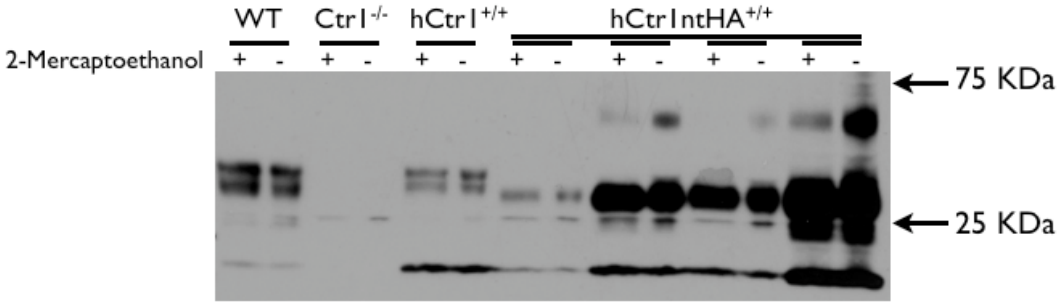

Figure 23. Ctr1 mobility does not change with reducing agent. Immunoblot probed with anti-Ctr1 antibody. No obvious difference is seen between WT, hCtr1$^{+/+}$ and mutant hCtr1ntHA mobility in the band at 36 KDa with and without reducing agent added to cell lysate before loading on SDS-PAGE gel. In highly expressing mutant cells, a higher band around 60 KDa shows decrease in intensity with addition of reducing agent. The presence of this band and its decrease with reducing agent indicates that mutant protein can form multimers.

3.2.4 Discussion

The data presented here demonstrate for the first time a phenotype associated with mutation of the extracellular N-terminal histidines in hCtr1 or any Ctr protein. We show that cells expressing the hCtr1ntHA mutants demonstrate a phenotype consistent with an intermediate copper deficiency relative to cells expressing fully functional native Ctr1 or hCtr1. We have investigated the effect of this mutation on plasma membrane localization, multimer formation, and glycosylation status of the mutant Ctr1 protein and found no evidence to suggest that hCtr1ntHA mutant is being processed differently from native protein. Based on spectroscopic characterization of hCtr1 N-terminal model peptides binding to copper at physiological pH, we can predict that the defect in hCtr1ntHA function is most likely due to the loss of high affinity extracellular histidine copper binding sites.

Loss of high affinity binding sites at the N-terminal of hCtr1 should not block the protein's transport function, but should inhibit its ability to acquire copper from other extracellular copper binding proteins. The intermediate phenotype that is copper deficient compared to cells expressing wild type hCtr1, yet still have higher copper

levels than Ctr knockout cell lines, is consistent with a mutant protein that is less efficient at acquiring copper, yet retains fundamental transport function.

The discovery that hCtr1 N-terminal His domains are important for copper acquisition in cells has an important impact on the current dogma for copper transport in mammalian systems. The current model implies that Ctr1 Mets motifs are the only important domains for high affinity copper acquisition, and that an unidentified reductase is necessary for copper reduction. Here we suggest adjustment to the current model that allows for potential hCtr1 competition with extracellular proteins for copper binding (Figure 24). In addition, evidence from Chapter 2 suggests that albumin or hCtr1 itself might have the ability to facilitate copper reduction in the presence of physiological reducing agents, like ascorbate. This new mammalian model is different from the model of yeast copper acquisition in that Ctr1 at mammalian physiological pH of 7.4 requires histidine for Ctr1 extracellular copper acquisition. Yeast survive in an acidic environment and would have no use for histidine, which binds copper in a pH-dependent manner. Yeast might also have no need for a copper transporter with high affinity binding sites, since copper can be loosely bound by proteins or soluble in its aquated form at low pH.

If human Ctr1, and possibly other mammalian Ctr1, requires His residues for copper recruitment, why has functional significance for these histidines not been found in previous mutagenesis studies of this protein? In fact, hCtr1 has been thoroughly studied by at least two independent research groups, and both found that hCtr1 His mutation to Ala did not affect protein function and had no associated phenotype.[156] Why only now are we able to show that the His to Ala mutation of hCtr1's N-terminal domain yields an intermediate copper deficiency?

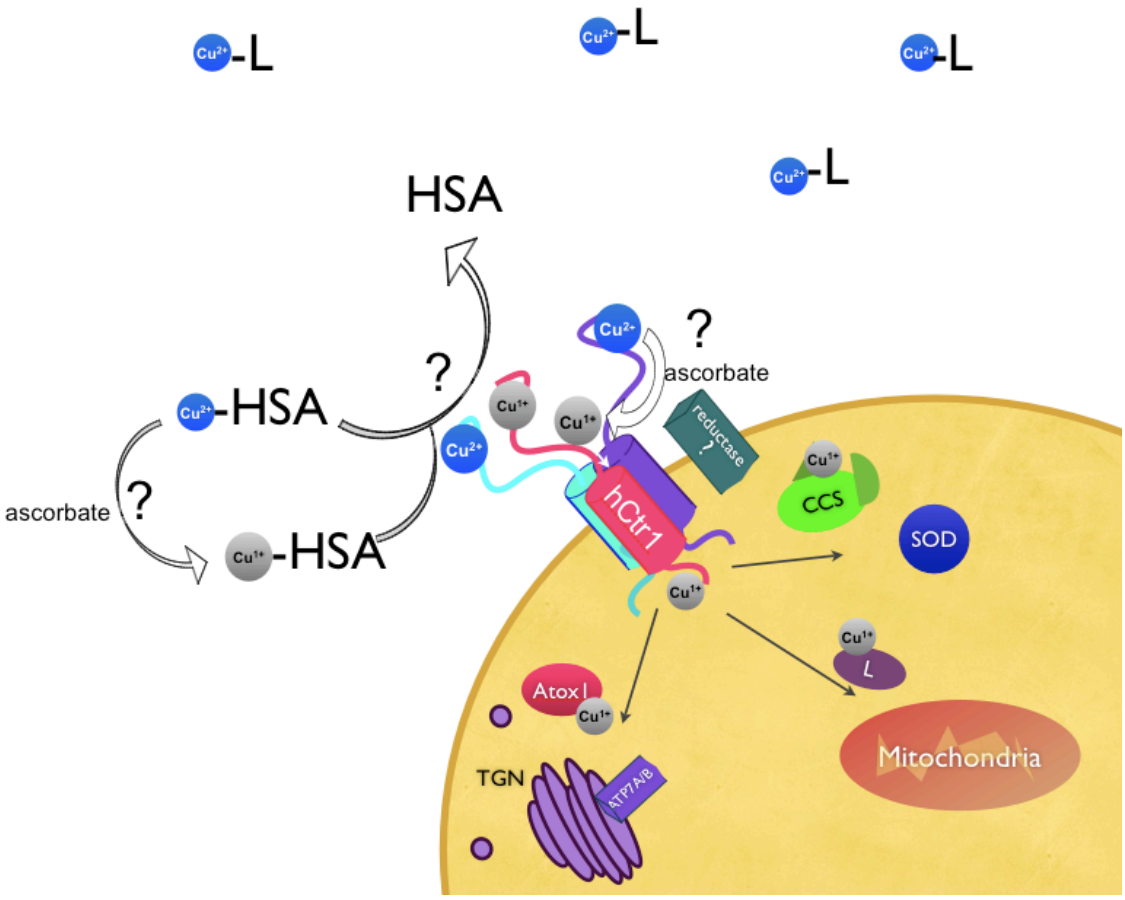

Figure 24. New model for human Ctr1-dependant cellular copper acquisition. Based on data presented in Chapters 2 and 3, we present a revised model for human copper acquisition by hCtr1. This new model includes potential Cu^{2+} as well as Cu^{+} binding to the N-terminal of hCtr1 ATCUN and His-rich clusters. In addition, a cell surface reductase may not be necessary in the presence of extracellular ascorbate reducing agent and potential facilitation of Cu(II) reduction when bound to either HSA or hCtr1. Further investigation is recommended to clarify the mechanism of copper reduction and the role of extracellular hCtr1 histidines in copper acquisition, reduction, and transport.

One potential reason that human Ctr1 histidines have been overlooked is that the founding members of the Ctr family were discovered in yeast. The best-studied Ctr1 protein is yeast Ctr1, which does not have extracellular histidine domains. In studies of both yCtr1 and hCtr1, emphasis was placed on the role of the methionines that are conserved across several species and necessary for Ctr1 function. However, despite the lack of histidine in yCtr1, the extracellular histidines in hCtr1 were not ignored.

The biochemical characterization that laid the groundwork for our understanding of hCtr1 was partly done in yeast model studies.[156] Yeast are excellent model organisms for studying a wide variety of basic biological mechanisms. We use a reductionist approach when employing yeast as a model for the biological processes of more complicated organisms, but in biology this approach is necessary and has proven fruitful. In fact, many biological processes in yeast are conserved in mammals, including the intracellular copper transport pathways. For this reason and the ease of genetic mutation, yeast are quite useful as a model for human biology. In the case of hCtr1 functional analysis, however, there is a flaw in the model that has likely interfered with the recognition of the role of extracellular hCtr1 histidines in copper transport function. That flaw is simply due to a difference in the extracellular environment between yeast and mammalian cells.

Yeast are well-known to acidify their extracellular environment to below pH 4 for optimal nutrient absorption. Growth of yeast cells is dependent on a pH gradient across the cell membrane that drives active transport of nutrients by H^+-symport.[197-199] At pH higher than 6.5, the yeast metabolism would likely slow down from lack of metabolite absorption. This is relevant to our discussion about extracellular His because His binding to metal is pH-dependent. The pK_a of the imidazole nitrogen is 6.0, and at low pH metal binding to this important nitrogen is blocked by protonation. As

discussed in previous sections, the histidine binding to copper, and especially binding by the ATCUN motif, is dependent on the anchoring ability of the histidine imidazole nitrogen. At pH below 6, where imidazole nitrogen would be protonated, His would no longer act as a copper binding residue. In other words, at the low pH in the extracellular environment of a yeast cell, His would be almost useless as a copper-binding residue. With this consideration, it is not surprising that studies of hCtr1 in yeast have found no role for extracellular Ctr1 histidines. It is also not surprising that yeast lack His in their N-terminal domain of Ctr1. Extracellular His would serve no Cu-binding purpose for the yeast.

In contrast, the extracellular environment of most human and mammalian cells is higher. At physiological pH of 7.4, His is a good ligand for copper. The presence of conserved His in the extracellular domains of mammalian copper transporters suggest that histidine might be involved in mammalian copper acquisition.

In the first several years of the hCtr1 saga, two groups independently performed biochemical characterizations of the protein in different model organisms. The Thiele lab at Duke University pioneered investigations of hCtr1 in yeast and set the foundation for our knowledge of Ctr proteins. Their characterization of hCtr1 was thorough in that it included studies not only in yeast, but also in the human model cell line, HEK293.[156, 157] Later, the Kaplan group performed a similar biochemical characterization in an insect model cell line, Sf9.[166, 167] The results from human and insect models were consistent with the yeast model and confirmed that the extracellular histidines were not necessary for hCtr1 function. There are several reasons why an intermediate phenotype, like the one described above, may not have been noticed in these original mammalian and insect model studies.

The Thiele lab did their pioneering work on hCtr1 in 2002. Since then there have been improvements in technology and great improvements of our understanding of hCtr1. For example, 2002 predates the use of a Ctr1-specific antibody. To recognize Ctr1 protein on the cell membrane or in an immunoblot, fusion proteins containing an N-terminal myc tag were used so that the Ctr1 protein could be identified using immunohistochemistry.[156, 166] Although use of myc-tags for identification of proteins using immunoblots and immunofluorescent imaging is a well-established technique that usually interferes minimally with most proteins, in this case it may have caused a significant drop in the protein's ability to bind Cu^{2+}. The addition of an N-terminal myc-tag to hCtr1 would essentially remove the ATCUN site from the protein. We have shown in Chapter 2 that capping of the N-terminal of an hCtr1 model peptide decreases its binding affinity by about two orders of magnitude.

If the ATCUN site is important for hCtr1 function, then studies of hCtr1 using an N-terminal myc tag would have a less efficient copper transporter to begin with. Mutation of His on the myc-tagged protein may yield an only slightly more defective protein. One could expect to see a smaller difference in phenotype between myc-tagged native hCtr1 and myc-tagged mutant protein compared to the difference when starting with the hCtr1 protein containing the intact ATCUN site. Because the phenotype difference between cells expressing hCtr1 and hCtr1ntHA is small even when the N-terminal ATCUN is not compromised in control cell lines (see data above), perhaps the phenotype for His mutation or N-terminal truncation was overlooked when it was compared to the myc-tagged hCtr1 control.

In addition to using myc-tagged proteins, when the hCtr1 characterizations were done both Thiele and Kaplan overexpressed hCtr1 in wild type mammalian and insect cell lines. These wild type cell lines also produced a level of endogenous fully functional

Ctr1. The practice of overexpression of Ctr1 could complicate experimental results due to heterotrimerization of endogenous and exogenous Ctr1 monomers (Figure 24a). It is unknown to what extent the functionality of the Ctr1 pore would be affected by substitution of only one or two native proteins by mutant. In the case of N-terminal His mutation or truncation, the transmembrane pore should be fully functional despite hetero or homotrimerization. We do not know the exact mechanism of Ctr1 copper acquisition, or whether it requires three intact N-terminal domains, or only one. It is likely however, that the possibility of heterotrimer formation could interfere by making the system less sensitive.

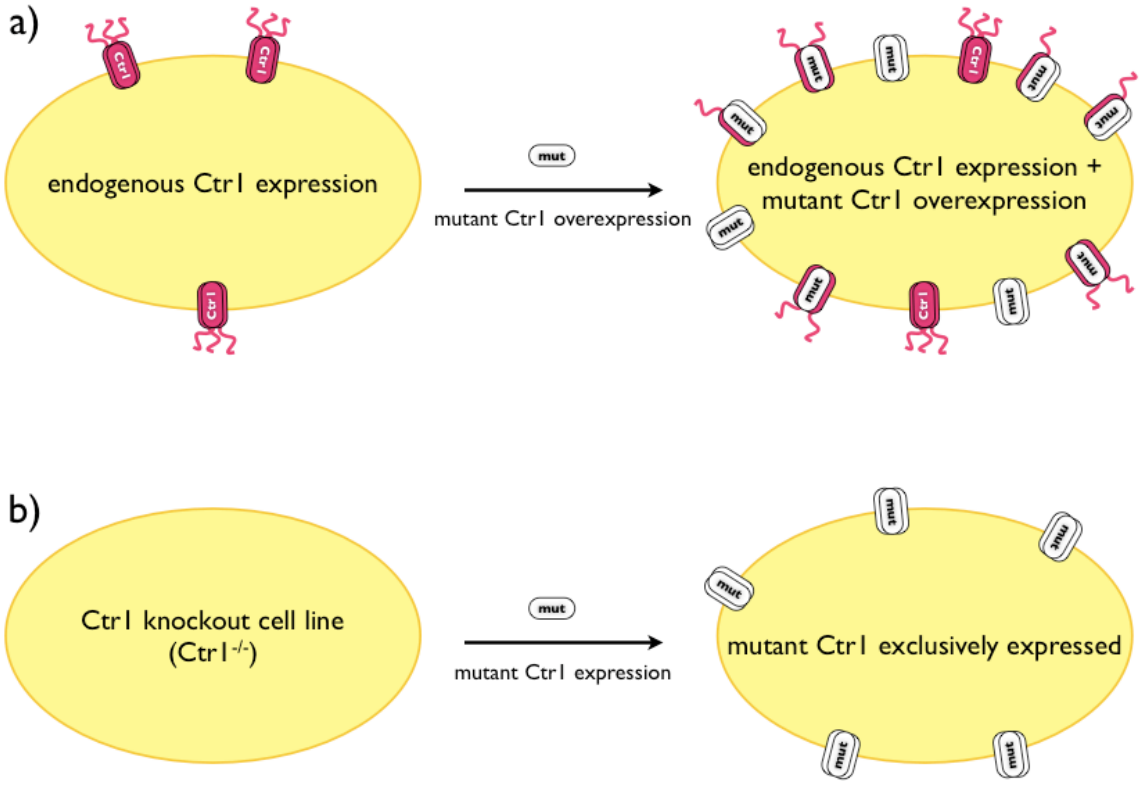

Figure 25. Overexpression of mutant Ctr1 in cells that express endogenous Ctr1 (a) is less sensitive than exclusive expression of mutant protein in a Ctr1 null cell line (b).

Fortunately, a more sensitive model system is now available. The Thiele lab has since generated the Ctr1 null ($Ctr1^{-/-}$) MEF cell line discussed above.[194] This cell line offers a blank slate for expression of wild type or mutant Ctr1, and the potential complication of heterotrimer formation can be avoided (Figure 24b). This more sensitive system has been used in the experiments in this work to exclusively express wild type hCtr1 or mutant hCtr1ntHA, both with an intact N-terminal ATCUN site.

We are fortunate to have access to both the more sensitive $Ctr1^{-/-}$ model cell line and the Ctr1 specific antibodies generated by the Thiele Lab. Using these more sensitive tools, we have repeated past experiments and found a phenotype that was missed before. The significance of ATCUN and other His in the N-terminal domain of hCtr1 and other mammalian Ctr1's has been brought to light, but is not yet fully understood. We still do not know whether the ATCUN site alone is important for copper acquisition and whether hCtr1 uses this site to compete for copper from extracellular copper carriers, like HSA. We do not fully understand the coordination of Cu^{+} and the role of hCtr1 or HSA in facilitation of copper reduction. Hopefully this work has provided some answers about the mechanism of human cellular copper acquisition, but has also stimulated new questions for future investigation.

3.3 Materials and Methods

Generation and Growth of Cell Lines

Mouse embryonic fibroblast (MEF) cells derived from wild type mice, MEF cells harboring mCtr1 deletion derived from $Ctr1^{-/-}$ mice (MEF $Ctr1^{-/-}$), and MEF Ctr1 knockout cells stably transfected with pcDNA3.1(+) expressing wild type human Ctr1 cDNA under control of the cytomegalovirus promoter (MEFΔhCtr1$^{+/+}$) were a generous gift from Dennis J. Thiele (Dept. of Pharmacology and Cancer Biology, Duke

University).[194] MEF cell lines were cultured in Dulbecco's modified eagle medium (DMEM (Invitrogen catalog # 11995) supplemented with 20% fetal bovine serum (FBS, Gibco), 100 units/mL penicillin, 100 μg/mL streptomycin, 1X nonessential amino acids (Gibco) and 55 μM 2-mercaptoethanol. To facilitate mitochondrial function under potentially low intracellular copper concentrations, 1 mM sodium pyruvate, and 0.5 μg/L uridine were also added to culture medium.[194] Where noted, 2-mercaptoethanol was omitted from media or cells were cultured in Opti-MEM supplemented with 100 units/mL penicillin, 100 μg/mL streptomycin, 1 mM sodium pyruvate, 0.5 μg/mL uridine, and 1X non-essential amino acids. Cells were split using 0.05% Trypsin incubated at 37°C for 2 min.

A pcDNA3.1(+) plasmid containing myc-tagged hCtr1 DNA with His cluster H1 (HSHH) mutated to A (ASAA) was gifted from the Thiele Lab.[156] The hCtr1 N-terminal protein contains two other histidine clusters, which were mutated to alanine using hCtr1-specific primers sets hCtr1H2A and hCtr1H3A listed in Table 9. The H2 (HHH) cluster was mutated to alanine (AAA) using primers hCtr1H2A and hCtr1H3A-F and -R and the H3 (HSH) cluster was mutated to alanine (ASA) using primers hCtr1H3A-F and -R (Table 9) in two steps using a Quikchange® Multi Site-Directed Mutagenesis Kit (Stratagene) and a standard Quikchange® PCR protocols. In each case, after mutagenesis, the 25 μL reaction was digested with 1 μL DPN1 enzyme, ethanol precipitated and taken up in 10 μL of elution buffer. This entire sample was transformed into XL10-Gold® Ultracompetant Cells (Strategene) and cells were incubated on LB plates containing ampicillin for 16 h at 37 °C. Individual colonies were inoculated into separate sterile culture tubes containing 3 mL of LB media plus ampicillin and incubated 16 h at 37 °C. Plasmid DNA was harvested with QIAprep Spin Miniprep Kit (QIAGEN). The hCtr1 insert was amplified using primers from table X to

remove the myc tag and add appropriate restriction sites, XhoI and EcoR1, for ligation of the insert into pcDNA 3.1 zeo (+) plasmid (Invitrogen). DNA was transformed into XL10-Gold Ultracompetant Cells and purified using Miniprep DNA kit. Miniprep DNA was then sequenced to insure proper mutation and amplification.

Table 9. DNA mutagenesis and amplification Primers

Primer/Set	Sequence
hCtr1H2A-F	5′-ATGGACTCCAACAGTACCATGCAACCTTCTGCCGCTGCCCCAACCACTTCAGCC-3′
hCtr1H2A-R	5′-GGCTGAAGTGGTTGGGGCAGCGGCAGAAGGTTGCATGGTACTGTTGGAGTCCAT-3′
hCtr1H3A-F	5′-CACCCAACCACTTCAGCCTCAGCCTCCGCTGGTGGAGGAG-3′
hCtr1H3A-R	5′-CTCCTCCACCAGCGGAGGCTGAGGCTGAAGTGGTTGGGTG-3′
hCtr1HA_EcoR1-F	5′-ATATGAATTCATGGATGCCTCCGCCTCCGCCGCCAT-3′
hCtr1HA_XhoI-R	5′-ATATCTCGAGTCAATGGCAATGCTCTGTGATATCC-3'

MEFΔCtr1$^{-/-}$ were transfected by electroporation with pcDNA3.1zeo(+) vector containing a Zeocin™ (Invitrogen) antibiotic resistance gene and the hCtr1ntHA cDNA under control of the cytomegalovirus promoter. Transiently transfected cells were put under selective pressure for stable expression using 750 μg/mL Zeocin™ (Invitrogen) antibiotic until all non transfected cells under the same Zeocin™ treatment were dead (~3 weeks). After selection, heterogeneous stable cells were trypsinized and harvested for selection of homogeneous stable cell lines. Cells were counted and plated in a 96 well plate at a density of 0.8 cells per well at a volume of 100 μL per well containing 750 μg/mL Zeocin™. After several days, approximately 30 wells contained viable stable cell lines. When cells became confluent, they were transferred in a graduated fashion to larger wells until there were enough cells of each homogeneous stable cell line to fill the wells of 6 well flat bottom plates. These cells were harvested and hCtr1ntHA expression was assessed. These mCtr1 knockout MEF cell lines stably expressing hCtr1ntHA

mutant DNA (MEF hCtr1ntHA$^{+/+}$) were selected for hCtr1ntHA expression levels similar to the expression level of hCtr1 in the MEF hCtr1$^{+/+}$ stable cell line.

Protein Isolation and Western Blotting Analysis

Confluent plates of MEF cells were rinsed two times with cold 1x PBS buffer then scraped from plates and pelleted by centrifugation at 15K rpm for 30 s. Pelleted cells were resuspended and incubated on ice for 30-60 min with 50-100 μL lysis buffer (1% TritonX100, 0.1%SDS, 1mM EDTA, and 1 cOmplete™ Mini EDTA-free protease inhibitor tablet (Roche) in 10 mL 1x PBS). Protein was isolated by centrifugation at 4°C and 15K rpm for 10 min. Supernatant was transferred to a clean 1.5 mL tube for protein quantification by using the Bio-Rad DC protein assay.

Samples were run on pre-cast Criterion Tris-HCl sodium dodecyl sulfite polyacrylamide gradient gels (Bio-Rad) using electrophoresis (SDS-PAGE) and transferred to a nitrocellulose or PVDF membrane. Where noted, loading buffer with and without 2-mercaptoethanol was used to determine multimerization of the hCtr1ntHA mutant compared to wild type. The membranes were blocked for at least 1 hour in 5% skim milk/TBS-T and allowed to incubate overnight in primary antibody diluted in blocking solution. Primary antibodies used are as follows: Rabbit anti-human Ctr1, described elsewhere,[200] was a gift from the Thiele lab and was used at 1:1000 dilution ; rabbit anti-CCS (FL-274) from Santa Cruz Biotechnology (1:200); mouse anti-CoxIV from Invitrogen (1:1000); mouse anti-Actin from BD Biosciences (1:1000); rabbit anti-Actin; rabbit anti-Tubulin. Secondary antibodies were donkey anti-rabbit and anti-mouse conjugated with horseradish peroxidase from Amersham Biosciences (1:5000).

Quantification of western blot data was performed using a Li-COR system and standard protocols.

N-Glycosidase Treatment

The comparison of N-glycosylation status of hCtr1 and hCtr1ntHA mutant protein was determined by treatment of total cell protein extract with N-Glycosidase F, also known as PNGaseF (New England Biolabs). A solution of 50 μg protein from cell lysate, 1 μL of 10x Glycoprotein Denaturing Buffer, and ddI H_2O at total volume of 10 μL was incubated for 10 min at 37°C. After incubation, 2 μL 10x G7 Buffer, 2 μL NP40, 2 μL PNGaseF enzyme and ddIH_2O were added to solutions to a new final volume of 20 μL. These solutions were incubated at 37°C for 72 hours and then directly loaded into precast gels for SDS-PAGE and Western Blot analysis as described above.

Immunofluorescence Microscopy

Cells were grown in 6 well plates for 24-48 hours on sterile glass cover slips. Cover slips were gently washed twice with 1 mL of cold 1x PBS and fixed for 30 seconds with 1:1 Acetone:ddI H_2O. Cells were permeabilized and blocked with 5% milk in TBS-T (contains 0.1% TritonX100) for 1 hour at room temperature. Protein was labeled using primary monoclonal antibody for hCtr1 raised in rabbit and a green fluorescent protein (GFP) labeled secondary anti-rabbit antibody. Confocal immunofluorescence microscopy was performed using a Zeiss Axio Observer wide field fluorescence microscope and images were processed using MetaMorph 7.5 system software at the Duke University Light Microscope Core Facility.

4. Caged Complexes for Selective Release of Copper[ii]

4.1 Background and Significance

Our desire to understand how the individual molecules that make up cells organize, interact, and communicate to form living systems has lead to the burgeoning field of chemical biology, an interfacial area of science that combines aspects of chemistry – the study of matter and its transformations, and biology – the study of living things and their interactions with the environment. The defining feature of chemical biology is the use of chemical approaches and small molecules to interrogate or manipulate biology.[201, 202] These small molecules can be synthetic or naturally occurring ones that, for example, bind to DNA to affect protein expression levels, bind to proteins to inhibit their function, interact with lipids to alter membrane integrity, or become fluorescent in response to a metabolic event. Small molecules are usually implied as being organic compounds that interact with biomolecules to alter or illuminate their function,[203] however, inorganic small molecules also have established a presence in biology. Because small molecules can affect biochemical function, there is a clear link to pharmacology and medicine[204] and there is also a long history of applying inorganic compounds to both biology and medicine. Ancient civilizations used gold and copper for healing purposes, and the modern era of drug discovery was ushered in when arsenic-containing salvorsan was discovered as an anti-syphilis agent to become the world's first blockbuster drug.[205] In many cases, inorganic compounds are particularly useful for probing or targeting biological systems due to their distinctive electronic, chemical, structural ,and photophysical properties.[17, 52, 206]

[ii] Parts of this chapter have been published in Ciesienski, K. L.; Haas, K. L.; Dickens, M. G.; Tesema, Y. T.; Franz, K. J., A photolabile ligand for light-activated release of caged copper. *J. Am. Chem. Soc.* **2008,** *130* (37), 12246. and Haas, K. L.; Franz, K. J., Application of Metal Coordination Chemistry To Explore and Manipulate Cell Biology. *Chem. Rev.* **2009,** *109* (10), 4921-4960.

While it is important to be able to use small molecule chelating agents to selectively reduce the concentration of bioavailable metals, as discussed in Chapter 1, it is also desirable to manipulate cellular metal ions by selectively increasing their concentration. Selective increase in a metal ion concentration in tissue culture experiments can be easily accomplished by adding a desired metal salt to the culture medium. This results in a global increase of a select metal ion.

It is also beneficial to deliver increased concentration of metal ion in a controlled way to a specific location in an organism or in a cell. The challenges associated with selective metal ion release have lead to a generation of caged metal complexes that are capable of releasing metal ions based on reactivity. The most well-developed compounds in this category belong to a class of molecules known as caged calcium, developed by both Tsien and Ellis-Davies.[26, 207, 208] These reagents operate by using light to trigger a chemical change that reduces a chelator's affinity for Ca^{2+}, thereby providing a sudden release of bioavailable Ca^{2+}. The chelating moieties are based on tetracarboxylate chelators BAPTA and EGTA that bind to Ca^{2+} with high affinity and sufficient selectivity over the most likely competing ions Na^{+}, K^{+}, and Mg^{2+}. Constructs based on EDTA are also available but do not discriminate Ca^{2+} from Mg^{2+} as effectively.

There are two general series of caged calcium, each using a different mechanism to reduce Ca^{2+} affinity, as shown in Figure 24a and b. In the nitr series (nitr-7, **16**), photoactivation converts the 2-nitrophenyl substituent to a more electron-withdrawing group that reduces the donor strength of a metal-binding nitrogen, thereby resulting in a 40-fold decrease in Ca^{2+} affinity.[209] In the series of compounds including NP-EGTA (**17**), a photoactive 2-nitrophenyl group is embedded into the backbone of the chelator so that illumination with UV light results in chelator fragmentation and a 40,000 – 600,000-

fold loss in Ca^{2+} affinity, depending on the derivative.[210, 211] There have been hundreds of studies that utilize caged calcium to explore biology.[26]

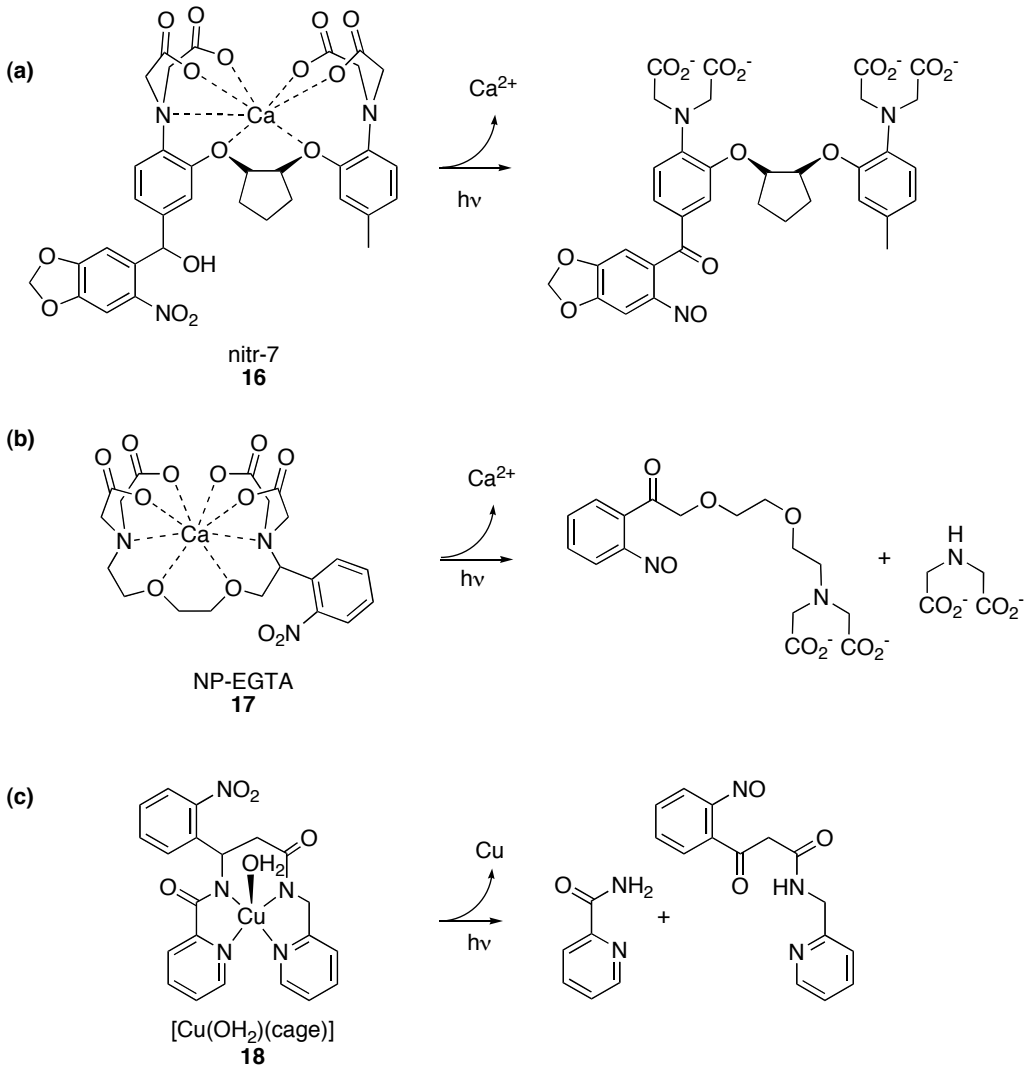

Figure 26. Photoactive Caged complexes that release metal.

The carboxylate-rich chelators DM-nitrophen and NP-EGTA used to cage Ca^{2+} have also been used for Sr^{2+}, Ba^{2+}, Mg^{2+}, Cd^{2+}, Mn^{2+}, and Co^{2+},[212] while photocleavable cryptands have been reported to release alkali ions[213] and a photoactive crown ether shows modest reversible photorelease of Sr^{2+}.[214] To the best of our knowledge, uncaging

biologically important d-block metal ions like iron, zinc, and copper using photoactive ligands had not been reported prior to our recent efforts.

In an effort to broaden the applicability of caged complexes to transition metals, our group has developed a series of photo-cleavable ligands that bind to Cu^{2+}.[40, 215] The redox activity of copper makes it an essential cofactor in numerous enzymes critical for life, but also renders it potentially toxic by promoting the formation of reactive oxygen species (ROS) that lead to cellular oxidative stress.[134, 216] As discussed in previous sections, understanding the trafficking pathways by which cells and organisms acquire, maintain, and utilize copper while suppressing its toxicity has important ramifications for health and disease.[138, 217] Copper's pro-oxidant property is also medicinally promising if it can be harnessed to induce oxidative stress as a cancer chemotherapy strategy.[218] New reagents that could deliver copper intracellularly in a site and time specific manner would therefore be useful both for targeted delivery of ROS-active agents and for delineating copper trafficking and utilization pathways. Toward these goals, we have designed and tested a series of caged copper complexes in which a photoactive nitrophenyl group is incorporated into the backbone of a high affinity copper chelator. Activation with UV light induces bond cleavage that releases components with lower affinity for copper compared to the intact complex (Figure 26c).

4.1.2 First Generation Caged Copper(II)

The design and synthesis of our first generation cage complex, as well as its pharmacological properties on living cells will be described in the dissertations of Katie Ciesienski and Lynne Heyman at Duke University. In short, by incorporation of a photocleavable nitrobenzyl group into the backbone of a copper chelator, light can be used as a switch for turning on metal-induced oxidative stress. In our first generation cage, H_2Cage (**18**) , two pyridyl groups were incorporated into a backbone containing

two other amide nitrogens that are capable of binding copper. The crystal structure of [Cu(OH$_2$)(cage)], is shown in Figure 27. [215] Two deprotonated amide nitrogens and two pyridyl nitrogens coordinate Cu^{2+} in a distorted trigonal bipyramidal geometry, with a water molecule lying in the trigonal plane at a Cu−O distance of 2.299(3) Å. The average Cu−N_{amide} distance of 1.943 Å and Cu−$N_{pyridine}$ distance of 2.034 Å are similar to other bispyridylamide Cu^{2+} complexes.[219-221]

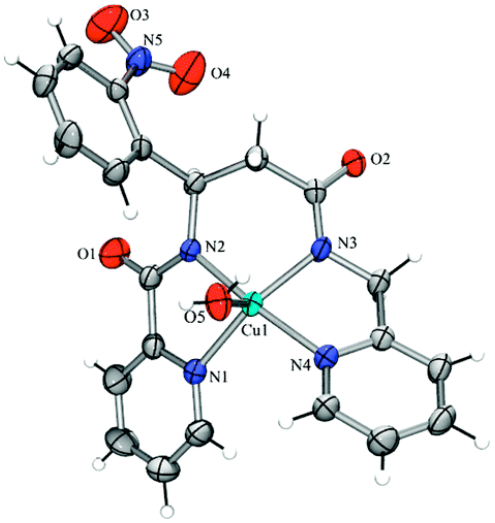

Figure 27. Crystal structure of [Cu(OH$_2$)(Cage)]

When solutions of [Cu(OH$_2$)(Cage)] in pH 7.4 phosphate buffer are exposed to 350 nm UV light (1-cm path length screw top quartz cuvette illuminated in a Rayonet RPR-100 Photochemical Reactor containing 16 bulbs, each 3500 Å) the ligand is cleaved within 4 minutes. The quantum yield of photolysis decreases from 0.73 for H_2Cage to 0.32 for [Cu(OH$_2$)(Cage)], indicating that coordination by Cu^{2+} decreases photolysis efficiency but does not prevent it. Exposure of either H_2Cage or [Cu(OH$_2$)(Cage)] results in the photoproducts shown in Figure 26c. The uncaged copper is likely bound to these photoproducts in solution, but with significantly diminished affinity compared to the

intact ligand **18**. Reduction to Cu^{1+} is also possible as a result of photolysis, although it would likely reoxidize to Cu^{2+} under these experimental conditions.

To show that photolysis of [Cu(OH_2)(Cage)] causes a change in the reactivity of the caged versus uncaged copper, the compound's pre- and post-photolysis ability to generate $OH^{\bullet}$ radicals was monitored by subjecting them to the deoxyribose assay. Hydroxyl radicals are generated in this assay by Fenton-like chemistry in the presence of copper, ascorbic acid, and H_2O_2. These hydroxyl radicals degrade deoxyribose to give thiobarbituric acid (TBA)-reactive products with absorbance at 532 nm. H_2Cage in the presence of Cu^{2+} provides 50% protection of copper-dependent deoxyribose degradation compared to the background reaction of adding Cu^{2+} alone. In the presence of Cu^{2+} the photoproducts increase the level of $OH^{\bullet}$ produced.

This new photoactive ligand can cage copper in a tetracoordinate binding site and upon activation with UV light uncages the metal cargo by cleaving the ligand backbone to release photoproducts with diminished affinity for Cu^{2+}. The ability of copper to undergo Fenton-like reactivity and promote $OH^{\bullet}$ formation increases by 160% following light-induced uncaging. This is a promising step in developing compounds that are triggered by light to increase oxidative stress.

As a potential therapeutic agent, it is critical that our caged copper complexes be stable under biological conditions. $Copper^{2+}$ is an intrinsically labile metal ion, which can be stabilized in complex with multidentate, thermodynamically stable chelators. The stability constants of H_2Cage with copper or other metal ions necessarily should be higher than other biological chelators. Understanding the thermodynamic properties of H_2Cage and other potential caging ligands and their metal complexes will allow us to predict complex stability in the presence of other biologically relevant metals and

chelators. The following sections describe the determination of copper binding constants for first generation and subsequent generation caged copper complexes.

4.2 Results

4.2.1 Potentiometric and Spectrophotometric Characterization of Copper Binding to H_2Cage

Potentiometric titration of H_2Cage and the copper complex,[Cu(OH_2)Cage], were preformed to determine the pK_a's of dissociable protons and the absolute β value for the association of Cu^{2+} and Cage. The potentiometric titration of the apo ligand, H_2Cage, (Figure 28) shows that it contains no dissociable protons between pH 2 and 12. This is not surprising, based on literature pK_a values of amide protons ($pK_a > 20$) and relevant substituted pyridine rings ($pK_a < 2$).[222]

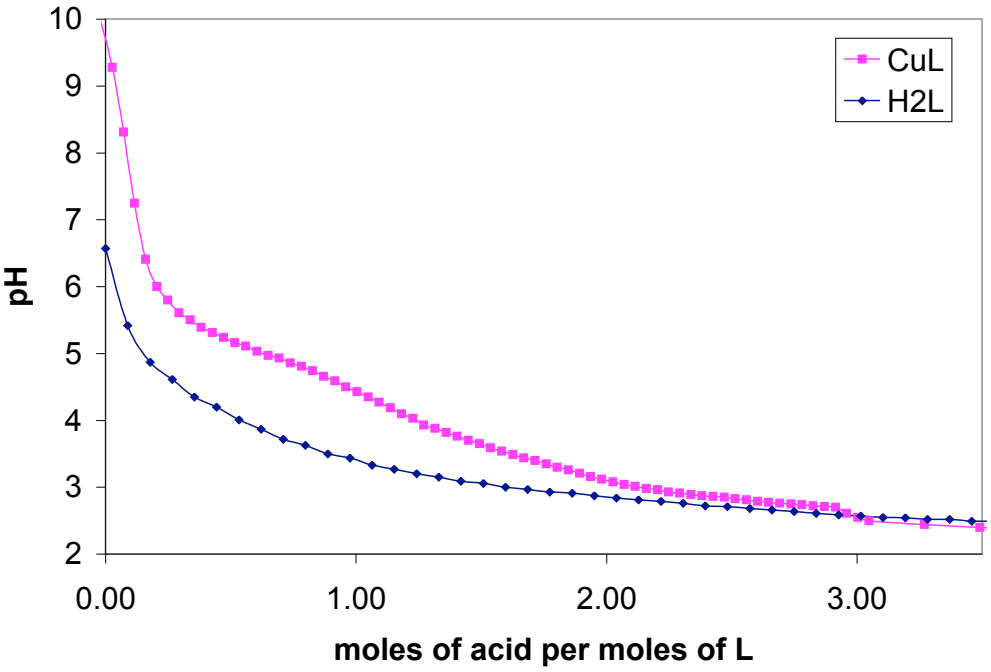

Figure 28. Potentiometric titration curves of H_2Cage and CuCage. Titration data for H_2Cage are shown as blue diamonds, [L] = 1.46 mM and titration data for CuCage are shown as pink squares, [CuL] = 1.33 mM), where L = $Cage^{2-}$. T = 25 °C, μ = 0.1 M $NaClO_4$.

Titration data for the 1:1 mixture of $Cu(ClO_4)_2$ and H_2Cage over the pH range from 2 to 12 shows that in the presence of Cu^{2+}, two protons are released from H_2Cage below pH 5, consistent with deprotonation of both amides (Figure 28). The pH-dependent spectra for the $[Cu(OH_2)(Cage)]$ complex is shown in Figure 29. These data were fit using Specfit software (Spectrum Software Associates, version 3.0.30) and Hyperquad software[223] according to the model in Table 10, where β is the absolute pH-independent binding constant for the association of L, Cu^{2+}, and H^+ defined by Equation 36 for the general equilibrium reaction in Equation 37 where L = $Cage^{2-}$. The Specfit and Hyperquad programs produced log β values of 15.63 and 18.96 for the CuLH and $CuLH_2$ species respectively, which correspond to the pKa values of 4.83 and 3.33. The deprotonation of a coordinated water molecule in $[Cu(OH_2)(Cage)]$ is not observable in the tested pH range. This is not surprising based on the known hydrolysis constants of copper[76] and the neutral character of $[Cu(OH_2)Cage]$. The calculated speciation curve is shown in Figure 29b.

$$\beta_{lmh} = \frac{[Cu_m L_l H_h]}{[Cu]^m [L]^l [H]^h} \qquad \textbf{Equation 36}$$

$$m\mathrm{Cu} + l\mathrm{L} + h\mathrm{H} \rightarrow \mathrm{Cu}_m\mathrm{L}_l\mathrm{H}_h \qquad \textbf{Equation 37}$$

Analysis of the pH-dependent spectrophotometric titration of a 1:1 mixture of H_2Cage and Cu^{2+} with Hyperquad software shows that the predominant species in solution from pH 5−12 is the neutral compound $[Cu(OH_2)(Cage)]$, with an overall stability constant of log $\beta_1 = 10.8$. The constant, β_1, is defined as the pH independent or absolute association constant. It is often denoted β_{lm} according to Equation 35 where

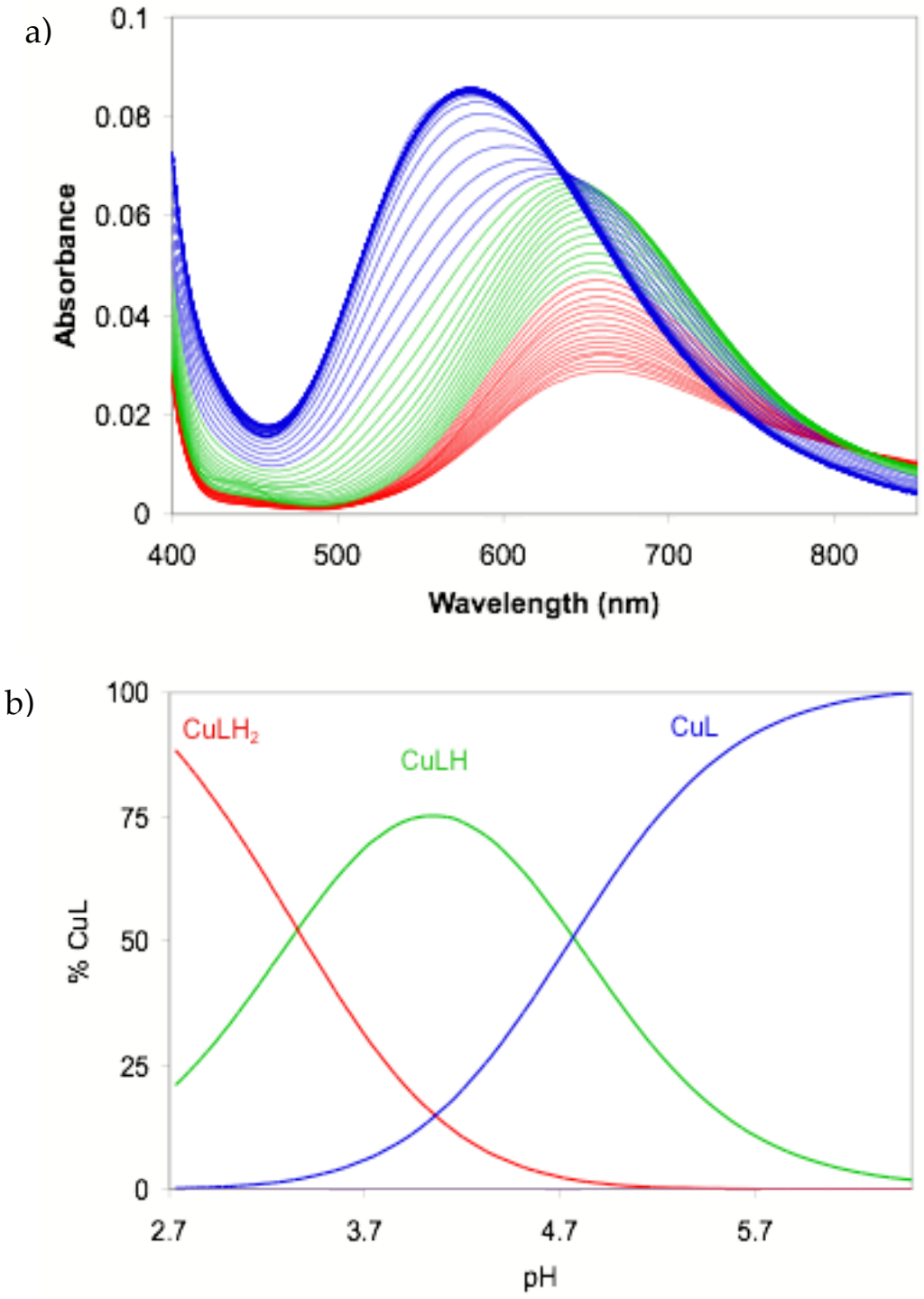

Figure 29. Potentiometric spectrophotometric titration of [Cu(OH$_2$)(Cage)]. a) pH-Dependent spectrophotometric titration of [Cu(Cage)] from pH 2.7 to 12. T = 25 °C, [Cu] = [cage] = 0.71 mM, μ = 0.1 M $NaClO_4$. b) Calculated species distribution for Cu^{2+} complexes of L, where L = $cage^{2-}$. T = 25 °C, μ = 0.1 M $NaClO_4$.

hydrogen is left out. The subscript *m* and *l* denote the complex M_mL_l, and when *m*=1 the second subscript is omitted.

The absolute β_1 can be converted to a pH-dependent conditional association constant by equations 38-40. The pH-dependent value is denoted β_{lm}' or K_l, and is also sometimes referred to as the conditional or effective association constant (K_{eff}). The conditional constant, β_{lm}' or K_l, is useful when comparing association constants of various ligands and metals at a given pH. Conditional stability constants are defined by Equation 38 in terms of the equilibrium between a metal complex and its components, except that the free metal ion and free ligand concentrations are replaced by the terms defined in Equations 39 and 40. The total concentration of free metal ion not bound to ligand (including hydrolyzed metal ion and metal bound to other complexing species) is represented as α_M in Equation 39, and the total concentration of all ligand species not bound to the metal ion is represented by α_L according to Equation 40.[75]

$$\beta_{lm}' = \frac{\beta_{lm}}{(\alpha_M)^m(\alpha_L)^l} \qquad \textbf{Equation 38}$$

$$\alpha_M = \frac{([\mathrm{M}] + [\mathrm{MOH}] + [\mathrm{M(OH)_2}] + \ldots)}{[M]} \qquad \textbf{Equation 39}$$

$$\alpha_L = \frac{([\mathrm{L}] + [\mathrm{HL}] + [\mathrm{LH_2}] + \ldots)}{[L]} \qquad \textbf{Equation 40}$$

For simplicity, the expressions for α_M and α_L can be reduced to Equations 38 and 39. The proof for this simplification is found in Appendix A.

$$\alpha_M = 1 + 10^{(pH - pK_{a1})} + 10^{(2pH - pK_{a1} - pK_{a2})} + \ldots \quad \textbf{Equation 41}$$

$$\alpha_L = 1 + 10^{(pK_{a1} - pH)} + 10^{(pK_{a1} + pK_{a2} - 2pH)} + \ldots \quad \textbf{Equation 42}$$

Conversion of absolute association constant, $\beta = 10.8$, using equations 38, 41, and 42 gives the pH-dependent value $\beta_1' = K_{CuCage} = 10.7$ for association of H_2Cage and Cu^{2+} at pH 7.4.

4.2.2 Competition between H_2Cage and NTA for Cu^{2+}

The pH-dependent value of $K_{CageCu} = 10.7$ determined above was further confirmed by a copper competition reaction between H_2Cage and the common chelator nitrilotriacetic acid (NTA), which has a K_{CuNTA} of 10.68 for Cu^{2+} at pH 7.4. Solutions of 1:1 Cage:Cu(II) were titrated with 2 equivalents of NTA and reactions were monitored by UV-Vis (Figure 30). Using Specfit software, and the model shown in Table 11 , we derived the apparent constant, $K_{CuCage} = 10.79$. This apparent constant does not account for the ternary species formed by association of HEPES to NTACu(II). We do not know to what extent HEPES may interfere with the CageCu(II) complex, but due to close agreement between the conditional and apparent values calculated from both potentiometric spectrophotometric titration and from the NTA competition study at pH 7.4, it is likely that the HEPES interferes similarly with both NTACu(II) and CageCu(II).

Despite potential interference from other solution components, the apparent binding constant for H_2Cage and Cu(II) at pH 7.4 calculated here agrees well with the value of the pH-dependent conditional constant derived from potentiometric spectrophotometric titrations of H_2Cage and [Cage(OH_2)Cu] described in the previous section. This association constant converts to a conditional dissociation constant, K_D, at pH 7.4 for Cu-Cage of 16 picomolar.

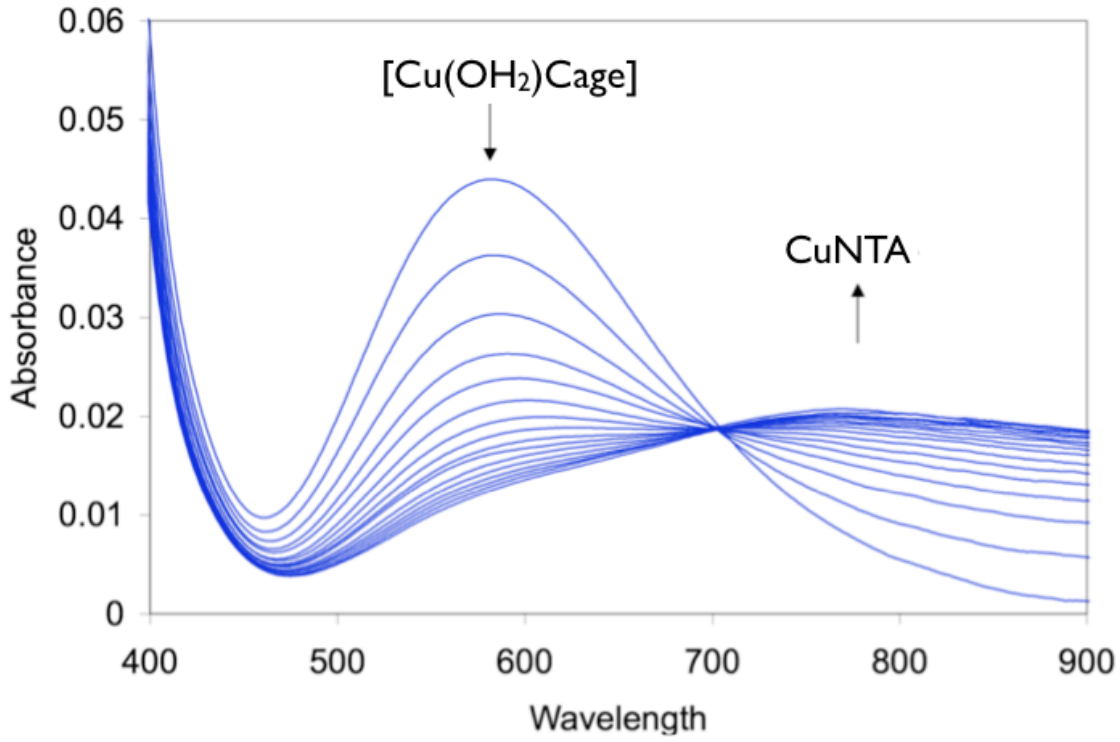

Figure 30. Titration spectra from competition of H_2Cage and NTA for Cu^{2+}. Two equivalents of NTA were titrated into a 500 μM [Cu(OH_2)Cage] in 50 mM HEPES at pH 7.4.

4.2.3 Second Generation Caged Complexes

The 16 picomolar (log K_{CuCage}= 10.7) affinity of our first-generation caged copper (**18**), while significant, may not be strong enough to keep copper sequestered in the presence of endogenous copper-binding proteins. For example, human serum albumin (HSA) binds Cu^{2+} with 1 picomolar affinity at pH 7.4 and could likely exchange copper with Cage pre-photolysis. To address the relatively weak affinity of Cage for copper, several other chelators were designed with a focus on improving the stability of caged copper complexes, as well as applying these photoactive ligands to other biologically interesting metals. Some of these new ligands (Figure 31) were screened for improved

copper binding using competition with NTA, as described above. Conditional affinity constants were calculated for any ligands that showed significant competition with NTA.

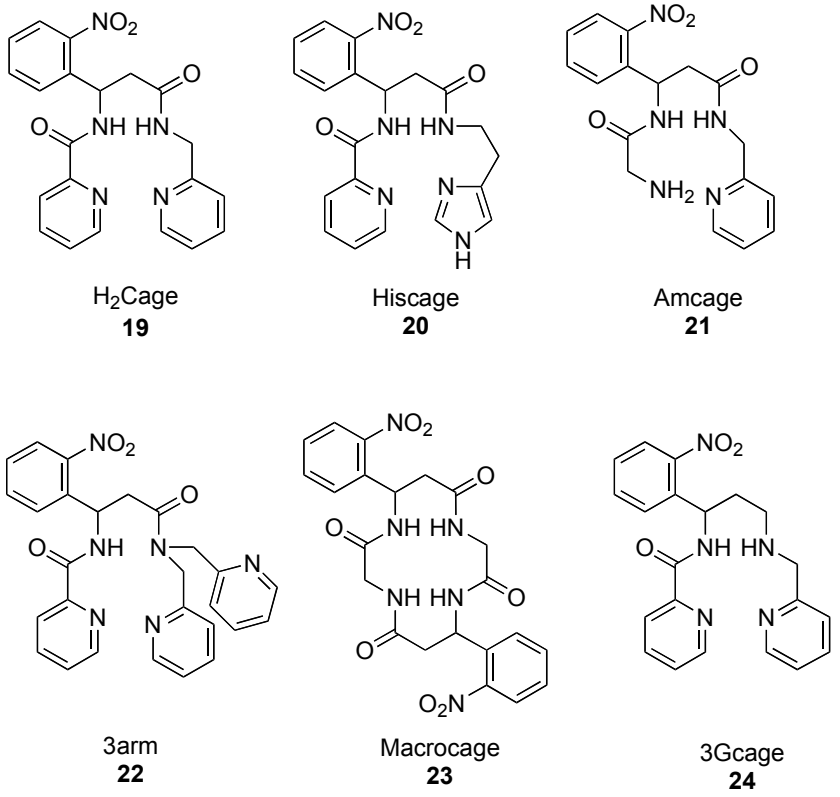

Figure 31. First and second generation cage ligands designed to bind Cu^{2+}.

Each of the ligands shown in Figure 31 were subjected to a copper competition titration with NTA. In short, the ligand-copper complex was titrated with excess NTA at pH 7.4 in 50 mM HEPES. This copper competition essentially served as a 'litmus test' to determine whether the ligands have higher binding affinity than the first generation chelator, H_2Cage (**19**). Ligands that have significantly higher binding affinity than **19** should easily retain copper in the presence of excess of NTA. Ligands with similar copper affinity to **19** should compete with NTA for copper in the same way as H_2Cage

(Figure 30), and ligands with much weaker affinity for copper should stoichiometrically exchange copper with NTA.

The second generation ligands Hiscage (**20**) and 3arm cage (**22**) had much lower binding affinity with Cu^{2+} at pH 7.4 than the first generation H_2Cage. Hiscage and 3arm cage could not compete with NTA for copper at this pH. Macrocage (**23**) also showed relatively low binding affinity for copper at pH 7.4 and demonstrated extremely poor water solubility. Amcage (**21**) competed with NTA for copper, but to a much lower extent than **18**. Because Amcage competed to only a small extent and was evidently weaker than NTA, a copper competition study was done in the reverse direction in which excess Amcage was titrated into a solution of 1:1 NTA:Cu(II). From this experiment the affective binding constant of log $K_{AmcageCu}$= 9.7 was determined using Specfit and the equilibrium model in Table 11. These ligands will not likely be able to maintain copper sequestration in biological systems, but perhaps would be medicinally useful for selected release of other metal ions.

3Gcage (**24**) is the only second generation ligand that showed improvement on the 16 picomolar K_D (log K_{CageCu}=10.7) and was significantly stronger than NTA. Titration of NTA into a solution of 1:1 Cu^{2+}:3Gcage showed that even in excess, NTA does not have sufficient binding affinity to compete for copper in the presence of **24**. In the case of 3Gcage, EDTA was required to remove copper from the 3Gcage(II) complex. The absolute binding constant has not yet been determined, but it is clear from the competition with EDTA that 3Gcage binds copper with significantly higher affinity that the other caged copper ligands and is likely stronger than biologically relevant copper chelators.

3Gcage and future generations of these cage ligands will be valuable tools for on-demand delivery of copper. These small inorganic molecules can be used as tools to

study mechanisms of metal ion trafficking, as well as applications such as chemotherapy where toxic metal ions could be released to induce cell death.

These caged ligands also have potential as valuable tools for selective delivery of other metal ions. H_2Cage, for example, has already shown promise as a caged platinum drug.[40] Platinum drug treatment is currently limited due to dose-restricting toxicity and inherent or acquired cellular resistance. Because of these limitations on platinum therapy, as well as other drug treatment therapies, investigations have recently focused on drug delivery systems and prodrugs to selectively deliver high local concentrations of platinum and other drugs to tumor cells.[224, 225] CagePt may offer a solution to this problem by allowing for selective delivery of active platinum drug to tumor cells.

Future efforts will focus on the development of improved caged copper complexes, as well as application of these ligands to other biologically relevant transition metals. The use of caged complexes to deliver transition metals in a time and location specific way is a promising strategy toward development of reagents for probing and manipulating biological systems for the purpose of discovery and clinical therapy.

4.3 Materials and Methods.

Nitrilotriacetic acid (NTA) was purchased from Fluka. All solvents were reagent grade. UV-Vis spectra were recorded on a Cary 50 UV-Vis spectrophotometer or an SI Photonics (Tucson, AZ) model 420 fiber optic CCD array UV-Vis spectrophotometer.

Potentiometric and Spectrophotometric Titrations.

Cu^{2+} perchlorate solutions (0.1 M) were prepared from solid $Cu(ClO_4)_2 \bullet 6H_2O$ and standardized with 0.05 M EDTA to a mueroxide endpoint in ammonia buffer. NaOH, $HClO_4$, and $NaClO_4$ solutions (0.1 M) were prepared with boiled nanopure deionized water and were degassed upon cooling to remove dissolved carbonate.

NaOH solutions were standardized by titration with both 0.2 M HCl and potassium hydrogen phthalate to a phenolphthalein end point and were stored under Ar; $HClO_4$ stock solutions were prepared from concentrated perchloric acid and standardized by titration with standard NaOH to a phenolphthalein end point. All solutions were degassed with Ar for 45 minutes prior to each experimental run.

Titrations were carried out at 25 °C with 0.1 M $NaClO_4$ supporting electrolyte in a 3-mL cuvette equipped with a pH probe, titrator tip, and stir bar, and blanketed in Ar to preserve an inert environment. The glass-bulb probe (Orion combination pH electrode model 8103BN filled with 3 M NaCl) was calibrated with pH 4 and 7 standard reference buffers (RICCA Chemical Company). Solutions of H_2Cage were prepared by dissolving the compound in a minimum volume of methanol and diluting with 0.1 M $NaClO_4$ in H_2O. Solutions of [Cu(Cage)] were prepared in the range of 0.5 mM by dissolving [Cu(OH_2)(Cage)] recrystallized from methanol in 0.1 M $NaClO_4$. Initial volumes were between 2 and 2.2 mL. A Schott Titronic® 110 plus autotitrator kept under constant Ar sparge was used to deliver 2 to 4 μL aliquots of acid or base through the titrator tip into the reaction cuvette. The solutions were stirred constantly and allowed to equilibrate at least 30 s after each addition before data were collected. All titrations were carried out from low to high and from high to low pH with similar results. Figure 28 shows the potentiometric titration curves of H_2Cage and [Cu(Cage)] (abbreviated as H_2L and CuL, respectively).

Table 10. Model used for the pH-dependent spectrophotometric titrations of CuL, where L = Cage^{2-}.

Species	Log β	Cu *m*	L *l*	H *h*	
CuL	10.80 ± 0.01	1	1	0	refined
CuLH	15.63 ± 0.08	1	1	1	refined
$CuLH_2$	18.96 ± 0.03	1	1	2	refined
CuOH	-8.2	1	0	-1	constant

$Cu(OH)_2$	-17.5	1	0	-2	constant
$Cu(OH)_3$	-27.8	1	0	-3	constant
$Cu(OH)_4$	-39.1	1	0	-4	constant
OH	-13.74	0	0	-1	constant

Competition study of NTA vs. Cage for Cu^{2+}

Solutions of [Cu(Cage)] were prepared by dissolving recrystallized [$Cu(OH_2)$Cage] into minimal methanol and diluting in 50 mM HEPES (N-(2-hydroxyethyl)-piperazine-N'-2-ethanesulfonic acid) buffer, pH 7.4, with initial concentrations ranging from 0.3–1.5 mM. The reaction vessel was a 3-mL cuvette and initial solution volumes were 1 mL. All titrations were carried out at 25 °C. Aliquots (1–2 μL) of the competitive chelator NTA (100 mM) were pipetted into [Cu(Cage)] solutions and monitored spectrophotometrically. After each addition, solutions were manually mixed and equilibrated for 5 min before data were collected. Data were fit to the model shown in Table 11 with Specfit software. Reported errors in log β were calculated from the standard deviation of three runs.

Table 11. Model for the Cu^{2+} competition study of NTA vs. L, where L = $Cage^{2-}$ or Amcage.

Species	Log β	Cu *m*	NTA *l*	L *l*	H *h*	
CuL	10.79 ± 0.06	1	0	1	0	refined
Cu(NTA)	12.7	1	1	0	0	Constant
$Cu(NTA)_2$	17.4	1	2	0	0	Constant
NTAH	9.46	0	1	0	1	Constant
$NTAH_2$	11.95	0	1	0	2	Constant
$NTAH_3$	13.76	0	1	0	3	Constant
$NTAH_4$	14.76	0	1	0	4	Constant
CuOH	-8.2	1	0	0	-1	Constant

Appendix A. Association Constants

A.1 Protonation Constants

General treatment of ligand protonation constants for a ligand with four dissociable protons is shown below.

Stepwise protonation equilibria:

(A) $L^{(n)} + H^+ \overset{\beta_1=K_{a1}}{\rightleftharpoons} LH^{(n+1)}$ $\qquad K_{a1} = \dfrac{[LH]}{[L][H]} = \beta_1$

(B) $LH^{(n+1)} + H^+ \overset{K_{a2}}{\rightleftharpoons} LH_2^{(n+2)}$ $\qquad K_{a2} = \dfrac{[LH_2]}{[LH][H]}$

(C) $LH_2^{(n+2)} + H^+ \overset{K_{a3}}{\rightleftharpoons} LH_3^{(n+3)}$ $\qquad K_{a3} = \dfrac{[LH_3]}{[LH_2][H]}$

(D) $LH_3^{(n+3)} + H^+ \overset{K_{a4}}{\rightleftharpoons} LH_4^{(n+4)}$ $\qquad K_{a4} = \dfrac{[LH_4]}{[LH_3][H]}$

Absolute protonation equilibria:

(A) $L^{(n)} + H^+ \overset{\beta_1=K_{a1}}{\rightleftharpoons} LH^{(n+1)}$ $\qquad \beta_1 = \dfrac{[LH]}{[L][H]} = K_{a1}$

(E) $L^{(n)} + 2H^+ \overset{\beta_2}{\rightleftharpoons} LH_2^{(n+2)}$ $\qquad \beta_2 = \dfrac{[LH_2]}{[L][H]^2} = K_{a1}K_{a2}$

(F) $L^{(n)} + 2H^+ \overset{\beta_3}{\rightleftharpoons} LH_3^{(n+3)}$ $\qquad \beta_3 = \dfrac{[LH_3]}{[L][H]^3} = K_{a1}K_{a2}K_{a3}$

(G) $L^{(n)} + 2H^+ \overset{\beta_4}{\rightleftharpoons} LH_4^{(n+4)}$ $\qquad \beta_4 = \dfrac{[LH_4]}{[L][H]^4} = K_{a1}K_{a2}K_{a3}K_{a4}$

For the purpose of defining protonation constants in terms of absolute values and stepwise values, it is useful to start with a specific example. Here we will use

glycine. Many of us are familiar with protonation constants as pK_a values, or stepwise protonation constants. For glycine, the stepwise protonation events can be defined as dissociation events or association events. The stepwise association equilibria for glycine are below. The dissociation equilibrium would be written in the apposite direction and their equilibria constants would be defined as the inverse of the association constant expression.

(H) $$Gly^{2-} + H^+ \overset{\beta_1=K_1}{\rightleftharpoons} GlyH^{1-} \qquad \beta_1 = K_1 = \frac{[GlyH^{-1}]}{[Gly^{-2}][H^+]}$$

(I) $$GlyH^{1-} + H^+ \overset{K_2}{\rightleftharpoons} GlyH_2 \qquad K_2 = \frac{[GlyH_2]}{[GlyH^{-1}][H^+]}$$

Take the log of K_1 or K_2 to find pK_1 or pK_2.

Many people are less familiar with the protonation constants that are defined as absolute association constants, or β values. For the first protonation event of glycine (Equation H), the β_1 is defined by the same equilibrium constant expression as the more familiar K_1. However, for the second protonation event, the β value is defined as two protons associating with the unprotonated ligand (Equation J).

(J) $$Gly^{2-} + 2H^+ \overset{\beta_2=K_1K_2}{\rightleftharpoons} GlyH_2 \qquad \beta_2 = \frac{[GlyH_2]}{[Gly^{-2}][H^+]^2} = K_1K_2$$

By multiplying the expression for K_1 and K_2 (Equations H & J), we arrive at the equilibrium constant express ion for β_2. Notice that β values are absolute and are defined by association of protons to ligand in a single step. K values are stepwise protonation events.

A.2 Metal – Ligand Association Constants

The constant, β, is defined as the pH independent absolute association constant and is often denoted β_{lm} according to the equation below. M is metal, L is ligand, and *l* and *m* denote the complex M_mL_l. When m=1 the second subscript is omitted. Sometimes H^+ ion is incorporated into this expression, as seen with Equation 36. If H^+ ion is incorporated, then the resulting β_{lmh} is pH dependant because it depends on the hydrogen ion concentration [H]. For the purposes here, H is left out of the equation and we use β_{lm} as defined here.

(K) $$m\mathrm{M} + l\mathrm{L} \overset{\beta_{lm}}{\rightleftharpoons} \mathrm{M}_m\mathrm{L}_l \qquad \beta_{lm} = \frac{[\mathrm{M}_m\mathrm{L}_l]}{[M]^m[L]^l}$$

The association of metal and ligand can involve exchange of protons, which can effect the affinity of ligand for metal depending on the pH of solution. The conditional β value is denoted β′ or K. β′ is the pH dependent constant, and is also referred to as the conditional constant or effective association constant. The absolute β value can be converted into a pH-dependant conditional value as follows:

(L) $$\beta_{lm}' = \frac{\beta_{lm}}{(\alpha_M)^{\mathrm{m}}(\alpha_L)^{\mathrm{n}}}$$

(M) $$\alpha_M = \frac{\left([\mathrm{M}] + [\mathrm{MOH}] + [\mathrm{M(OH)_2}] + \ldots\right)}{[M]}$$

(N) $$\alpha_L = \frac{\left([\mathrm{L}] + [\mathrm{LH}] + [\mathrm{LH_2}] + \ldots\right)}{[L]}$$

The expressions for α_M and α_L correspond to the fractions of metal and ligand in solution that do not exist as complexed species with OH or L, respectively. These expressions can be reduced to the following equations.

(O) $$\alpha_M = 1 + 10^{(\mathrm{pH}-\mathrm{pK_{a1}})} + 10^{(2\mathrm{pH}-\mathrm{pK_{a1}}-\mathrm{pK_{a2}})} + \ldots$$

(P) $$\alpha_L = 1 + 10^{(\mathrm{pK_{a1}}-\mathrm{pH})} + 10^{(\mathrm{pK_{a1}}+\mathrm{pK_{a2}}-2\mathrm{pH})} + \ldots$$

Proof for Simplification of α_M (Conversion of Equation M to Equation O):

Equation M can be expressed as the following (Q):

(Q) $$\alpha_M = \frac{[M]}{[M]} + \frac{[MOH]}{[M]} + \frac{[M(OH)_2]}{[M]} + \ldots$$

The expression for metal hydroxide formation is

(R) $$M + OH \rightleftharpoons \mathrm{MOH} \qquad \mathrm{K_1} = \frac{[\mathrm{MOH}]}{[\mathrm{M}][\mathrm{OH}]}$$

This expression can put in terms of [H] by multiplying by the equilibrium constant expression for the dissociation of water:

(S) $$\mathrm{K_W} = [OH][H]$$

(T) $$\mathrm{K_1} = K_1 K_W = \frac{[\mathrm{MOH}]}{[\mathrm{M}][\mathrm{OH}]} \times [OH][H] = \frac{[MOH][H]}{[M]}$$

Rearrange the expression and put [H] in terms of pH and K_1 in terms of pK_1.

(U) $$\frac{[\mathrm{MOH}]}{[\mathrm{M}]} = \frac{\mathrm{K_1}}{[\mathrm{H}]} = \frac{10^{-\mathrm{pK_1}}}{10^{-\mathrm{pH}}} = 10^{\mathrm{pH}-\mathrm{pK_1}}$$

Treat the second hydrolysis component similarly:

(V) $$M + 2(OH) \rightleftharpoons \mathrm{M(OH)_2}$$

(W) $$\beta_2 = \frac{[\mathrm{M(OH)_2}]}{[\mathrm{M}][\mathrm{OH}]^2} = \beta_2(\mathrm{K_W})^2 = \frac{[M(OH)_2][H]^2}{[M]}$$

(X) $$\frac{[\mathrm{M(OH)_2}]}{[\mathrm{M}]} = \frac{\beta_2}{[\mathrm{H}]^2} = \frac{\mathrm{K_1K_2}}{[\mathrm{H}]^2} = \frac{10^{-\mathrm{pK_1}-\mathrm{pK_2}}}{10^{-2\mathrm{pH}}} = 10^{2pH-\mathrm{pK_1}-\mathrm{pK_2}}$$

Substitute (U) and (X) into (Q) to get Equation O.

Proof for Simplification of α_L (Conversion of Equation N to Equation P):

Equation N can be expressed as the following (Y):

(Y) $$\alpha_M = \frac{[M]}{[M]} + \frac{[MOH]}{[M]} + \frac{[M(OH)_2]}{[M]} + \ldots$$

The equilibrium expression for protonation of L is shown in (A). For the fist protonation, The Expression for K_{a1} in (A) can be rearranged to Equation Z and put in terms of pH and pK_{a1} instead of [H] and K_{a1}:

(Z) $$\frac{[HL]}{\mathrm{L}} = \frac{[\mathrm{H}]}{[\mathrm{K_{a1}}]} = \frac{10^{-\mathrm{pH}}}{10^{-\mathrm{pK_{a1}}}} = 10^{\mathrm{pK_{a1}}-\mathrm{pH}}$$

Treat the term for the second protonation similarly using the expression of β_2 from Equation E. The expression for β_2 can be rearranged and put in terms of pH and pK_a's (recall that $\beta_2=K_{a1}K_{a2}$) .

(AA) $$\frac{[H_2L]}{[\mathrm{L}]} = \frac{[\mathrm{H}]^2}{[\beta_2]} = \frac{[\mathrm{H}]^2}{[\mathrm{K_{a1}K_{a2}}]} = \frac{10^{-2\mathrm{pH}}}{10^{-\mathrm{pK_{a1}}-\mathrm{pK_{a2}}}} = 10^{\mathrm{pK_{a1}}+\mathrm{pK_{a2}}-2\mathrm{pH}}$$

Substitute (Z) and (AA) into (Y) to get Equation P.

Please note that for the equations above, the pK_{a1} value is the highest pK_a value for any given ligand. We define pK_a as an ASSOCIATION constant. In many sources, the K_a or pK_a values given are actually ACID DISSOCIATION constants defined by the dissociation rather than association of ligand and proton. It is very important to use the association constant value for the least acidic proton for pK_{a1} to get the correct values using the α_M and α_L equations above.

Other components in solution, such as buffer or competing ligand can affect the measured stability constant. The apparent stability constant (K_{app}) is defined as the constant measured in the presence of other species (salt, buffer components) that may interfere with determination of the pure pH-dependant conditional association constant.

A.3 Useful Constants for Commonly Used Copper Chelators

Hydroxide ion (OH^-)[76]

$Cu^{2+} + OH^- \xrightarrow{\beta_1 = K_1} CuOH^+$	$\log \beta_1 = 6.1$
$Cu^{2+} + 2OH^- \xrightarrow{\beta_2 = K_1K_2} Cu(OH)_2$	$\log \beta_2 = 11.2$
$Cu^{2+} + 3OH^- \xrightarrow{\beta_2 = K_1K_2} Cu(OH)_3^-$	$\log \beta_3 = 14.5$
***At pH 7.4 for Cu^{2+} $\alpha_{Cu} = 1.25$ and $\log \alpha_{Cu} = 0.097$**	

Glycine (Gly)

Ligand Protonation Equilibria:[76]		
$H^+ + Gly^- \xrightarrow{K_{a1}} HGly$	$\log K_{a1} = 9.57$	
$H^+ + HGly \xrightarrow{K_{a2}} H_2Gly$	$\log K_{a1} = 2.63$	
at pH 7.4 $\alpha_{Gly} = 148.91$, $\log \alpha_{Gly} = 2.17$		
Complexation Equilibria:	pH Independent[76]	Calculated at pH 7.4
$Cu^{2+} + Gly^- \xrightarrow{\beta_1 = K_1} CuGly^+$	$\log \beta_1 = 8.15$	$\log \beta_1' = 5.88$
$Cu^{2+} + 2Gly^- \xrightarrow{\beta_2 = K_1K_2} CuGly_2$	$\log \beta_2 = 15.03$	$\log \beta_2' = 10.59$
$CuGly^+ + Gly^- \xrightarrow{K_2} CuGly_2$	$\log K_2 = \log \beta_2 - \log \beta$	$\log K_2 = 4.71$

Ethylenediamminetetraacetic acid (EDTA)

Ligand Protonation Equilibria:[76]		
$H^+ + EDTA^{4-} \xrightarrow{K_{a1}} HEDTA^{3-}$	$\log K_{a1} = 10.3$	
$H^+ + HEDTA^{3-} \xrightarrow{K_{a2}} H_2EDTA^{2-}$	$\log K_{a2} = 6.13$	
$H^+ + H_2EDTA^{2-} \xrightarrow{K_{a3}} H_3EDTA^-$	$\log K_{a3} = 2.79$	
$H^+ + H_3EDTA^- \xrightarrow{K_{a4}} H_4EDTA$	$\log K_{a4} = 2$	
at pH 7.4 $\alpha_{EDTA} = 566.87$, $\log \alpha_{EDTA} = 2.75$		
Complexation Equilibria:	pH Independent[76]	Calculated at pH 7.4
$Cu^{2+} + EDTA^{4-} \xrightarrow{\beta_1 = K_1} CuEDTA^{2-}$	$\log \beta_1 = 18.78$	$\log \beta_1' = 16.03$

Ethyleneglycoltetraacetic acid (EGTA)

Ligand Protonation Equilibria:[76]		
$H^+ + EGTA^{4-} \xrightarrow{K_{a1}} HEGTA^{3-}$	$\log K_{a1} = 9.5$	
$H^+ + HEGTA^{3-} \xrightarrow{K_{a2}} H_2EGTA^{2-}$	$\log K_{a2} = 8.8$	
$H^+ + H_2EGTA^{2-} \xrightarrow{K_{a3}} H_3EGTA^{-}$	$\log K_{a3} = 2.7$	
$H^+ + H_3EGTA^{-} \xrightarrow{K_{a4}} H_4EGTA$	$\log K_{a4} < 2$	
at pH 7.4 $\alpha_{EGTA} = 3289.23$, $\log \alpha_{EGTA} = 3.52$		
Complexation Equilibria:	pH Independent[76]	Calculated at pH 7.4
$Cu^{2+} + EGTA^{4-} \xrightarrow{\beta_1 = K_1} CuEGTA^{2-}$	$\log \beta_1 = 17.7$	$\log \beta_1' = 14.09$

Ethylenediiminodiacetic acid (EDDA)

Ligand Protonation Equilibria:[76]		
$H^+ + EDDA^{4-} \xrightarrow{K_{a1}} HEDDA^{3-}$	$\log K_{a1} = 9.61$	
$H^+ + HEDDA^{3-} \xrightarrow{K_{a2}} H_2EDDA^{2-}$	$\log K_{a2} = 6.55$	
$H^+ + H_2EDDA^{2-} \xrightarrow{K_{a3}} H_3EDDA^{-}$	$\log K_{a3} = 2.12$	
$H^+ + H_3EDDA^{-} \xrightarrow{K_{a4}} H_4EDDA$	$\log K_{a4} \sim 1.3$	
at pH 7.4 $\alpha_{EDDA} = 186.09$, $\log \alpha_{EDDA} = 2.27$		
Complexation Equilibria:	pH Independent[76]	Calculated at pH 7.4
$Cu^{2+} + EDDA^{4-} \xrightarrow{\beta_1 = K_1} CuEDDA^{2-}$	$\log \beta_1 = 16.2$	$\log \beta_1' = 13.93$

Acetohydroxamic acid

Ligand Protonation Equilibria:[76]		
$H^+ + L^- \xrightarrow{K_{a1}} HL$	$\log K_{a1} = 9.29$	
at pH 7.4 $\alpha_L = 78.62$, $\log \alpha_L = 1.89$		
Complexation Equilibria:	pH Independent[76]	Calculated at pH 7.4
$Cu^{2+} + L^- \xrightarrow{\beta_1 = K_1} CuL^+$	$\log \beta_1 = 7.90$	$\log \beta_1' = 6.01$
$Cu^{2+} + 2L^- \xrightarrow{\beta_2 = K_1K_2} CuL_2$	$\log \beta_2 = 12.18$	$\log \beta_2' = 12.18$
$CuL^+ + L^- \xrightarrow{K_2} CuL_2$	$\log K_2 = \log \beta_2 - \log \beta$	$\log K_2 = 6.07$

Nitrilotriacetic acid (NTA)

Ligand Protonation Equilibria:[76]	
$H^+ + NTA^{3-} \xrightarrow{K_{a1}} HNTA^{2-}$	$\log K_{a1} = 9.46$
$H^+ + HNTA^{2-} \xrightarrow{K_{a2}} H_2NTA^-$	$\log K_{a2} = 2.52$
$H^+ + H_2NTA^- \xrightarrow{K_{a3}} H_3NTA$	$\log K_{a3} = 1.81$
$H^+ + H_3NTA \xrightarrow{K_{a3}} H_4NTA^+$	$\log K_{a3} = 1.0$
at pH 7.4 $\alpha_{NTA} = 115.82$, $\log \alpha_{NTA} = 2.06$	

Complexation Equilibria:	pH Independent[76]	Calculated at pH 7.4
$Cu^{2+} + NTA^{3-} \xrightarrow{\beta_1 = K_1} CuNTA^-$	$\log \beta_1 = 12.7$	$\log \beta_1' = 10.64$
$Cu^{2+} + 2NTA^{3-} \xrightarrow{\beta_2 = K_1K_2} CuNTA_2^{4-}$	$\log \beta_2 = 17.4$	$\log \beta_2' = 15.34$
$CuNTA^- + NTA^{3-} \xrightarrow{K_2} CuNTA_2^{4-}$	$\log K_2 = \log \beta_2 - \log \beta$	$\log K_2 = 4.7$

N,N,N'N'-Tetra-2-picolylethylenediamine (TPEN)

Ligand Protonation Equilibria:[76]	
$H^+ + TPEN \xrightarrow{K_{a1}} HTPEN^+$	$\log K_{a1} = 7.12$
$H^+ + HTPEN^+ \xrightarrow{K_{a2}} H_2TPEN^{2+}$	$\log K_{a2} = 4.81$
$H^+ + HTPEN^{2+} \xrightarrow{K_{a3}} H_3TPEN^{3+}$	$\log K_{a3} = 3.30$
$H^+ + HTPEN^{2+} \xrightarrow{K_{a3}} H_3TPEN^{3+}$	$\log K_{a3} = 2.88$
at pH 7.4 $\alpha_{TPEN} = 1.53$, $\log \alpha_{TPEN} = 0.18$	

Complexation Equilibria:	pH Independent[76]	Calculated at pH 7.4
$Cu^{2+} + TPEN \xrightarrow{\beta_1 = K_1} CuTPEN^{2+}$	$\log \beta_1 = 20.2$	$\log \beta_1' = 20.02$

Tris(2-aminoethyl)amine (Tren)

Ligand Protonation Equilibria:[76]		
$H^+ + Tren \xrightarrow{K_{a1}} HTren^+$	$\log K_{a1} = 10.13$	
$H^+ + HTren^+ \xrightarrow{K_{a2}} H_2Tren^{2+}$	$\log K_{a2} = 9.43$	
$H^+ + H_2Tren^{2+} \xrightarrow{K_{a3}} H_3Tren^{3+}$	$\log K_{a3} = 8.42$	
at pH 7.4 $\alpha_{Tren} = 660641.61$, $\log \alpha_{Tren} = 5.82$		
Complexation Equilibria:	pH Independent[76]	Calculated at pH 7.4
$Cu^{2+} + Tren \xrightarrow{\beta_1 = K_1} CuTren^{2+}$	$\log \beta_1 = 18.8$	$\log \beta_{110}' = 12.98$
$Cu^{2+} + 2Tren \xrightarrow{\beta_2 = K_1K_2} CuTren_2^{2+}$	$\log \beta_2 = 21.7$	

Triethylamine (Trien)

Ligand Protonation Equilibria:[76]		
$H^+ + Trien \xrightarrow{K_{a1}} HTrien^+$	$\log K_{a1} = 9.75$	
$H^+ + HTrien^+ \xrightarrow{K_{a2}} H_2Trien^{2+}$	$\log K_{a2} = 9.07$	
$H^+ + H_2Trien^{2+} \xrightarrow{K_{a3}} H_3Trien^{3+}$	$\log K_{a3} = 6.57$	
$H^+ + H_3Trien^{2+} \xrightarrow{K_{a3}} H_4Trien^{3+}$	$\log K_{a3} = 3.27$	
at pH 7.4 $\alpha_{Trien} = 2857.17$, $\log \alpha_{Tren} = 3.46$		
Complexation Equilibria:	pH Independent[76]	Calculated at pH 7.4
$Cu^{2+} + Trien \xrightarrow{\beta_1 = K_1} CuTrien^{2+}$	$\log \beta_1 = 20.06$	$\log \beta_{110}' = 16.60$

L-histidyl-L-histidine (Bishis)

Ligand Protonation Equilibria:[76]		
$H^+ + Bishis^- \xrightarrow{K_{a1}} HBishis$	$\log K_{a1} = 7.52$	
$H^+ + HBishis \xrightarrow{K_{a2}} H_2Bishis^+$	$\log K_{a2} = 6.70$	
$H^+ + H_2Bishis^+ \xrightarrow{K_{a3}} H_3Bishis^{2+}$	$\log K_{a3} = 5.66$	
$H^+ + H_3Bishis^{2+} \xrightarrow{K_{a3}} H_4Bishis^{3+}$	$\log K_{a3} = 2.60$	
at pH 7.4 $\alpha_{Bishis} = 2.59$, $\log \alpha_{Bishis} = 0.41$		
Complexation Equilibria:	pH Independent[76]	Calculated at pH 7.4
$Cu^{2+} + Bishis^- \xrightarrow{\beta_1 = K_1} CuBishis^+$	$\log \beta_1 = 11.10$	$\log \beta_1' = 10.69$

6,6'-Bis(aminomethyl)-2,2'-bipyridyl (BABP)

Ligand Protonation Equilibria:[76]		
$H^+ + L \xrightarrow{K_{a1}} HL^+$	$\log K_{a1} = 7.52$	
$H^+ + HL^+ \xrightarrow{K_{a2}} H_2L^{2+}$	$\log K_{a2} = 6.70$	
$H^+ + H_2L^{2+} \xrightarrow{K_{a3}} H_3L^{3+}$	$\log K_{a3} = 5.66$	
at pH 7.4 $\alpha_L = 553.47$, $\log \alpha_L = 2.74$		
Complexation Equilibria:	pH Independent[76]	Calculated at pH 7.4
$Cu^{2+} + L \xrightarrow{\beta_1 = K_1} CuL^{2+}$	$\log \beta_1 = 15.05$	$\log \beta_1' = 12.31$

5. References

1. Bertini, I.; Gray, H. B.; Stiefel, E. I.; Valentine, J. S., *Biological Inorganic Chemistry: Structure and Reactivity*. University Science Books: Sausalito, CA, 2007.

2. Silva, J. J. R. F. d.; Williams, R. J. P., *The Biological Chemistry of the Elements*. 2nd ed.; Oxford University Press: Oxford, 2001.

3. Lippard, S. J.; Berg, J. M., *Principles of Bioinorganic Chemistry*. University Science Books: Mill Valley, CA, 1994.

4. Mann, S., Biominerals and Biomineralization. In *Biological Inorganic Chemistry: Structure and Reactivity*, Bertini, I.; Gray, H. B.; Stiefel, E. I.; Valentine, J. S., Eds. University Science Books: Sausalito, CA, 2007; pp 79-93.

5. Evenas, J.; Malmendal, A.; Forsen, S., Calcium. *Curr. Opin. Chem. Biol.* **1998,** *2* (2), 293-302.

6. Pyle, A., Metal Ions in the Structure and Function of RNA. *J. Biol. Inorg. Chem.* **2002,** *7* (7), 679-690.

7. Vinod K. Misra, D. E. D., On the Role of Magnesium Ions in RNA Stability. *Biopolymers* **1998,** *48* (2-3), 113-135.

8. Winge, D. R., Metal Ion Receptors and Signaling. In *Biological Inorganic Chemistry: Structure and Reactivity*, Bertini, I.; Gray, H. B.; Stiefel, E. I.; Valentine, J. S., Eds. University Science Books: Sausalito, CA, 2007; pp 613-627.

9. Frederickson, C. J.; Koh, J.-Y.; Bush, A. I., The Neurobiology of Zinc in Health and Disease. *Nat. Rev. Neurosci.* **2005,** *6* (6), 449-462.

10. Chen, P. R.; He, C., Selective Recognition of Metal Ions by Metalloregulatory Proteins. *Curr. Opin. Chem. Biol.* **2008,** *12* (2), 214-221.

11. Pennella, M. A.; Giedroc, D. P., Structural Determinants of Metal Selectivity in Prokaryotic Metal-Responsive Transcriptional Regulators. *BioMetals* **2005,** *18* (4), 413-428.

12. Cowan, J. A., Hydrolytic Chemistry. In *Biological Inorganic Chemistry: Structure and Reactivity*, Bertini, I.; Gray, H. B.; Stiefel, E. I.; Valentine, J. S., Eds. University Science Books: Sausalito, CA, 2007; pp 175-194.

13. Thomas, D. D.; Ridnour, L. A.; Isenberg, J. S.; Flores-Santana, W.; Switzer, C. H.; Donzelli, S.; Hussain, P.; Vecoli, C.; Paolocci, N.; Ambs, S.; Colton, C. A.; Harris, C. C.; Roberts, D. D.; Wink, D. A., The Chemical Biology of Nitric Oxide: Implications in Cellular Signaling. *Free Radical Biol. Med.* **2008,** *45* (1), 18-31.

14. Holm, R. H.; Kennepohl, P.; Solomon, E. I., Structural and Functional Aspects of Metal Sites in Biology. *Chem. Rev.* **1996,** *96* (7), 2239-2314.

15. Valentine, J. S., Oxygen Metalbolism. In *Biological Inorganic Chemistry: Structure and Reactivity*, Bertini, I.; Gray, H. B.; Stiefel, E. I.; Valentine, J. S., Eds. University Science Books: Sausalito, CA, 2007; pp 319-440.

16. Meggers, E., Targeting Proteins with Metal Complexes. *Chem. Commun.* **2009**, -.

17. David, S. S.; Meggers, E., Inorganic Chemical Biology: From Small Metal Complexes in Biological Systems to Metalloproteins. *Curr. Opin. Chem. Biol.* **2008,** *12* (2), 194-196.

18. Meggers, E., Exploring Biologically Relevant Chemical Space with Metal Complexes. *Curr. Opin. Chem. Biol.* **2007,** *11* (3), 287-292.

19. Meggers, E.; Atilla-Gokcumen, G. E.; Bregman, H.; Maksimoska, J.; Mulcahy, S. P.; Pagano, N.; Williams, D. S., Exploring Chemical Space with Organometallics: Ruthenium Complexes as Protein Kinase Inhibitors. *Synlett* **2007,** (8), 1177-1189.

20. Zeglis, B. M.; Pierre, V. C.; Barton, J. K., Metallo-Intercalators and Metallo-Insertors. *Chem. Commun.* **2007,** (44), 4565-4579.

21. Boon, E. M.; Kisko, J. L.; Barton, J. K., Detection of DNA Base Mismatches Using DNA Intercalators. In *Redox Cell Biology and Genetics, Pt B*, 2002; Vol. 353, pp 506-522.

22. Erkkila, K. E.; Odom, D. T.; Barton, J. K., Recognition and Reaction of Metallointercalators with DNA. *Chem. Rev.* **1999,** *99* (9), 2777-2795.

23. Reed, J. E.; Arnal, A. A.; Neidle, S.; Vilar, R., Stabilization of G-Quadruplex DNA and Inhibition of Telomerase Activity by Square-Planar Nickel(II) Complexes. *J. Am. Chem. Soc.* **2006,** *128* (18), 5992-5993.

24. Bertrand, H.; Monchaud, D.; De Cian, A.; Guillot, R.; Mergny, J. L.; Teulade-Fichou, M. P., The Importance of Metal Geometry in the Recognition of G-Quadruplex-DNA by Metal-Terpyridine Complexes. *Org. Biomol. Chem.* **2007,** *5* (16), 2555-2559.

25. Haas, K. L.; Franz, K. J., Application of Metal Coordination Chemistry to Explore and Manipulate Cell Biology. *Chemical Reviews* **2009,** *109* (10), 4921-4960.

26. Ellis-Davies, G. C. R., Neurobiology with Caged Calcium. *Chem. Rev.* **2008,** *108* (5), 1603-1613.

27. Grant, K. B.; Kassai, M., Major Advances in the Hydrolysis of Peptides and Proteins by Metal Ions and Complexes. *Curr. Org. Chem.* **2006,** *10* (9), 1035-1049.

28. Montgomery, C. P.; Murray, B. S.; New, E. J.; Pal, R.; Parker, D., Cell-Penetrating Metal Complex Optical Probes: Targeted and Responsive Systems Based on Lanthanide Luminescence. *Accounts of Chemical Research* **2009,** *42* (7), 925-937.

29. Major, J. L.; Meade, T. J., Bioresponsive, Cell-Penetrating, and Multimeric Mr Contrast Agents. *Acc. Chem. Res.* **2009,** *42* (7), 893-903.

30. Wadas, T. J.; Wong, E. H.; Weisman, G. R.; Anderson, C. J., Copper Chelation Chemistry and Its Role in Copper Radiopharmaceuticals. *Curr. Pharm. Des.* **2007,** *13* (1), 3-16.

31. Liu, S., The Role of Coordination Chemistry in the Development of Target-Specific Radiopharmaceuticals. *Chem. Soc. Rev.* **2004,** *33* (7), 445-461.

32. Zhuang, T. D.; Lee, H. S.; Imperiali, B.; Prestegard, J. H., Structure Determination of a Galectin-3-Carbohydrate Complex Using Paramagnetism-Based Nmr Constraints. *Protein Sci.* **2008,** *17* (7), 1220-1231.

33. Silvaggi, N. R.; Martin, L. J.; Schwalbe, H.; Imperiali, B.; Allen, K. N., Double-Lanthanide-Binding Tags for Macromolecular Crystallographic Structure Determination. *J. Am. Chem. Soc.* **2007,** *129* (22), 7114-7120.

34. Martin, L. J.; Hahnke, M. J.; Nitz, M.; Wohnert, J.; Silvaggi, N. R.; Allen, K. N.; Schwalbe, H.; Imperiali, B., Double-Lanthanide-Binding Tags: Design, Photophysical Properties, and Nmr Applications. *J. Am. Chem. Soc.* **2007,** *129* (22), 7106-7113.

35. Sculimbrene, B. R.; Imperiali, B., Lanthanide-Binding Tags as Luminescent Probes for Studying Protein Interactions. *J. Am. Chem. Soc.* **2006,** *128* (22), 7346-7352.

36. Nitz, M.; Sherawat, M.; Franz, K. J.; Peisach, E.; Allen, K. N.; Imperiali, B., Structural Origin of the High Affinity of a Chemically Evolved Lanthanide-Binding Peptide. *Angew. Chem.-Int. Edit.* **2004,** *43* (28), 3682-3685.

37. Wohnert, J.; Franz, K. J.; Nitz, M.; Imperiali, B.; Schwalbe, H., Protein Alignment by a Coexpressed Lanthanide-Binding Tag for the Measurement of Residual Dipolar Couplings. *J. Am. Chem. Soc.* **2003,** *125* (44), 13338-13339.

38. Franz, K. J.; Nitz, M.; Imperiali, B., Lanthanide-Binding Tags as Versatile Protein Coexpression Probes. *ChemBioChem* **2003,** *4* (4), 265-271.

39. Nitz, M.; Franz, K. J.; Maglathlin, R. L.; Imperiali, B., A Powerful Combinatorial Screen to Identify High-Affinity Terbium(III)-Binding Peptides. *ChemBioChem* **2003,** *4* (4), 272-276.

40. Ciesienski, K. L.; Heyman, L. H.; Yang, D. T.; Haas, K. L.; Dickens, M. G.; Franz, K. J., A Photo-Caged Platinum(II) Complex That Increases Cytotoxicity Upon Light Activation. *Eur. J. Inorg. Chem.* **2010,** *Accepted for Publication.*

41. Ciesienski, K. L.; Haas, K. L.; Dickens, M. G.; Tesema, Y. T.; Franz, K. J., A Photolabile Ligand for Light-Activated Release of Caged Copper. *J. Am. Chem. Soc.* **2008,** *130* (37), 12246-12247.

42. Charkoudian, L. K.; Dentchev, T.; Lukinova, N.; Wolkow, N.; Dunaief, J. L.; Franz, K. J., Iron Prochelator Bsih Protects Retinal Pigment Epithelial Cells against Cell Death Induced by Hydrogen Peroxide. *J. Inorg. Biochem.* **2008,** *102* (12), 2130-2135.

43. Charkoudian, L. K.; Pham, D. M.; Kwan, A.; Vangeloff, A.; Franz, K. J., Modifications of Boronic Ester Pro-Chelators Triggered by Hydrogen Peroxide Tune

Reactivity to Inhibit Metal-Promoted Oxidative Stress. *Dalton Trans.* **2007,** (43), 5031-5042.

44. Charkoudian, L. K.; Pham, D. M.; Franz, K. J., A Pro-Chelator Triggered by Hydrogen Peroxide Inhibits Iron-Promoted Hydroxyl Radical Formation. *J. Am. Chem. Soc.* **2006,** *128* (38), 12424-12425.

45. Bayly, S.; Beer, P., Metal-Based Anion Receptor Systems. In *Recognition of Anions*, 2008; pp 45-94.

46. Tamaru, S.-i.; Hamachi, I., Recent Progress of Phosphate Derivatives Recognition Utilizing Artificial Small Molecular Receptors in Aqueous Media. In *Recognition of Anions*, 2008; pp 95-125.

47. O'Neil, E. J.; Smith, B. D., Anion Recognition Using Dimetallic Coordination Complexes. *Coord. Chem. Rev.* **2006,** *250* (23-24), 3068-3080.

48. Adams, J. A., Kinetic and Catalytic Mechanisms of Protein Kinases. *Chem. Rev.* **2001,** *101* (8), 2271-2290.

49. Lawrence, D. S.; Wang, Q., Seeing Is Believing: Peptide-Based Fluorescent Sensors of Protein Tyrosine Kinase Activity. *ChemBioChem* **2007,** *8* (4), 373-378.

50. Jacobsen, F. E.; Buczynski, M. W.; Dennis, E. A.; Cohen, S. M., A Macrophage Cell Model for Selective Metalloproteinase Inhibitor Design. *ChemBioChem* **2008,** *9* (13), 2087-2095.

51. Agrawal, A.; Romero-Perez, D.; Jacobsen, J. A.; Villarreal, F. J.; Cohen, S. M., Zinc-Binding Groups Modulate Selective Inhibition of Mmps. *ChemMedChem* **2008,** *3* (5), 812-820.

52. Cohen, S. M., New Approaches for Medicinal Applications of Bioinorganic Chemistry. *Curr. Opin. Chem. Biol.* **2007,** *11* (2), 115-120.

53. Jacobsen, F. E.; Lewis, J. A.; Cohen, S. M., The Design of Inhibitors for Medicinally Relevant Metalloproteins. *ChemMedChem* **2007,** *2* (2), 152-171.

54. Jacobsen, F. E.; Lewis, J. A.; Cohen, S. M., A New Role for Old Ligands: Discerning Chelators for Zinc Metalloproteinases. *J. Am. Chem. Soc.* **2006,** *128* (10), 3156-3157.

55. Puerta, D. T.; Mongan, J.; Tran, B. L.; McCammon, J. A.; Cohen, S. M., Potent, Selective Pyrone-Based Inhibitors of Stromelysin-1. *J. Am. Chem. Soc.* **2005,** *127* (41), 14148-14149.

56. Puerta, D. T.; Cohen, S. M., A Bioinorganic Perspective on Matrix Metalloproteinase Inhibition. *Curr. Top. Med. Chem.* **2004,** *4* (15), 1551-1573.

57. Soh, N., Selective Chemical Labeling of Proteins with Small Fluorescent Molecules Based on Metal-Chelation Methodology. *Sensors* **2008,** *8* (2), 1004-1024.

58. Lowe, M. P., Activated Mr Contrast Agents. *Curr. Pharm. Biotech.* **2004,** *5* (6), 519-528.

59. Jasanoff, A., Mri Contrast Agents for Functional Molecular Imaging of Brain Activity. *Current Opinion in Neurobiology* **2007,** *17* (5), 593-600.

60. Sitlani, A.; Long, E. C.; Pyle, A. M.; Barton, J. K., DNA Photocleavage by Phenanthrenequinone Diimine Complexes of Rhodium(III) - Shape-Selective Recognition and Reaction. *J. Am. Chem. Soc.* **1992,** *114* (7), 2303-2312.

61. Cowan, J. A., Catalytic Metallodrugs. *Pure Appl. Chem.* **2008,** *80*, 1799-1810.

62. Lee, H. S.; Schultz, P. G., Biosynthesis of a Site-Specific DNA Cleaving Protein. *J. Am. Chem. Soc.* **2008**.

63. Suh, J.; Chei, W. S., Metal Complexes as Artificial Proteases: Toward Catalytic Drugs. *Curr. Opin. Chem. Biol.* **2008,** *12* (2), 207-213.

64. Li, L.; Murthy, N. N.; Telser, J.; Zakharov, L. N.; Yap, G. P. A.; Rheingold, A. L.; Karlin, K. D.; Rokita, S. E., Targeted Guanine Oxidation by a Dinuclear Copper(II) Complex at Single Stranded/Double Stranded DNA Junctions. *Inorg. Chem.* **2006,** *45* (18), 7144-7159.

65. Ito, T.; Thyagarajan, S.; Karlin, K. D.; Rokita, S. E., Recognition of Guanines at a Double Helix-Coil Junction in DNA by a Trinuclear Copper Complex. *Chem. Commun.* **2005,** (38), 4812-4814.

66. Li, L.; Karlin, K. D.; Rokita, S. E., Changing Selectivity of DNA Oxidation from Deoxyribose to Guanine by Ligand Design and a New Binuclear Copper Complex. *J. Am. Chem. Soc.* **2005,** *127* (2), 520-521.

67. Humphreys, K. J.; Karlin, K. D.; Rokita, S. E., Targeted Strand Scission of DNA Substrates by a Tricopper(II) Coordination Complex. *J. Am. Chem. Soc.* **2002,** *124* (27), 8055-8066.

68. Hancock, R. D.; Martell, A. E., Ligand Design for Selective Complexation of Metal-Ions in Aqueous-Solution. *Chemical Reviews* **1989,** *89* (8), 1875-1914.

69. Martell, A. E.; Hancock, R. D.; Motekaitis, R. J., Factors Affecting Stabilities of Chelate, Macrocyclic and Macrobicyclic Complexes in Solution. *Coordination Chemistry Reviews* **1994,** *133*, 39-65.

70. Martell, A. E.; Hancock, R. D., *Metal Comlexes in Aqueous Solution*. Plenum Press: New York, 1996.

71. Hancock, R. D.; Melton, D. L.; Harrington, J. M.; McDonald, F. C.; Gephart, R. T.; Boone, L. L.; Jones, S. B.; Dean, N. E.; Whitehead, J. R.; Cockrell, G. M., Metal Ion Recognition in Aqueous Solution by Highly Preorganized Non-Macrocyclic Ligands. *Coord. Chem. Rev.* **2007,** *251* (13-14), 1678-1689.

72. Andersen, O., Chemical and Biological Considerations in the Treatment of Metal Intoxications by Chelating Agents. *Mini-Reviews in Medicinal Chemistry* **2004,** *4* (1), 11-21.

73. Sigel, H.; McCormick, D. B., On Discriminating Behavior of Metal Ions and Ligands with Regard to Their Biological Significance. *Accounts Chem. Res.* **1970,** *3* (6), 201-208.

74. Pearson, R. G., Hard and Soft Acids and Bases. *Journal of the American Chemical Society* **1963,** *85* (22), 3533-3539.

75. Perrin, D. D.; Dempsey, B., *Buffers for Ph and Metal Ion Control*. London : Chapman and Hall ; New York : Distributed in the U.S.A. by Halsted Press, 1979, c1974.

76. Martell, A. E.; M., S. R. *Nist Critically Selected Stability Constants of Metal Complexes*, 6.0; NIST: Gaithersburg, MD, 2001.

77. Martell, A. E.; Smith, R. M., *Critical Stability Constants*. Plenum Press: New York, 1974.

78. Miessler, G. L.; Tarr, D. A., *Inorganic Chemistry*. 3rd ed.; Pearson Education: Upper Saddle River, N.J. :, 2004.

79. Shriver; Atkins, *Inorganic Chemistry*. 4th ed.; W. H. Freeman New York, 2006.

80. Walling, C., Intermediates in the Reactions of Fenton Type Reagents. *Accounts Chem. Res.* **1998,** *31* (4), 155-157.

81. Prousek, J., Fenton Chemistry in Biology and Medicine. *Pure Appl Chem* **2007,** *79* (12), 2325-2338.

82. Fenton, H. J., *Chem. Soc. Trans.* **1894,** *65*.

83. Pierre, J. L.; Fontecave, M., Iron and Activated Oxygen Species in Biology: The Basic Chemistry. *Biometals* **1999,** *12* (3), 195-199.

84. Liu, Z. D.; Hider, R. C., Design of Iron Chelators with Therapeutic Application. *Coord. Chem. Rev.* **2002,** *232* (1-2), 151-171.

85. Crumbliss, A. L.; Harrington, J. M., Iron Sequestration by Small Molecules: Thermodynamic and Kinetic Studies of Natural Siderophores and Synthetic Model Compounds. *Adv. Inorg. Chem.* **2009,** *61*, 179-250.

86. Glickstein, H.; Ben El, R.; Shvartsman, M.; Cabantchik, Z. I., Intracellular Labile Iron Pools as Direct Targets of Iron Chelators: A Fluorescence Study of Chelator Action in Living Cells. *Blood* **2005,** *106* (9), 3242-3250.

87. Halliwell, B., Use of Desferrioxamine as a Probe for Iron-Dependent Formation of Hydroxyl Radicals - Evidence for a Direct Reaction between Desferal and the Superoxide Radical. *Biochem. Pharmacol.* **1985,** *34* (2), 229-233.

88. Balcerczyk, A.; Sowa, K.; Bartou, G., Metal Chelators React Also with Reactive Oxygen and Nitrogen Species. *Biochem. Biophys. Res. Commun.* **2007,** *352* (2), 522-525.

89. Scott, L. E.; Orvig, C., Medicinal Inorganic Chemistry Approaches to Passivation and Removal of Aberrant Metal Ions in Disease. *Chem. Rev.* **2009,** *109* (10), 4885-4910.

90. Kalinowski, D. S.; Richardson, D. R., The Evolution of Iron Chelators for the Treatment of Iron Overload Disease and Cancer. *Pharmacol. Rev.* **2005,** *57* (4), 547-583.

91. Simunek, T.; Boer, C.; Bouwman, R. A.; Vlasblom, R.; Versteilen, A. M. G.; Sterba, M.; Gersl, V.; Hrdina, R.; Ponka, P.; de Lange, J. J.; Paulus, W. J.; Musters, R. J. P., Sih - a Novel Lipophilic Iron Chelator - Protects H9c2 Cardiomyoblasts from Oxidative Stress-Induced Mitochondrial Injury and Cell Death. *J. Mol. Cell Cardiol.* **2005,** *39* (2), 345-354.

92. Zhang, A. S.; Sheftel, A. D.; Ponka, P., Intracellular Kinetics of Iron in Reticulocytes: Evidence for Endosome Involvement in Iron Targeting to Mitochondria. *Blood* **2005,** *105* (1), 368-375.

93. Horackova, M.; Ponka, P.; Byczko, Z., The Antioxidant Effects of a Novel Iron Chelator Salicylaldehyde Isonicotinoyl Hydrazone in the Prevention of H2o2 Injury in Adult Cardiomyocytes. *Cardiovasc. Res.* **2000,** *47* (3), 529-536.

94. Richardson, D. R.; Ponka, P., Pyridoxal Isonicotinoyl Hydrazone and Its Analogs: Potential Orally Effective Iron-Chelating Agents for the Treatment of Iron Overload Disease. *J. Lab. Clin. Med.* **1998,** *131* (4), 306-315.

95. Hermes-Lima, M.; Nagy, E.; Ponka, P.; Schulman, H. M., The Iron Chelator Pyridoxal Isonicotinoyl Hydrazone (Pih) Protects Plasmid Puc-18 DNA against (Oh)-O-Center Dot-Mediated Strand Breaks. *Free Radical Biol. Med.* **1998,** *25* (8), 875-880.

96. Hermes-Lima, M.; Ponka, P.; Schulman, H. M., The Iron Chelator Pyridoxal Isonicotinoyl Hydrazone (Pih) and Its Analogues Prevent Damage to 2-Deoxyribose Mediated by Ferric Iron Plus Ascorbate. *Biochim. Biophys. Acta* **2000,** *1523* (2-3), 154-160.

97. Petrat, F.; de Groot, H.; Sustmann, R.; Rauen, U., The Chelatable Iron Pool in Living Cells: A Methodically Defined Quantity. *Biol. Chem.* **2002,** *383* (3-4), 489-502.

98. Esposito, B. P.; Epsztejn, S.; Breuer, W.; Cabantchik, Z. I., A Review of Fluorescence Methods for Assessing Labile Iron in Cells and Biological Fluids. *Anal. Biochem.* **2002,** *304* (1), 1-18.

99. Richardson, D. R.; Hefter, G. T.; May, P. M.; Webb, J.; Baker, E., Iron Chelators of the Pyridoxal Isonicotinoyl Hydrazone Class. *BioMetals* **1989,** *2*, 161-167.

100. Kovarikova, P.; Mrkvickova, Z.; Klimes, J., Investigation of the Stability of Aromatic Hydrazones in Plasma and Related Biological Material. *J. Pharm. Biomed. Anal.* **2008,** *47* (2), 360-370.

101. Rutherford, J. C.; Ojeda, L.; Balk, J.; Muhlenhoff, U.; Lill, R.; Winge, D. R., Activation of the Iron Regulon by the Yeast Aft1/Aft2 Transcription Factors Depends on Mitochondrial but Not Cytosolic Iron-Sulfur Protein Biogenesis. *J. Biol. Chem.* **2005,** *280* (11), 10135-10140.

102. Chen, O. S.; Crisp, R. J.; Valachovic, M.; Bard, M.; Winge, D. R.; Kaplan, J., Transcription of the Yeast Iron Regulon Does Not Respond Directly to Iron but Rather to Iron-Sulfur Cluster Biosynthesis. *J. Biol. Chem.* **2004,** *279* (28), 29513-29518.

103. Blair, D.; Diehl, H., Bathophenanthrolinedisulphonic Acid and Bathocuproinedisulphonic Acid, Water Soluble Reagents for Iron and Copper. *Talanta* **1961/2,** *7* (3-4), 163-174.

104. Cowart, R. E.; Singleton, F. L.; Hind, J. S., A Comparison of Bathophenanthrolinedisulfonic Acid and Ferrozine as Chelators of Iron(II) in Reduction Reactions. *Anal. Biochem.* **1993,** *211* (1), 151-155.

105. Philpott, C. C.; Rashford, J.; Yamaguchi-Iwai, Y.; Rouault, T. A.; Dancis, A.; Klausner, R. D., Cell-Cycle Arrest and Inhibition of G(1) Cyclin Translation by Iron in Aft1-1(up) Yeast. *EMBO J.* **1998,** *17* (17), 5026-5036.

106. Courel, M.; Lallet, S.; Camadro, J. M.; Blaiseau, P. L., Direct Activation of Genes Involved in Intracellular Iron Use by the Yeast Iron-Responsive Transcription Factor Aft2 without Its Paralog Aft1. *Mol. Cell Biol.* **2005,** *25* (15), 6760-6771.

107. Shakoury-Elizeh, M.; Tiedeman, J.; Rashford, J.; Ferea, T.; Demeter, J.; Garcia, E.; Rolfes, R.; Brown, P. O.; Botstein, D.; Philpott, C. C., Transcriptional Remodeling in Response to Iron Deprivation in Saccharomyces Cerevisiae. *Mol. Biol. Cell* **2004,** *15* (3), 1233-1243.

108. Berlett, B. S.; Levine, R. L.; Chock, P. B.; Chevion, M.; Stadtman, E. R., Antioxidant Activity of Ferrozine-Iron-Amino Acid Complexes. *Proc. Natl Acad. Sci. USA* **2001,** *98* (2), 451-456.

109. Mitsumoto, A.; Kim, K. R.; Oshima, G.; Nakagawa, Y., Chelation of Cellular Cu(I) Raised the Degree of Glyoxalase I Inactivation in Human Endothelial Cells Upon Exposure to S-Nitrosoglutathione through Stabilization of S-Nitrosothiols. *Biol. Pharm. Bull.* **2001,** *24* (4), 336-341.

110. Ogra, Y.; Aoyama, M.; Suzuki, K. T., Protective Role of Metallothionein against Copper Depletion. *Arch. Biochem. Biophys.* **2006,** *451* (2), 112-118.

111. Watanabe, M.; Tezuka, M., Copper Is Required for Retinoic Acid Receptor-Dependent Transcription and Neuronal Differentiation in P19 Embryonal Carcinoma Cells. *Journal of Health Science* **2006,** *52* (5), 540-548.

112. Gordge, M. P.; Meyer, D. J.; Hothersall, J.; Neild, G. H.; Payne, N. N.; Noronhadutra, A., Copper Chelation-Induced Reduction of the Biological-Activity of S-Nitrosothiols. *Brit. J. Pharmacol.* **1995,** *114* (5), 1083-1089.

113. Kang, J. H.; Lin, C. J.; Chen, J.; Liu, Q., Copper Induces Histone Hypoacetylation through Directly Inhibiting Histone Acetyltransferase Activity. *Chem. Biol. Interact.* **2004,** *148* (3), 115-123.

114. Armstrong, C.; Leong, W.; Less, G. J., Comparative Effects of Metal Chelating Agents on the Neuronal Cytotoxicity Induced by Copper (Cu^{+2}), Iron (Fe^{+3}) and Zinc in the Hippocampus. *Brain Research* **2001,** *892* (1), 51-62.

115. Li, Y. B.; Seacat, A.; Kuppusamy, P.; Zweier, J. L.; Yager, J. D.; Trush, M. A., Copper Redox-Dependent Activation of 2-Tert-Butyl(1,4)Hydroquinone: Formation of Reactive Oxygen Species and Induction of Oxidative DNA Damage in Isolated DNA and Cultured Rat Hepatocytes. *Mut. Res.* **2002,** *518* (2), 123-133.

116. Lappin, A. G.; Youngblood, M. P.; Margerum, D. W., Electron-Transfer Reactions of Copper(I) and Copper(III) Complexes. *Inorg. Chem.* **1980,** *19* (2), 407-413.

117. Sayre, L. M., Alzheimer's Precursor Protein and the Use of Bathocuproine for Determining Reduction of Copper(II). *Science* **1996,** *274* (5294), 1933-1934.

118. Laggner, H.; Hermann, M.; Gmeiner, B. M. K.; Kapiotis, S., Cu^{2+} and Cu^{+} Bathocuproine Disulfonate Complexes Promote the Oxidation of the Ros-Detecting Compound Dichlorofluorescin (Dcfh). *Analytical and Bioanalytical Chemistry* **2006,** *385* (5), 959-961.

119. Mandal, S.; Kazmi, N. H.; Sayre, L. M., Ligand Dependence in the Copper-Catalyzed Oxidation of Hydroquinones. *Arch. Biochem. Biophys.* **2005,** *435* (1), 21-31.

120. Messori, L.; Casini, A.; Gabbiani, C.; Sorace, L.; Muniz-Miranda, M.; Zatta, P., Unravelling the Chemical Nature of Copper Cuprizone. *Dalton Trans.* **2007,** (21), 2112-2114.

121. Fritsky, I. O.; Kozlowski, H.; Sadler, P. J.; Yefetova, O. P.; Swatek-Kozlowska, J.; Kalibabchuk, V. A.; Glowiak, T., Template Synthesis of Square-Planar Nickel(II) and Copper(III) Complexes Based on Hydrazide Ligands. *Dalton Trans.* **1998,** (19), 3269-3274.

122. Fritsky, I. O.; Kozlowski, H.; Kanderal, O. M.; Haukka, M.; Swiatek-Kozlowska, J.; Gumienna-Kontecka, E.; Meyer, F., Efficient Stabilization of Copper(III) in Tetraaza Pseudo-Macrocyclic Oxime-and-Hydrazide Ligands with Adjustable Cavity Size. *Chem. Commun.* **2006,** (39), 4125-4127.

123. Zatta, P.; Raso, M.; Zambenedetti, P.; Wittkowski, W.; Messori, L.; Piccioli, F.; Mauri, P. L.; Beltramini, M., Copper and Zinc Dismetabolism in the Mouse Brain Upon Chronic Cuprizone Treatment. *Cell. Mol. Life Sci.* **2005,** *62* (13), 1502-1513.

124. Choi, S. M.; Choi, K. O.; Lee, N.; Oh, M.; Park, H., The Zinc Chelator, N,N,N ',N '-Tetrakis (2-Pyridylmethyl) Ethylenediamine, Increases the Level of Nonfunctional HIF-1 Alpha Protein in Normoxic Cells. *Biochem. Biophys. Res. Commun.* **2006,** *343* (4), 1002-1008.

125. Segurado, M.; Lopez-Aragon, R.; Calera, J. A.; Fernandez-Abalos, J. M.; Leal, F., Zinc-Regulated Biosynthesis of Immunodominant Antigens from Aspergillus Spp. *Infection and Immunity* **1999,** *67* (5), 2377-2382.

126. Seve, M.; Favier, A.; Osman, M.; Hernandez, D.; Vaitaitis, G.; Flores, N. C.; McCord, J. M.; Flores, S. C., The Human Immunodeficiency Virus-1 Tat Protein Increases Cell Proliferation, Alters Sensitivity to Zinc Chelator-Induced Apoptosis, and Changes Sp1 DNA Binding in Hela Cells. *Arch. Biochem. Biophys.* **1999,** *361* (2), 165-172.

127. Chimienti, F.; Seve, M.; Richard, S.; Mathieu, J.; Favier, A., Role of Cellular Zinc in Programmed Cell Death: Temporal Relationship between Zinc Depletion, Activation of Caspases, and Cleavage of Sp Family Transcription Factors. *Biochem. Pharmacol.* **2001,** *62* (1), 51-62.

128. Parat, M. O.; Richard, M. J.; Favier, A.; Amblard, P.; Beani, J. C., Zinc and DNA Fragmentation in Keratinocyte Apoptosis. *J. Invest. Dermatol.* **1996,** *107* (2), C26-C26.

129. Hashemi, M.; Ghavami, S.; Eshraghi, M.; Booy, E. P.; Los, M., Cytotoxic Effects of Intra and Extracellular Zinc Chelation on Human Breast Cancer Cells. *Eur. J. Pharmacol.* **2007,** *557* (1), 9-19.

130. Jackson, K. A.; Helston, R. M.; McKay, J. A.; O'Neill, E. D.; Mathers, J. C.; Ford, D., Splice Variants of the Human Zinc Transporter Znt5 (Slc30a5) Are Differentially Localized and Regulated by Zinc through Transcription and Mrna Stability. *J. Biol. Chem.* **2007,** *282* (14), 10423-10431.

131. Anderegg, G.; Hubmann, E.; Podder, N. G.; Wenk, F., Pyridine-Derivatives as Complexing Agents .11. Thermodynamics of Metal-Complex Formation with Bis[(2-Pyridyl)Methyl]-Amine, Tris[(2-Pyridyl)Methyl]-Amine and Tetrakis[(2-Pyridyl)Methyl]-Amine. *Helv. Chim. Acta* **1977,** *60* (1), 123-140.

132. A. E. Martell, R. M. S., *Critical Stability Constants*. Plenum Press: New York and London, 1977.

133. Sigdel, T. K.; Easton, J. A.; Crowder, M. W., Transcriptional Response of Escherichia Coli to Tpen. *J. Bacteriol.* **2006,** *188* (18), 6709-6713.

134. Pena, M. M. O.; Lee, J.; Thiele, D. J., A Delicate Balance: Homeostatic Control of Copper Uptake and Distribution. *J. Nutr.* **1999,** *129* (7), 1251-1260.

135. Macomber, L.; Imlay, J. A., The Iron-Sulfur Clusters of Dehydratases Are Primary Intracellular Targets of Copper Toxicity. *Proc. Natl. Acad. Sci. U. S. A.* **2009,** *106* (20), 8344-8349.

136. Predki, P. F.; Sarkar, B., Effect of Replacement of Zinc Finger Zinc on Estrogen-Receptor DNA Interactions. *J. Biol. Chem.* **1992,** *267* (9), 5842-5846.

137. Waggoner, D. J.; Bartnikas, T. B.; Gitlin, J. D., The Role of Copper in Neurodegenerative Disease. *Neurobiol. Dis.* **1999,** *6* (4), 221-230.

138. Madsen, E.; Gitlin, J. D., Copper and Iron Disorders of the Brain. *Annu. Rev. Neurosci.* **2007,** *30*, 317-337.

139. Petris, M. J.; Voskoboinik, I.; Cater, M.; Smith, K.; Kim, B. E.; Llanos, R. M.; Strausak, D.; Camakaris, J.; Mercer, J. F. B., Copper-Regulated Trafficking of the Menkes Disease Copper Atpase Is Associated with Formation of a Phosphorylated Catalytic Intermediate. *J. Biol. Chem.* **2002,** *277* (48), 46736-46742.

140. Wong, P. C.; Rothstein, J. D.; Price, D. L., The Genetic and Molecular Mechanisms of Motor Neuron Disease. *Curr. Opin. Neurobiol.* **1998,** *8* (6), 791-799.

141. Turski, M. L.; Thiele, D. J., New Roles for Copper Metabolism in Cell Proliferation, Signaling, and Disease. *J. Biol. Chem.* **2009,** *284* (2), 717-721.

142. Kim, B. E.; Nevitt, T.; Thiele, D. J., Mechanisms for Copper Acquisition, Distribution and Regulation. *Nat. Chem. Biol.* **2008,** *4* (3), 176-185.

143. Puig, S.; Rees, E. M.; Thiele, D. J., The Abcds of Periplasmic Copper Trafficking. *Structure* **2002,** *10* (10), 1292-1295.

144. Puig, S.; Thiele, D. J., Molecular Mechanisms of Copper Uptake and Distribution. *Curr. Opin. Chem. Biol.* **2002,** *6* (2), 171-180.

145. Huffman, D. L.; O'Halloran, T. V., Function, Structure, and Mechanism of Intracellular Copper Trafficking Proteins. *Annu. Rev. Biochem.* **2001,** *70*, 677-701.

146. O'Halloran, T. V.; Culotta, V. C., Metallochaperones, an Intracellular Shuttle Service for Metal Ions. *J. Biol. Chem.* **2000,** *275* (33), 25057-25060.

147. Rae, T. D.; Schmidt, P. J.; Pufahl, R. A.; Culotta, V. C.; O'Halloran, T. V., Undetectable Intracellular Free Copper: The Requirement of a Copper Chaperone for Superoxide Dismutase. *Science* **1999,** *284* (5415), 805-808.

148. Rosenzweig, A. C.; O'Halloran, T. V., Structure and Chemistry of the Copper Chaperone Proteins. *Curr. Opin. Chem. Biol.* **2000,** *4* (2), 140-147.

149. Knight, S. A. B.; Kwon, L. F.; Kosman, D. J.; Thiele, D. J., High Affinity Copper Transport in Yeast. *Faseb J* **1996,** *10* (3), 1685-1685.

150. Dancis, A.; Haile, D.; Yuan, D. S.; Klausner, R. D., The Saccharomyces-Cerevisiae Copper Transport Protein (Ctr1p) - Biochemical, Characterization, Regulation by Copper, and Physiological-Role in Copper Uptake. *J. Biol. Chem.* **1994,** *269* (41), 25660-25667.

151. Dancis, A.; Yuan, D. S.; Haile, D.; Askwith, C.; Eide, D.; Moehle, C.; Kaplan, J.; Klausner, R. D., Molecular Characterization of a Copper Transport Protein in

Saccharomyces-Cerevisiae - an Unexpected Role for Copper in Iron Transport. *Cell* **1994,** *76* (2), 393-402.

152. Rees, E. M.; Lee, J.; Thiele, D. J., Mobilization of Intracellular Copper Stores by the Ctr2 Vacuolar Copper Transporter. *J. Biol. Chem.* **2004,** *279* (52), 54221-54229.

153. Rees, E. M.; Thiele, D. J., Identification of a Vacuole-Associated Metalloreductase and Its Role in Ctr2-Mediated Intracellular Copper Mobilization. *J. Biol. Chem.* **2007,** *282* (30), 21629-21638.

154. De Feo, C. J.; Aller, S. G.; Siluvai, G. S.; Blackburn, N. J.; Unger, V. M., Three-Dimensional Structure of the Human Copper Transporter Hctr1. *Proc. Natl. Acad. Sci. U. S. A.* **2009,** *106* (11), 4237-4242.

155. Aller, S. G.; Unger, V. M., Projection Structure of the Human Copper Transporter Ctr1 at 6-a Resolution Reveals a Compact Trimer with a Novel Channel-Like Architecture. *Proc. Natl. Acad. Sci. U. S. A.* **2006,** *103* (10), 3627-3632.

156. Puig, S.; Lee, J.; Lau, M.; Thiele, D. J., Biochemical and Genetic Analyses of Yeast and Human High Affinity Copper Transporters Suggest a Conserved Mechanism for Copper Uptake. *J. Biol. Chem.* **2002,** *277* (29), 26021-26030.

157. Lee, J.; Pena, M. M. O.; Nose, Y.; Thiele, D. J., Biochemical Characterization of the Human Copper Transporter Ctr1. *J. Biol. Chem.* **2002,** *277* (6), 4380-4387.

158. Hassett, R.; Kosman, D. J., Evidence for Cu(II) Reduction as a Component of Copper Uptake by Saccharomyces-Cerevisiae. *J. Biol. Chem.* **1995,** *270* (1), 128-134.

159. Georgatsou, E.; Mavrogiannis, L. A.; Fragiadakis, G. S.; Alexandraki, D., The Yeast Fre1p/Fre2p Cupric Reductases Facilitate Copper Uptake and Are Regulated by the Copper-Modulated Mac1p Activator. *J. Biol. Chem.* **1997,** *272* (21), 13786-13792.

160. Knutson, M. D., Steap Proteins: Implications for Iron and Copper Metabolism. *Nutr. Rev.* **2007,** *65* (7), 335-340.

161. Lamb, A. L.; Torres, A. S.; O'Halloran, T. V.; Rosenzweig, A. C., Heterodimeric Structure of Superoxide Dismutase in Complex with Its Metallochaperone. *Nat. Struct. Biol.* **2001,** *8* (9), 751-755.

162. Rae, T. D.; Torres, A. S.; Pufahl, R. A.; O'Halloran, T. V., Mechanism of Cu,Zn-Superoxide Dismutase Activation by the Human Metallochaperone Hccs. *J. Biol. Chem.* **2001,** *276* (7), 5166-5176.

163. Lamb, A. L.; Wernimont, A. K.; Pufahl, R. A.; Culotta, V. C.; O'Halloran, T. V.; Rosenzweig, A. C., Crystal Structure of the Copper Chaperone for Superoxide Dismutase. *Nat. Struct. Biol.* **1999,** *6* (8), 724-729.

164. Rosenzweig, A. C., Copper Delivery by Metallochaperone Proteins. *Accounts Chem. Res.* **2001,** *34* (2), 119-128.

165. Boal, A. K.; Rosenzweig, A. C., Structural Biology of Copper Trafficking. *Chem. Rev.* **2009,** *109* (10), 4760-4779.

166. Eisses, J. F.; Kaplan, J. H., Molecular Characterization of Hctr1, the Human Copper Uptake Protein. *J. Biol. Chem.* **2002,** *277* (32), 29162-29171.

167. Eisses, J. F.; Kaplan, J. H., The Mechanism of Copper Uptake Mediated by Human Ctr1 - a Mutational Analysis. *J. Biol. Chem.* **2005,** *280* (44), 37159-37168.

168. Nose, Y.; Rees, E. M.; Thiele, D. J., Structure of the Ctr1 Copper Trans'pore'ter Reveals Novel Architecture. *Trends Biochem.Sci.* **2006,** *31* (11), 604-607.

169. De Feo, C. J.; Aller, S. G.; Unger, V. M. In *A Structural Perspective on Copper Uptake in Eukaryotes*, Springer: 2007; pp 705-716.

170. Jiang, J. F.; Nadas, I. A.; Kim, M. A.; Franz, K. J., Mets Motif Peptide Found in Copper Transport Proteins Selectively Binds Cu(I) with Methionine-Only Coordination. *Inorg. Chem.* **2005,** *44* (26), 9787-9794.

171. Deschamps, P.; Kulkarni, P. P.; Gautam-Basak, M.; Sarkar, B., The Saga of Copper(II)-L-Histidine. *Coordin Chem Rev* **2005,** *249* (9-10), 895-909.

172. Rózga, M.; Sokołowska, M.; Protas, A.; Bal, W., Human Serum Albumin Coordinates Cu(II) at Its N-Terminal Binding Site with 1 pm Affinity. *Journal of Biological Inorganic Chemistry* **2007,** *12* (6), 913-918.

173. Melino, S.; Garlando, L.; Patamia, M.; Paci, M.; Petruzzelli, R., A Metal-Binding Site Is Present in the Amino Terminal Region of the Bioactive Iron Regulator Hepcidin-25. *J. Pept. Res.* **2005,** *66*, 65-71.

174. Cabras, T.; Patamia, M.; Melino, S.; Inzitari, R.; Messana, I.; Castagnola, M.; Petruzzelli, R., Pro-Oxidant Activity of Histatin 5 Related Cu(II)-Model Peptide Probed by Mass Spectrometry. *Biochem. Biophys. Res. Commun.* **2007,** *358* (1), 277-284.

175. Harford, C.; Sarkar, B., Amino Terminal Cu(II)- and Ni(II)-Binding (Atcun) Motif of Proteins and Peptides: Metal Binding, DNA Cleavage, and Other Properties. *Accounts Chem. Res.* **1997,** *30* (3), 123-130.

176. Harford, C.; Sarkar, B., Neuromedin-C Binds Cu(II) and Ni(II) Via the Atcun Motif - Implications for the Cns and Cancer Growth. *Biochem. Biophys. Res. Commun.* **1995,** *209* (3), 877-882.

177. Kolozsi, A.; Jancso, A.; Nagy, N. V.; Gajda, T., N-Terminal Fragment of the Anti-Angiogenic Human Endostatin Binds Copper(II) with Very High Affinity. *J. Inorg. Biochem.* **2009,** *103* (7), 940-947.

178. Shearer, J.; Soh, P., The Copper(II) Adduct of the Unstructured Region of the Amyloidogenic Fragment Derived from the Human Prion Protein Is Redox-Active at Physiological Ph. *Inorg. Chem.* **2007,** *46* (3), 710-719.

179. Shearer, J.; Szalai, V. A., The Amyloid-Beta Peptide of Alzheimer's Disease Binds Cu-I in a Linear Bis-His Coordination Environment: Insight into a Possible Neuroprotective Mechanism for the Amyloid-Beta Peptide. *J. Am. Chem. Soc.* **2008,** *130* (52), 17826-17835.

180. Shearer, J.; Soh, P.; Lentz, S., Both Met(109) and Met(112) Are Utilized for Cu(II) Coordination by the Amyloidogenic Fragment of the Human Prion Protein at Physiological Ph. *J. Inorg. Biochem.* **2008,** *102* (12), 2103-2113.

181. Himes, R. A.; Park, G. Y.; Barry, A. N.; Blackburn, N. J.; Karlin, K. D., Synthesis and X-Ray Absorption Spectroscopy Structural Studies of Cu(I) Complexes of Histidylhistidine Peptides: The Predominance of Linear 2-Coordinate Geometry. *J. Am. Chem. Soc.* **2007,** *129* (17), 5352-5353.

182. Himes, R. A.; Park, G. Y.; Siluvai, G. S.; Blackburn, N. J.; Karlin, K. D., Structural Studies of Copper(I) Complexes of Amyloid-Beta Peptide Fragments: Formation of Two-Coordinate Bis(Histidine) Complexes. *Angew. Chem.-Int. Edit.* **2008,** *47* (47), 9084-9087.

183. Yatsunyk, L. A.; Rosenzweig, A. C., Cu(I) Binding and Transfer by the N Terminus of the Wilson Disease Protein. *J. Biol. Chem.* **2007,** *282* (12), 8622-8631.

184. Perrone, L.; Mothes, E.; Vignes, M.; Mockel, A.; Figueroa, C.; Miquel, M.-C.; Maddelein, M.-L.; Faller, P., Copper Transfer from Cu-Abeta to Human Serum Albumin Inhibits Aggregation, Radical Production and Reduces Abeta Toxicity. *ChemBioChem* **2009,** *11* (1), 110-118.

185. Pace, C. N.; Vajdos, F.; Fee, L.; Grimsley, G.; Gray, T., How to Measure and Predict the Molar Absorption Coefficient of a Protein. *Protein Science* **1995,** *4* (11), 2411-2423.

186. Edelhoch, H., Spectroscopic Determination of Tryptophan and Tyrosine in Proteins *Biochemistry* **1967,** *6* (7), 1948-&.

187. Flaschka, H. A., *Edta Titrations: An Introduction to Theory and Practice*. Pergamon Press: New York, 1959.

188. Xiao, Z.; Loughlin, F.; George, G. N.; Howlett, G. J.; Wedd, A. G., C-Terminal Domain of the Membrane Copper Transporter Ctr1 from Saccharomyces Cerevisiae Binds Four Cu(I) Ions as a Cuprous-Thiolate Polynuclear Cluster: Sub-Femtomolar Cu(I) Affinity of Three Proteins Involved in Copper Trafficking. *J. Am. Chem. Soc.* **2004,** *126* (10), 3081-3090.

189. Gampp, H.; Maeder, M.; Meyer, C. J.; Zuberbuhler, A. D., Calculation of Equilibrium-Constants from Multiwavelength Spectroscopic Data .1. Mathematical Considerations. *Talanta* **1985,** *32* (2), 95-101.

190. Gampp, H.; Maeder, M.; Meyer, C. J.; Zuberbuhler, A. D., Calculation of Equilibrium-Constants from Multiwavelength Spectroscopic Data .4. Model-Free Least-Squares Refinement by Use of Evolving Factor-Analysis. *Talanta* **1986,** *33* (12), 943-951.

191. Xiao, Z.; Donnelly, P. S.; Zimmermann, M.; Wedd, A. G., Transfer of Copper between Bis(Thiosemicarbazone) Ligands and Intracellular Copper-Binding Proteins. Insights into Mechanisms of Copper Uptake and Hypoxia Selectivity. *Inorg. Chem.* **2008,** *47* (10), 4338-4347.

192. Chong, L. X.; Ash, M.-R.; Maher, M. J.; Hinds, M. G.; Xiao, Z.; Wedd, A. G., Unprecedented Binding Cooperativity between Cui and Cuii in the Copper Resistance Protein Copk from Cupriavidus Metallidurans Ch34: Implications from Structural

Studies by Nmr Spectroscopy and X-Ray Crystallography. *J. Am. Chem. Soc.* **2009,** *131* (10), 3549-3564.

193. Kamau, P.; Jordan, R. B., Complex Formation Constants for the Aqueous Copper(I)-Acetonitrile System by a Simple General Method. *Inorg. Chem.* **2001,** *40* (16), 3879-3883.

194. Lee, J.; Petris, M. J.; Thiele, D. J., Characterization of Mouse Embryonic Cells Deficient in the Ctr1 High Affinity Copper Transporter - Identification of a Ctr1-Independent Copper Transport System. *J. Biol. Chem.* **2002,** *277* (43), 40253-40259.

195. Maryon, E. B.; Molloy, S. A.; Kaplan, J. H., O-Linked Glycosylation at Threonine 27 Protects the Copper Transporter Hctr1 from Proteolytic Cleavage in Mammalian Cells. *J. Biol. Chem.* **2007,** *282* (28), 20376-20387.

196. Maryon, E. B.; Zhang, J.; Jellison, J. W.; Kaplan, J. H., Human Copper Transporter 1 Lacking O-Linked Glycosylation Is Proteolytically Cleaved in a Rab9-Positive Endosomal Compartment. *J. Biol. Chem.* **2009,** *284* (41), 28104-28114.

197. Serrano, R.; Kiellandbrandt, M. C.; Fink, G. R., Yeast Plasma-Membrane Atpase Is Essential for Growth and Has Homology with (Na^++K^+), K^+- and Ca-$^{2+}$-Atpases. *Nature* **1986,** *319* (6055), 689-693.

198. Lefebvre, B.; Boutry, M.; Morsomme, P., The Yeast and Plant Plasma Membrane H^+ Pump Atpase: Diveraent Reaulation for the Same Function. In *Progress in Nucleic Acid Research and Molecular Biology, Vol 74*, Academic Press Inc: San Diego, 2003; Vol. 74, pp 203-237.

199. Carmelo, V.; Santos, H.; S·-Correia, I., Effect of Extracellular Acidification on the Activity of Plasma Membrane Atpase and on the Cytosolic and Vacuolar Ph of Saccharomyces Cerevisiae. *Biochimica et Biophysica Acta (BBA) - Biomembranes* **1997,** *1325* (1), 63-70.

200. Nose, Y.; Kim, B. E.; Thiele, D. J., Ctr1 Drives Intestinal Copper Absorption and Is Essential for Growth, Iron Metabolism, and Neonatal Cardiac Function. *Cell Metab.* **2006,** *4* (3), 235-244.

201. Schreiber, S. L., Small Molecules: The Missing Link in the Central Dogma. *Nat. Chem. Biol.* **2005,** *1* (2), 64-66.

202. Doudna, J. A., Chemical Biology at the Crossroads of Molecular Structure and Mechanism. *Nat Chem Biol* **2005,** *1* (6), 300-303.

203. Stockwell, B. R., Exploring Biology with Small Organic Molecules. *Nature* **2004,** *432* (7019), 846-854.

204. Tomi, K. S., Chemical Biology and Drug Design: Three-Dimensional, Dynamic, and Mechanistic Nature of Two Multidisciplinary Fields. *Chem. Biol. Drug Des.* **2006,** *67* (3), 196-200.

205. Fricker, S. P., Metal Based Drugs: From Serendipity to Design. *Dalton Trans.* **2007,** (43), 4903-4917.

206. Lippard, S. J., The Inorganic Side of Chemical Biology. *Nat Chem Biol* **2006,** *2* (10), 504-507.

207. Ellis-Davies, G. C. R., Development and Application of Caged Calcium. *Methods Enzymol* **2003,** *360*, 226-238.

208. Adams, S. R.; Tsien, R. Y., Controlling Cell Chemistry with Caged Compounds. *Ann. Rev. Physiol.* **1993,** *55*, 755-784.

209. Adams, S. R.; Kao, J. P. Y.; Grynkiewicz, G.; Minta, A.; Tsien, R. Y., Biologically Useful Chelators That Release Ca^{2+} Upon Illumination. *J. Am. Chem. Soc.* **1988,** *110* (10), 3212-3220.

210. Ellis-Davies, G. C. R.; Kaplan, J. H., Nitrophenyl-Egta, a Photolabile Chelator That Selectively Binds Ca^{2+} with High-Affinity and Releases It Rapidly Upon Photolysis. *Proc. Natl. Acad. Sci. U.S.A.* **1994,** *91* (1), 187-191.

211. Ellis-Davies, G. C. R.; Barsotti, R. J., Tuning Caged Calcium: Photolabile Analogues of Egta with Improved Optical and Chelation Properties. *Cell Calcium* **2006,** *39* (1), 75-83.

212. Kishimoto, T.; Liu, T. T.; Ninomiya, Y.; Takagi, H.; Yoshioka, T.; Ellis-Davies, G. C. R.; Miyashita, Y. W.; Kasai, H., Ion Selectivities of the Ca^{2+} Sensors for Exocytosis in Rat Phaeochromocytoma Cells. *Journal of Physiology-London* **2001,** *533* (3), 627-637.

213. Grell, E.; Warmuth, R., Caged Cations. *Pure Appl Chem* **1993,** *65* (3), 373-379.

214. Plaza, P.; Leray, I.; Changenet-Barret, P.; Martin, M. M.; Valeur, B., Reversible Bulk Photorelease of Strontium Ion from a Crown Ether-Linked Merocyanine. *Chemphyschem* **2002,** *3* (8), 668-674.

215. Ciesienski, K. L.; Haas, K. L.; Dickens, M. G.; Tesema, Y. T.; Franz, K. J., A Photolabile Ligand for Light-Activated Release of Caged Copper. *J. Am. Chem. Soc.* **2008,** *130* (37), 12246-12247.

216. Gaggelli, E.; Kozlowski, H.; Valensin, D.; Valensin, G., Copper Homeostasis and Neurodegenerative Disorders (Alzheimer's, Prion, and Parkinson's Diseases and Amyotrophic Lateral Sclerosis). *Chem. Rev.* **2006,** *106* (6), 1995-2044.

217. Schlief, M. L.; Gitlin, J. D., Copper Homeostasis in the Cns - a Novel Link between the Nmda Receptor and Copper Homeostasis in the Hippocampus. *Mol. Neurobiol.* **2006,** *33* (2), 81-90.

218. Filomeni, G.; Cerchiaro, G.; Ferreira, A. M. D.; De Martino, A.; Pedersen, J. Z.; Rotilio, G.; Ciriolo, M. R., Pro-Apoptotic Activity of Novel Isatin-Schiff Base Copper(II) Complexes Depends on Oxidative Stress Induction and Organelle-Selective Damage. *J. Biol. Chem.* **2007,** *282* (16), 12010-12021.

219. Tsuboyama, S.; Sakurai, T.; Kobayashi, K.; Azuma, N.; Kajikawa, Y.; Ishizu, K., Ph-Dependence of Binding-Site in Complexation of Cu-11 with Picolinamide Groups - Crystallographic Studies of Mono- and Binuclear Complexes with N,N'-Dipicolinoyl-1,3-Propanediamine. *Acta Crystallogr. Sect. B-Struct. Commun.* **1984,** *40* (OCT), 466-473.

220. Stephens, F. S.; Vagg, R. S., Studies on the Metal Amide Bond .17. The Crystal and Molecular-Structure of the Alpha-Form of Aqua-[N,N'-Bis(2'-Pyridinecarboxamido)-1,3-Propane] Copper(II) Dihydrate. *Inorg Chim a-Art Let* **1984,** *88* (1), 7-14.

221. Comba, P.; Goll, W.; Nuber, B.; Varnagy, K., Transition Metal Coordination Compounds of Bisamidobispyridyl Ligands. *Eur. J. Inorg. Chem.* **1998,** (12), 2041-2049.

222. Conley, H. L.; Martin, R. B., Cupric Ion Catalyzed Hydrolyses of Glycine Ethyl Ester Glycinamide and Picolinamide. *J Phys Chem-Us* **1965,** *69* (9), 2914-&.

223. Gans, P.; Sabatini, A.; Vacca, A., Investigation of Equilibria in Solution. Determination of Equilibrium Constants with the Hyperquad Suite of Programs. *Talanta* **1996,** *43* (10), 1739-1753.

224. Reedijk, J., Platinum Anticancer Coordination Compounds: Study of DNA Binding Inspires New Drug Design. *Eur. J. Inorg. Chem.* **2009,** (10), 1303-1312.

225. Bruijnincx, P. C. A.; Sadler, P. J., Controlling Platinum, Ruthenium, and Osmium Reactivity for Anticancer Drug Design. In *Adv Inorg Chem*, Elsevier Academic Press Inc: San Diego, 2009; Vol. 61, pp 1-62.

6. Biography

Kathryn Louise Haas was born October 9, 1981 in Harrisburg Pennsylvania. She also lived in York and Dover Pennsylvania. After graduating with Honors from Dover Area High School, Kathryn attended Gettysburg College to pursue a Bachelors of Science Degree in Chemistry. She graduated *summa cum laude* and with Chemistry Department Honors from Gettysburg College in 2004. In Fall 2004, Kathryn began her graduate career as a student of the Center for Biologically Inspired Materials and Materials Science (CBIMMS) at Duke University in Durham, North Carolina. She joined the lab of Katherine J. Franz in the Chemistry Department at Duke and started doing research on the effect of posttranslational peptide modifications on metal ion binding. After briefly working on another project toward elucidating the structural components of sepia melanin, Kathryn finally settled on a project dealing with copper membrane transport proteins. During her tenure at Duke University, Kathryn received several awards and fellowships including an National Science Foundation Integrated Graduate Education and Research Traineeship, the John Herbert Pearson Teaching Award, and the Pelham Wilder Jr. Fellowship for outstanding teaching assistants. Kathryn also contributed to work published in journals such as the Journal of the American Chemical Society, Chemical Reviews, The European Journal of Inorganic Chemistry and the Journal of Chemical Education. Kathryn also designed a new course for undergraduate students with four other chemistry graduate students under the supervision of Dr. James Bonk. After graduate school, Kathryn will pursue a postdoctoral position in the field of metal regulation of epigenetic DNA modifications.